Master's thesis

NTNU
Norwegian University of Science and Technology
Faculty of Information Technology and Electrical Engineering
Department of Electric Power Engineering

Jonas Eidsvåg Rostad

Frequency Control Evaluation for a Variable Speed Wind Power Plant in an Isolated Power System

Master's thesis in Energy and Environmental Engineering
Supervisor: Kjetil Uhlen
June 2023

NTNU
Norwegian University of
Science and Technology

Jonas Eidsvåg Rostad

Frequency Control Evaluation for a Variable Speed Wind Power Plant in an Isolated Power System

Master's thesis in Energy and Environmental Engineering
Supervisor: Kjetil Uhlen
June 2023

Norwegian University of Science and Technology
Faculty of Information Technology and Electrical Engineering
Department of Electric Power Engineering

NTNU
Norwegian University of
Science and Technology

Preface

This thesis marks the conclusion of studies in Energy and Environmental Engineering at the Norwegian University of Science and Technology, serving as the final requirement for my masters degree. The masters thesis builds upon the work initiated during my specialisation project from autumn 2022, as documented in citation [34]. Certain sections of the theory presented in section 2 and 3 are reused, as well as aspects of the model explanation in section 4. While the specialisation project utilised a simple model, this thesis aims to develop a sophisticated model that accurately represents the actual behaviour of power systems and the connected wind power plants. The enhanced model employed in the masters thesis captures a more comprehensive depiction of the power system dynamics, surpassing the limitations of the model previously used in the specialisation project.

I would like to express my gratitude to my supervisor, Professor Kjetil Uhlen, for continuous support and guidance throughout the duration of this academic year. His extensive expertise on the topic and valuable feedback has contributed to the success of this research. I would also like to thank PhD student Hallvar Haugdal for granting permission to utilise his dynamic power system simulation program, and for support and clarification regarding the simulation model.

Finally, I would like to express my appreciation to my friends and family. Their presence in in my life is invaluable, being a constant source of motivation and joy throughout my academic journey. I am forever grateful.

Trondheim, 09.06.2023
Jonas Eidsvåg Rostad

Abstract

The demand for renewable energy is experiencing a continuous growth. In future power systems, a substantial portion of energy generation will be derived from renewable energy sources such as wind, hydro and solar energy. Utilisation of renewable energy sources provides a significant environmental advantage, particularly in terms of reducing emission from non-renewable gases. This introduces new challenges regarding power system transmission and stability. Unlike conventional energy sources, Wind and solar energy cannot be easily stored and dispatched at the needed time. Hydro power stands out among renewable energy sources as it allows for storage, because water can be stored in reservoirs. It must be noted that hydro power storage still is subject to geographical and environmental factors. Nonetheless, hydro power offers a more reliable storage mechanism compared to wind and solar energy which lack inherent storage mechanisms. In general, the integration of renewable energy sources in the power system leads to a reduction system inertia levels. This decrease in system inertia creates challenges in terms of maintaining stability during transient events in the power system. Enhanced control measures and strategies must be implemented in the system to allow safe and stable operation of the power system in the presence of increased renewable energy integration.

Wind energy, which is the main focus of this thesis, have the ability to provide a fair amount of synthetic inertia. This is achieved by the implementation of variable speed wind turbines, which is more flexible than their fixed speed counterpart. The variable speed element of the turbines allow for faster and safer control as the turbines are decoupled from the power grid.

In this thesis, the frequency control will be evaluated for a variable speed wind power plant connected to an isolated grid. Initially, a base case is established for the isolated grid to examine the systems behaviour during a load deviation. Subsequently, the wind farm model is incorporated in the same power system configuration to examine the frequency support and impact of synthetic inertia provided by the wind farm.

Additionally, two scenarios involving continuous support from the wind farm over an extended time period is examined. In the first scenario, continuous support from the wind farm is provided until the rotor speed surpasses the controllers limit for safe operation, and the active power contribution to the system is reduced. In the second scenario, frequency restoration reserves are introduced, subsequently replacing the primary control reserve provided by the wind farm. This enables the analysis of the autonomous restoration of the wind farm without external intervention after providing synthetic inertia.

The integration of a variable speed wind farm shows promising results in enhancing the stability of the power system by providing frequency support. The wind farm plays a crucial role in reducing the initial drop in frequency caused by the load deviation. Additionally, it is important to note

that the provision of frequency support from the wind farm is only temporary. During a sudden load increase, a portion of the kinetic energy stored in the system is released. The synthetic inertia regulator of the wind farm detects this and signals the wind farm to contribute power. As the load increase leads to a decrease in rotor speed decreases, the operating point on the $C_P - \lambda$ curve shifts. By initially operating on the right side of the curve, the wind farm is able to provide support for a significantly longer duration, as operating on the right side allows it to delay reaching the rotor speed limits, in contrast to operating on the left side. This positioning of the curve's operating point facilitates the prolonged support of the wind farm during transient events.

The power system used for this simulation study is Kundur's Two Area System, which serves as a simplified representation of small- to medium-sized electric power systems. The system is commonly employed to explore various concepts and phenomena related to power systems. By manipulating the parameters of buses, generators, transformers, lines and governors, different scenarios can be created that yield realistic responses within the power system. The simulations are performed in the DynPSSimPy software, which is an open source software developed in Python used for dynamic power system simulation. The utilisation of DynPSSimPy facilitate accurate representations and analysis of dynamic behaviour of the power system during the simulated scenarios.

Sammendrag

Behovet for fornybare energikilder vokser kontinuerlig. Energiproduksjonen i fremtidens kraftsystemer vil i store deler bestå av fornybare energikilder som vindkraft, vannkraft og solenergi. Selv om bruk av fornybare energikilder er en stor fordel med tanke på miljøaspektet, spesielt med tanke på utslipp av ikke-fornybare gasser, medbringer det også utfordringer for transmisjon og stabilitet i kraftsystemet. I motsetning til konvensjonelle energikilder, kan ikke vindkraft og solenergi lagres og brukes ved senere behov. Her skiller vannkraft seg ut blant de fornybare energikildene, da vann kan lagres i reservoarer som vannmagasin. Det må bemerkes at lagring av vannkraft fortsatt utsettes for geografiske og miljømessige faktorer, slik at ikke heller det kan være hundre prosent sikkert. Likevel er det betraktelig mer pålitelig å lagre vann sammenlignet med vind og sol, der lagring ikke er mulig. Generelt fører integrering av fornybare energikilder i kraftsystemet til en reduksjon i systemets totale svingmasse. Reduksjonen i svingmasse medfører problemer for å opprettholde stabiliteten i systemet dersom en uforutsett situasjon skulle oppstå. Forsterkede reguleringstiltak må iverksettes i systemet for å sikre sikker og stabil drift ved for økt integrering av fornybar energi.

Vindkraft, som er hovedfokuset for denne masteroppgaven, har evnen til å produsere syntetisk svingmasse. Gode nivåer av dette kan oppnås ved implementering av vindturbiner med varierende rotasjonshastighet, da disse er mye mer fleksible enn turbinene med konstant hastighet. Turbinenes evne til å variere rotasjonshastigheten gir raskere og mer sikker regulering ettersom disse også ikke er direkte koblet til kraftnettet.

I denne masteroppgaven vil frekvensreguleringen til et vindkraftverk med variabel hastighet koblet til et isolert kraftnett bli evaluert. Først vil en base case bli etablert for det isolerte kraftnettet for å analysere systemets oppførsel under et lastavvik. Deretter vil vindparkmodellen integreres i den samme kraftsystemkonfigurasjonen for å undersøke hvordan frekvensresponsen endres, og virkningen av syntetisk svingmasse produsert av vindparken.

I tillegg vil to ulike scenarier som involverer kontinuerlig støtte fra vindparken over en lengre periode undersøkes. I det første scenariet vil vindparken gi kontinuerlig støtte til systemet helt til rotasjonshastigheten overstiger grensen for sikker drift. Da vil bidraget fra vindparken reduseres, slik at den kan gjenopprette normal drift. I det andre scenariet vil reserver som gjenoppretter frekvensen introduseres en stund inn i simuleringen, disse reservene erstatter vindparkens støtte. Dette gjør det mulig for vindparken å gjenopprette normal drift uten å måtte få ekstern støtte.

Integreringen av en vindpark med variabel hastighet i kraftsystemet viser lovende resultater ved å tilby frekvensstøtte for å forbedre stabiliteten i systemet. Vindparken spiller en viktig rolle i reduseringen av det initielle frekvensfallet forårsaket av lastavviket. Det er viktig å påpeke at frekvensstøtten vindparken tilbyr bare er midlertidig. Ved en brå økning av lasten vil en del av

den kinetiske energien lagret i systemet frigjøres. Dette fanges opp av regulatoren for syntetisk svingmasse, som signaliserer vindparken til å bidra med mer kraft. Økningen av lasten fører til at vind turbinenes rotasjonshastighet avtar. Dette fører til at arbeidspunktet på $C_P - \lambda$ kurven flyttes. Fordelen ved å initielt operere på høyre side av kurven er at vindparken kan tilby støtte i betydelig lengre tid. Ved å operere på høyre side vil det ta lengre tid før vindparken når arbeidsgrensen for rotasjonshastigheten, i motsetning til å operere på venstre side av kurven. Posisjoneringen av arbeidspunktet på kurven muliggjør derfor forlenget støtte fra vindparken under lastforstyrrelser.

Kraftsystemet som brukes i oppgaven er Kundurs Two Area System. Dette fungerer som en forenklet representasjon av små til mellomstore kraftsystemer. Systemet brukes ofte til å undersøke ulike konsepter og fenomener relatert til kraftsystemanalyse. Ved å manipulere parameterne til samleskinner, generatorer, transformatorer, linjer og regulatorer kan ulike scenarier formes, slik at de gir realistiske resultater. Simuleringene utføres i programvaren DynPSSimPy. Dette er en open-source programvare som er skrevet i Python, og brukes til dynamisk kraftsystemsimulering. Bruken av DynPSSimPy gjør det mulig å gjennomføre nøyaktige analyser av dynamikken i kraftsystemet ved de simulerte lastavvikene.

Table of Contents

List of Figures

List of Tables

Chapter 1

Introduction

1.1 Background and Motivation

The demand for electrical energy in Europe has has slow but relatively stable increase over the last 10 years. However, there has been some deviations the last couple of years. In 2020, the outbreak of the Covid-19 resulted in significant disruptions in across various sectors, including the electricity consumption, Lockdown measures and restrictions led to a reduction in electricity consumption. Additionally, in 2022, Europe experienced a decrease in electricity consumption by 4% compared to the levels of 2021. This decline can be attributed to the mild winter experienced in the region, and the geopolitical situation, particularly the invasion of Ukraine. Despite the fluctuations and challenges in the electricity market, the proportion of renewable energy sources in the overall generation mix has been steadily increasing since 2005 as seen in figure 1.1.1. [14]

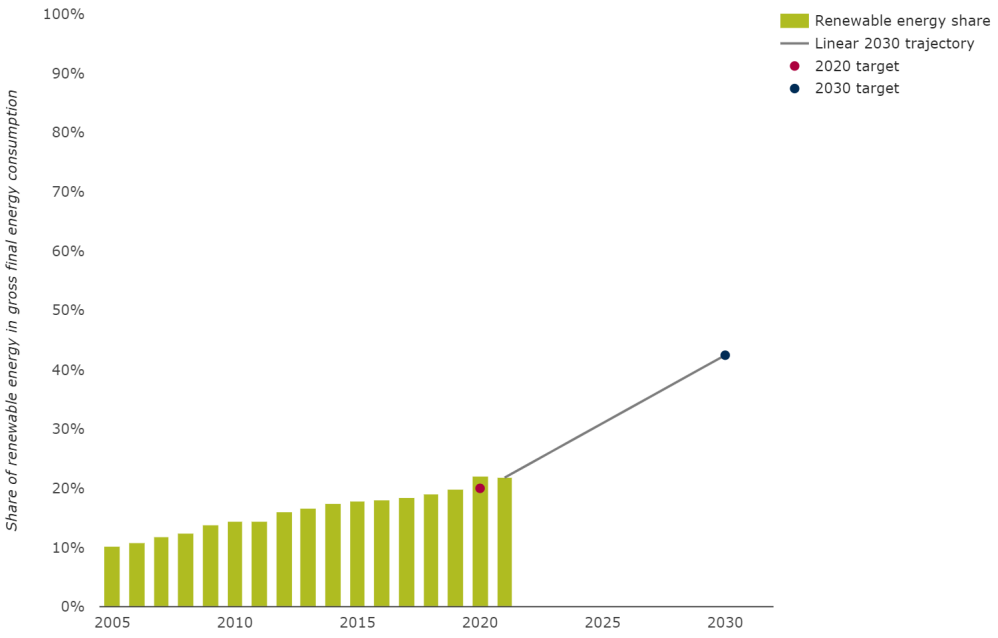

Figure 1.1.1: Share of energy consumption from renewable sources in Europe [18]

Renewable alternatives, such as wind, solar and hydro power have experienced significant technological advancements in the recent decades. The rise of offshore wind technology in particular, has gained considerable popularity in various influential regions, like Europe, China and the USA. [16] The year 2022 experienced a substantial growth in wind power production compared to 2021. This can be attributed to the continuous expansion of the wind energy infrastructure. In the UK, wind power production accounted for a quarter of the total electricity generation. [14]

The increasing demand for electrical power emphasise the importance of ensuring power system stability and reliable supply of power. To address these objectives, increasingly advanced methods are being developed to monitor and control the power system. An emerging approach for such a utility are Digital Twins, which are virtual representations of physical system that replicate the their characteristics, behaviours and performance. By constructing and updating Digital Twins with real-time data, operators and engineers can effectively model and simulate power system configurations and optimise system performance. [5]

An electric power system is characterised by two main parameters of great importance, voltage and frequency. Maintaining these parameters within the specified limits is essential for ensuring the desired operating conditions and reliable energy supply to all connected consumers. Deviations outside of these predefined limits can potentially lead to dangerous operation or even result in system failure in worst case scenario. Effective control of voltage and frequency is therefore a necessity to ensure the stability and functionality of the power system. [41]

1.2 Objective of the Project

The objective of this thesis is to develop a realistic model of a wind power plant, and study the dynamics of both the power system and the connected wind farm. The specific focus of this research is to investigate the power system frequency during a transient event, such as a load deviation, and analyse the contribution of frequency support from the wind farm.

The thesis includes specific objectives that are outlined as follows:

1. Develop a test case that accurately captures the frequency control response of the power system during a transient event. This involves defining the characteristics of the event, and setting up initial conditions of the power system.

2. Model a variable speed wind turbine. This involves capturing the turbine's dynamic behaviour, power characteristics, and control strategies.

3. Perform simulations for the developed test case, using different configurations of the power system. This includes scenarios with and without the wind farm.

4. Study the impact of wind farm control and operation on frequency control. Specifically, the thesis aims to analyse the capability of the wind farm to provide synthetic inertia and primary control to the grid.

1.3 Outline of the Project

This thesis consists of seven chapters in total, each addressing specific aspects of the research. The chapters are organised in a logical sequence to provide a comprehensive analysis.

Chapter 1 is an introduction of the objective of the thesis, as well as the motivation behind the work.

Chapter 2 provides a comprehensive overview of relevant theory on power system frequency and control mechanisms.

Chapter 3 provides a comprehensive overview of relevant theory on general wind energy. It includes subsections on wind turbines, energy production, grid codes and transmission schemes.

Chapter 4 is fundamental for the thesis as it explains the models developed and implemented in dynamic power system simulation, with relevant equations and figures.

Chapter 5 presents the results of the dynamic power system simulation.

Chapter 6 discuss main objective of the thesis, comparing the simulated results to the theory presented in chapter 2 and 3.

Chapter 7 is the conclusion on the thesis, providing some final words, in addition to visions for future work.

Each chapter is designed to contribute to the overall research objectives and understanding of the topic.

1.4 Reuse of Project Work from Autumn 2022

This thesis builds upon the work conducted during the specialisation project in autumn 2022. Some sections from the specialisation project have been reused or reworked, while others have been removed completely. Additionally, numerous new sections have been added to provide a more comprehensive and detailed analysis of the objective.

Section 2.2, 3.1, 3.5, 3.6, 3.7, 4.5 - 4.10, and 5.2 are reused or partially reworked, while section 2.1, 2.3, 3.4, 4.1 and 5.1 are reworked. all referring to the specialisation project *Power System Response to a Variable Speed Wind Power Plant* of Autumn 2022. [34]

Chapter 2

Frequency Control and System Inertia

2.1 Power System Frequency

Power systems are constructed to enable electricity and power generation in locations deemed suitable, ensuring generation in sufficient quantities to satisfy the consumers demand. The electrical energy delivered must have a high degree of reliability and quality. Additionally, the cost of electricity must be within a competitive price range while also striving for sustainability by incorporating environmentally friendly practices.

The power system frequency serves as an indication of the balance between generation and demand. The European power grid has a standard frequency of 50 Hz, while regions like North-America have a standard grid frequency of 60 Hz. [41] Preserving a constant frequency in the grid is essential for safe operation of the power system. In order to achieve this, the energy generated must match to the energy demand on a continuous basis. In the occurrence of a fault in the system, the synchronous generators must also be promptly synchronised after the clearance of said fault. The system ability to respond to such faults depends on the inertia in the system. [41]

Inertia refers to an objects resistance to any alteration in its velocity. A power system consists of multiple large and fast spinning generators. For a power system, inertia refers to the energy that is stored within these large rotating generators. This stored energy can temporarily compensate for lost power in the event of a substantial power plant failure. System inertia is therefore assumes a crucial role for maintaining power system stability. Failing to compensate when generation and/or load is lost results in frequency deviations in the power system. The different scenarios for frequency deviations are listed in table 2.1.1. [3]

Scenario	**Frequency**
Generation = demand	No change
Generation > demand	Increase
Generation < demand	Decrease

Table 2.1.1: Frequency deviation for changes in generation and demand of power

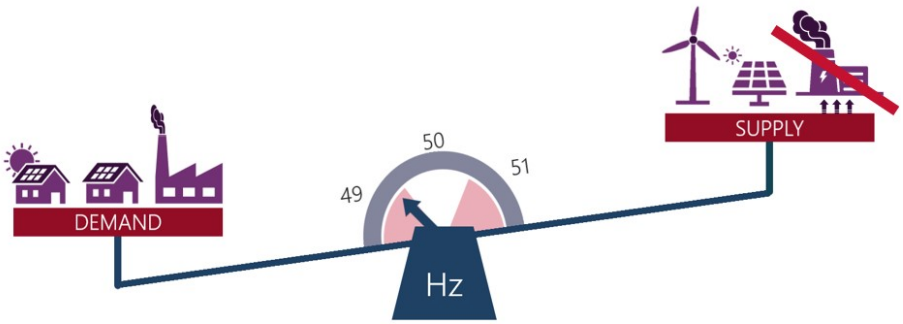

Figure 2.1.1: Frequency balance in the power system [2]

Another operational requirement for power systems is maintaining constant voltage at every bus. This maintains power system stability and ensures delivery of electricity with a consistent power quality. To achieve this requirement, generation and absorption of reactive power must be balanced to keep the voltage levels at each node in constant. Voltage level deviations are listed in table 2.1.2. [3]

Scenario	**Voltage Level**
$Q_{generated} = Q_{demand}$	No change
$Q_{generated} > Q_{demand}$	Too high
$Q_{generated} < Q_{demand}$	Too low

Table 2.1.2: Voltage level deviation for changes in generation and demand of reactive power

In the power system, ensuring reliability and quality of energy supply entails two main objectives. The first objective involves maintaining stability during both normal operation and unforeseen events. This encompasses ensuring that the power system remains in a stable state and operates within acceptable limits, even in the presence of a disturbance. The second objective involves the ability to withstand faults and disturbances, and subsequently recovering to a new steady state as fast as possible. This rapid restoration process is critical for ensuring safe supply of energy and minimising possible downtime. [3]

2.2 The Swing Equation

The power system consists multiple interconnected synchronous machines. The kinetic energy of the rotor dynamics of a synchronous machine is given by equation 2.2.1.

$$E_k = \frac{1}{2} J \omega_r^2 \tag{2.2.1}$$

The motion of these synchronous machines follows Newton's law of rotation, where product of the moment of inertia and angular acceleration must equal the net acceleration torque. Equation 2.2.2 shows the relationship.

$$J\dot{\omega}_m + D\omega_m = T_m - T_e \tag{2.2.2}$$

Where J is the moment of inertia in the rotating mass in $[kg \cdot m^2]$, $\dot{\omega}_m$ is the angular rotor acceleration in $[rad/s^2]$, D is the damping coefficient in $[Nm \cdot s]$, T_m is the mechanical torque and T_e is the electrical torque, both given in $[Nm]$.

The relation between the rotor speed and the mechanical angle is given by equation 2.2.3.

$$\omega_m = \frac{d\theta_n}{dt} \tag{2.2.3}$$

The measurement of the angular position in the rotating reference frame of the synchronous generator is given by equation 2.2.4.

$$\theta_m = \omega_m + \delta_m \tag{2.2.4}$$

where δ_m is the rotor angle in the synchronous generator with respect to the synchronous speed $\omega_{m,sync}$. The rotor angle is given in $[rad]$.

Substituting equation 2.2.4 into equation 2.2.2, gives the resulting equation 2.2.5.

$$J\frac{d^2\delta_m}{dt^2} + D\frac{\delta_m}{dt} = T_m - T_e \tag{2.2.5}$$

By multiplying each side of the equation with the synchronous speed of the rotor ω_s, and assuming steady-state ($\omega_m \approx \omega_s$), equation 2.2.6 is formed.

$$J\omega_s\frac{d^2\delta_m}{dt^2} + D\omega_s\frac{\delta_m}{dt} = P_m - P_e \tag{2.2.6}$$

Where the power is given as $P = T\omega_m$ for both mechanical and electrical torque.

The inertia constant of a synchronous generator is defined as ratio of the kinetic energy stored at synchronous speed to the apparent power of the generator. This is expressed by equation 2.2.7.

$$H = \frac{\frac{1}{2}J\omega_s^2}{S_{rated}} \tag{2.2.7}$$

To further simplify the equation, the damping power can be expressed as in equation 2.2.8.

$$P_D = D\frac{d\delta_m}{dt} \tag{2.2.8}$$

Substituting equation 2.2.7 and 2.2.8 into equation 2.2.5, gives the final equation 2.2.9.

$$\frac{2HS_{rated}}{\omega_s}\frac{d^2\delta_m}{dt^2} = P_m - P_e - P_D \tag{2.2.9}$$

The per unit swing equation 2.2.10 is achieved by dividing equation 2.2.9 by S_{rated}. [12]

$$\frac{2H}{\omega_s}\frac{d^2\delta}{dt^2} = p_{mp.u.} - p_{ep.u.} = p_{ap.u.} \tag{2.2.10}$$

2.3 Frequency Control

The power system frequency decreases whenever demand exceeds generation, while an increase in system frequency occurs whenever generation exceeds demand. Any abrupt loss of either supply or demand results in a deviation from the nominal system frequency. The rate of change of frequency, caused by the deviation, depends on the inertia of the power system. The system inertia is related to the synchronously rotating mass in the system as illustrated by the swing equation 2.2.9. [36]

During normal operation of the power system, the accepted frequency range is $F_n \pm 0.1$ Hz. In a 50 Hz network, if the frequency ranges from 47.5 to 51.5, the system operates under emergency condition or restoration conditions. When the power system frequency enters the emergency condition range, a control strategy is initiated to restore the system. [41]

Frequency control is commonly divided in to three levels, namely primary control (governor action), secondary control, and tertiary control. These three levels represent the sequential actions taken following a sudden loss of a generator, which causes a decrease in frequency. Figure 2.3.1 provides a graphical representation of these three levels during such an event.

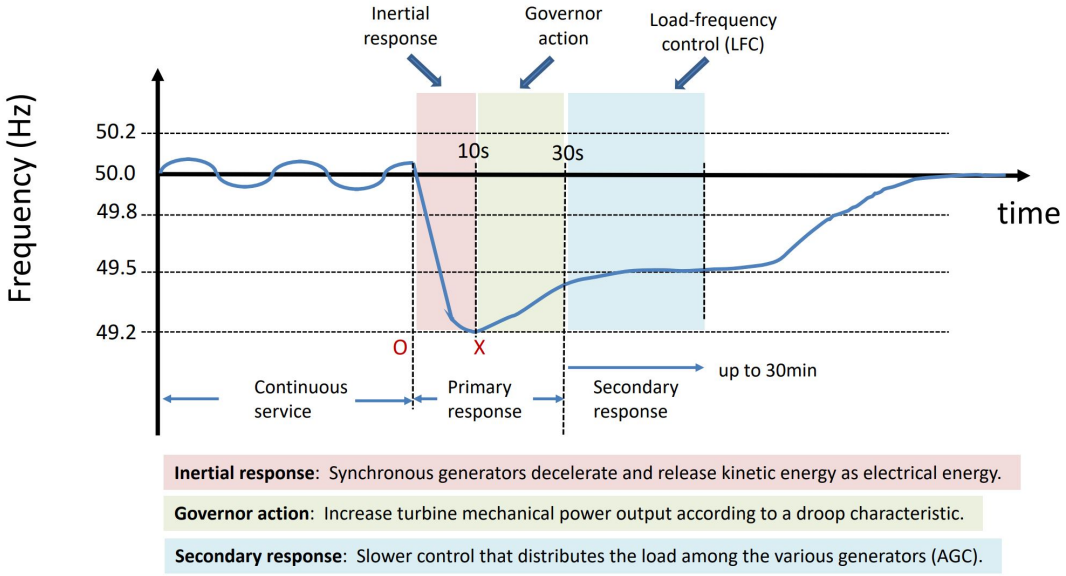

Figure 2.3.1: The control response to frequency deviations during loss of generation [4]

2.3.1 Primary Control

Primary control, also referred to as frequency response control, is an automatic response to frequency deviations. Among the three control levels, primary control has the fastest response time. The response time is almost immediate, and only lasts for a few seconds. The purpose of primary control is to clear the imbalance between generation and load. Primary control is a compulsory service for all generators in the system. [41]

In the occurrence of a frequency deviation due to an load increase, generated power is not immediately produced. To compensate for the load increase, the kinetic energy stored in the rotating generators is utilised. As a result, the generator's velocity is reduced. This mechanism is known as the inertial response, where inertia from the generators contributes to stabilising the frequency.

Following the inertial response, the governor action is activated. The speed controller, known as the governor, of each generator increases power generation as a response to the decreasing speed. This action aims to restore the balance in the system. In general, the generation units are expected to generate the additional power required to balance the system within 30 seconds, and maintain this power output for a duration of 15 minutes. All rotating generation units are obliged to supply this service. The exception are generation units with renewable energy sources such as solar and wind. As the integration of renewable energy sources gradually increase in the power systems, each generation unit must have a dedicated reserve power to fulfil the regulation requirements when needed. [41]

The governor utilises a droop-characteristic to determine the change in turbine mechanical power output in response to the change in rotational speed. This is illustrated by the block diagram shown in figure 2.3.2, where feedback loop incorporates the system droop. [3]

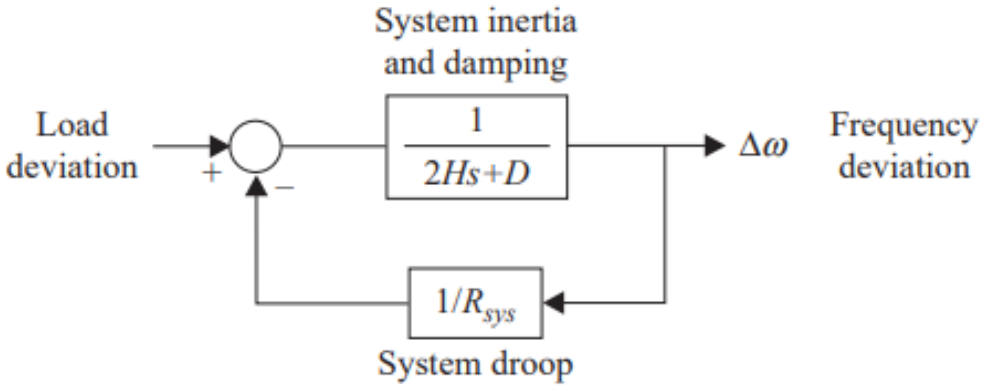

Figure 2.3.2: Block diagram of the system frequency response control [17]

Where R_{sys} in the system droop-block represents the relationship between the deviation in frequency and power, given by equation 2.3.1. Additionally, this is visualised in figure 2.3.3.

$$-R_{sys} = \frac{\Delta f}{\Delta P_m} \tag{2.3.1}$$

The change in mechanical power output due to a frequency deviation for a single generating unit is given by equation 2.3.2.

$$\Delta P_m = \Delta P_{ref} - \frac{1}{R}\Delta f \tag{2.3.2}$$

The turbine-governors response to a frequency deviation in an interconnected power system is given by equation 2.3.3.

$$\Delta P_m = \Delta P_{ref} - \beta \Delta f \tag{2.3.3}$$

Where β is the system frequency bias, which is the sum of the regulation constants given by equation 2.3.4. The units for the system frequency bias β is MW/Hz.

$$\beta = \frac{1}{R_{sys}} = (\frac{1}{R_1} + \frac{1}{R_2} + ...) \tag{2.3.4}$$

The speed droop of of a system refers to the change of speed required to make the prime mover control mechanism transition from fully closed to fully open. The control valve is opened a specified amount depending on the disturbance observed by the governor. Thus, the magnitude of the governor response is regulated by the speed droop characteristic. Figure 2.3.3 visualises the speed droop characteristic. [3]

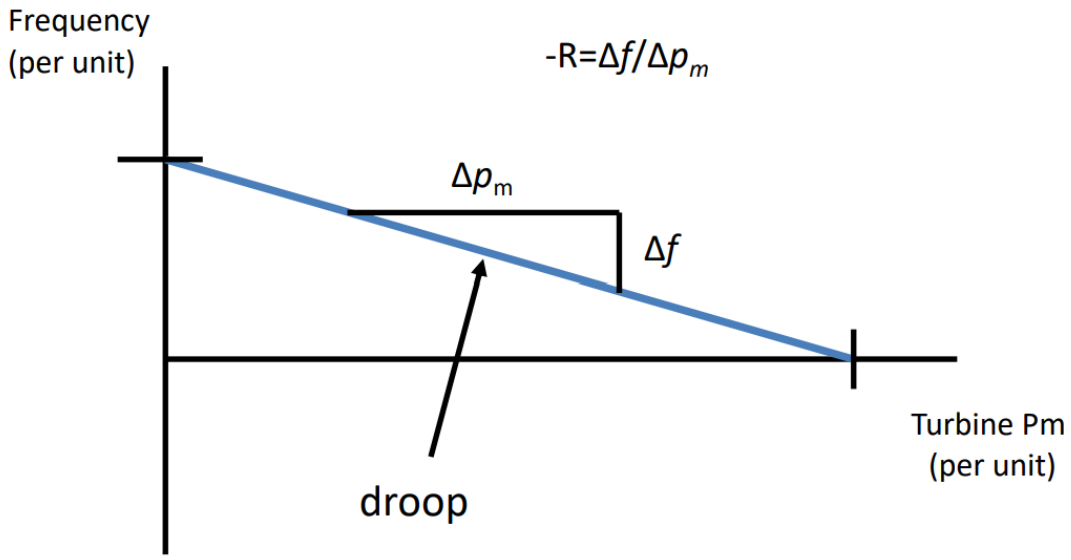

Figure 2.3.3: The speed-droop characteristic in the control system [3]

2.3.2 Secondary Control

Upon completion of the primary control actions, the system frequency will be stabilised but may deviate from the nominal value. Additionally, the power reserves of the generators will be partially or completely depleted. The power exchange between interconnected power system may also differ from the predefined value. In order to fully restore the power system to desired operating conditions, secondary control is introduced. [41]

The implementation of secondary control involve specific generators dedicated to performing the secondary control action. These generators have a dedicated power reserve based on the requirement set by the Transmission System Operator. Typically, the reserve power percentage of the system's maximum power, with a minimum threshold to guarantee independence from each generators maximum power. When the frequency deviated below nominal value, additional generation capacity must be added or load must be reduced to restore the frequency. Conversely, if the frequency exceeds the nominal value, generation capacity must be reduced or load must be increased to bring the frequency back to the desired level. Similar to primary control, secondary control is generally implemented as an automatic process. [41]

Load frequency control (LFC) plays a crucial role in maintaining a stable frequency throughout the power system, improving transient performance and minimising area control error. [23] The objectives of LFC and economic dispatch are achieved by adjusting the power settings reference

of the turbine-governor through the use of Automatic Generation Control (AGC). AGC facilitates the coordination of both of these objectives to ensure optimal operation of the power system. Through AGC, the system operators can regulate the power output of generators in real time by receiving signals from the communication link based on frequency and power deviations. Figure 2.3.4 illustrates the concept of AGC.

The Automatic Generation Control System is responsible for ensuring the smooth and efficient operation of the power system. The primary purpose of the AGC regulate and maintain power system frequency within specified limits and to ensure accurate control of the interchange power level. [42]

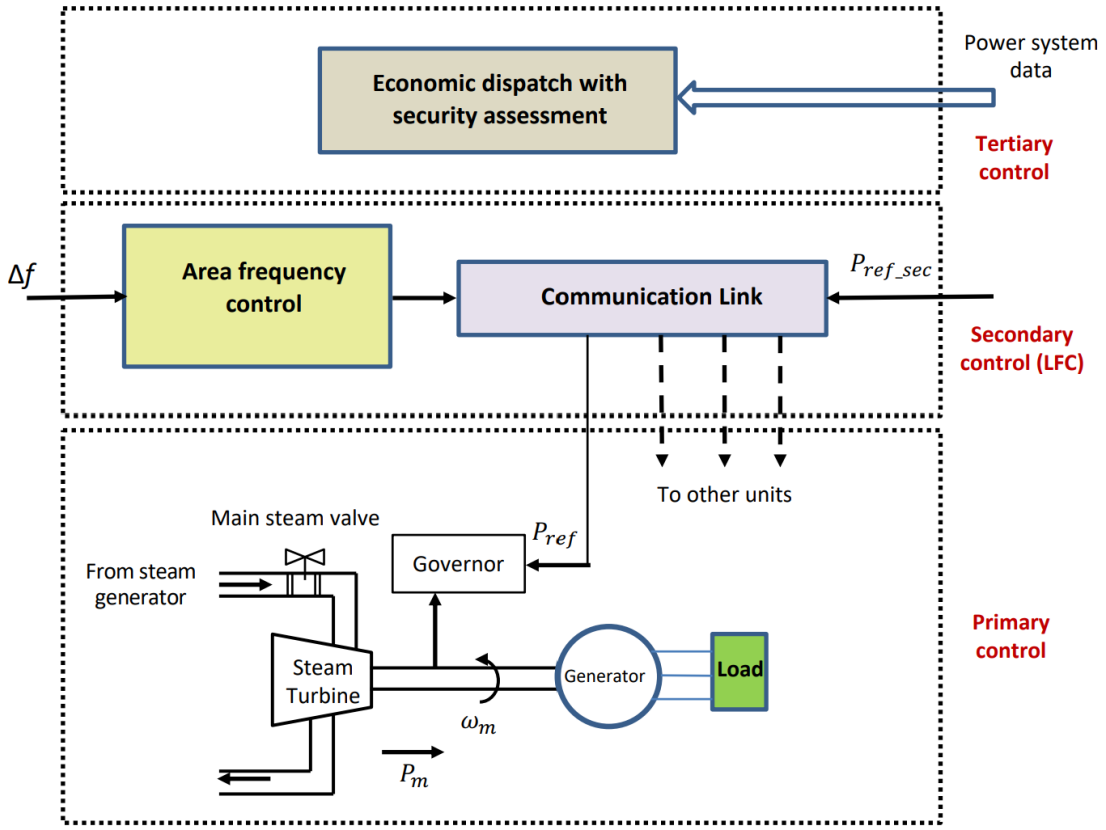

Figure 2.3.4: Automatic Generation Control [3]

2.3.3 Tertiary Control

Tertiary control represents the final stage of frequency control and is initiated upon the request of from the grid operator. Upon completion of all secondary control actions, the reserve of the generators specific to secondary control needs to be restored. This serves as the main purpose of tertiary control. The process of restoring the reserves of the generation units involves providing operating instructions to producers. These instructions specify power adjustments for generators already in operation, and potential activation of start-up generators to meet the demand requirements. Unlike primary and secondary control, tertiary control is not an automatic process, but a process executed through the collaborative efforts between the grid operator and producers. [41]

2.4 Fast Frequency Reserves

Inertia serves as the first line of defence to large disturbances in the power system. Systems with higher inertia slows the rate at which frequency changes due to the system disturbance, allowing for more time to react and mitigate the impact of the disturbance. Inertia is provided by generators with large spinning rotors. Typically, these generators are hydro, coal, or gas powered. However, with an increasing prominence of renewable energy sources, these generators are gradually forming a smaller part of the overall energy system. Wind and solar energy are inverter-based technology which lack inherent inertia. Alternative methods like fast frequency reserves are employed to ensure stable operation of power systems with lower inertia. [2]

Fast frequency reserves are critical for quickly addressing frequency drops caused by faults in the power system. These reserves are characterised by their fast response time, enabling swift compensation for frequency deviations. In line with this, Statnett initiated a test project in 2020 and 2021 to procure fast frequency reserves. Subsequently, in 2022 a commercial market dedicated to acquisition of fast frequency reserves was established. [39]

Fast frequency reserves typically activates within approximately 1 second, when the system frequency drops below a predetermined limit. The possible frequency range for activation is 49.5 Hz to 49.7 Hz. Opting for a lower activation frequency necessitates a faster response in order achieve the desired outcome. Based on tests conducted by Statnett, the frequency range is set low enough that an occurrence is infrequent, not happening on an annual basis. As a result, activation of the fast frequency response is considered a rare event. [39]

Chapter 3

Wind Energy and Transmission Schemes

3.1 Wind Resource

Wind data is typically collected by use of meteorological masts and instruments, such as anemometers and wind vanes. Cup anemometers are a commonly used for measuring wind speed. These consists of three or four symmetrically arranged cups in a vertical spindle. Modern day instruments are designed in such a way that the rate of rotation in the cups is directly proportional to the wind speed, with a high degree of accuracy within a small error margin. [25]

The wind direction is measured using a wind vane. The vane consists of a thin horizontal arm which carries a vertical flat plate at one end and a weighted pointer at the other end, resembling an arrow. The horizontal arm is attached to a vertical spindle mounted on bearings, enabling the free movement of the vane in response to the wind. Both the anemometer and the vane are typically installed at the top of the mast to ensure unobstructed wind flow and minimise interference from land formations or vegetation, resulting in the most accurate and reliable measurements. [25]

3.1.1 Wind Speed

Wind speed is a critical factor when locating a wind farm site. Wind speed refers to the magnitude of the wind's velocity and is considered the most important factor due to the direct influence on mechanical power generation at the wind farm site. To gain a comprehensive understand of wind speed, it is best represented as a distribution rather than a collection of discrete values. The Weibull distribution is most commonly employed to represent the distribution of wind speeds. The wind is measured and organised into wind speed bins. Subsequently, the collected wind data is sorted and used to create histogram. This is visualised by the the example in figure 3.1.1. [11]

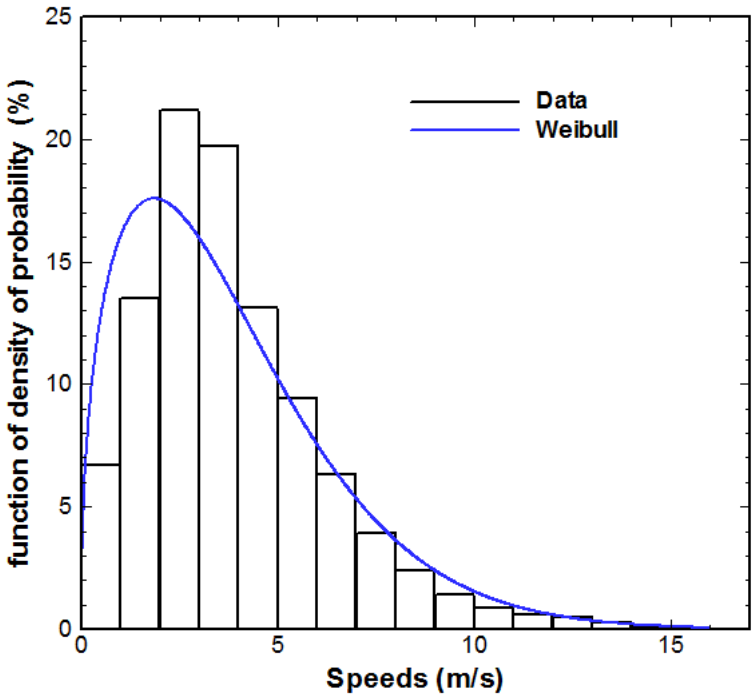

Figure 3.1.1: Histogram of wind speed frequencies modelled by a Weibull distribution [1]

For the majority wind farm sites, the frequency distribution of wind speeds can be accurately represented by the two parameter Weibull distribution. This distribution provides a density function that allows for random sampling of wind speeds. The density function randomly sampled for a wind speed with value U is given by the equation 3.1.1.

$$p(U) = (\frac{k}{C})(\frac{U}{C})^{(k-1)} e^{-(\frac{U}{C})^k} \tag{3.1.1}$$

This frequency distribution also has a corresponding cumulative density function, which provides the probability that a wind speed is less than or equal to a given value. The cumulative density function is expressed by equation 3.1.2.

$$Q(U < V) = 1 - e^{-(\frac{V}{C})^k} \tag{3.1.2}$$

The two parameters in the distribution, namely the scale parameter C and the shape parameter k, can be estimated based on the average wind speed and standard deviation observed at the specific location. The scale parameter C is given by equation 3.1.3, while the shape parameter k is given by 3.1.4. [22]

$$C \approx 2\frac{\overline{U}}{\sqrt{\pi}} \tag{3.1.3}$$

$$k \approx (\frac{\sigma}{\overline{U}})^{-1.086} \tag{3.1.4}$$

3.1.2 Wind Direction

Wind direction can vary significantly over a defined time period. A common method for visualising the wind direction is through the use of a wind rose. A wind rose represents a frequency graph in polar coordinates, where the angle of the widgets indicate the wind direction and the magnitude represents the frequency of occurrence for that wind direction. [11]

An example of a wind rose is shown below in figure 3.1.2, which depicts the average wind rose in Trondheim in 2021.

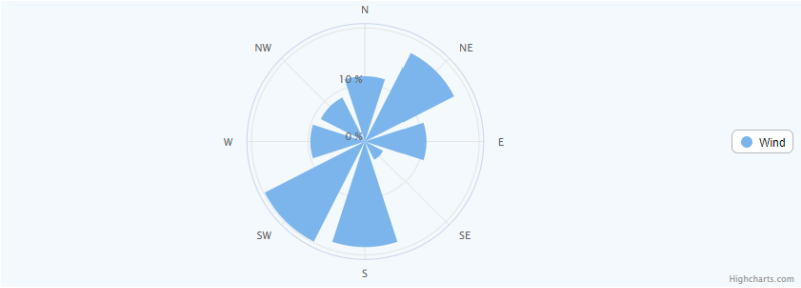

Wind direction graph in Trondheim using average values according to our data.

N ▼ Northern	NE ▲ Northeastern	E ◄ Eeastern	SE ➤ Southeastern	S ▲ Southern	SW ◄ Southwestern	W ➤ Western	NW ▲ Northwestern
11.5%	17.5%	10.7%	3.6%	18.6%	19.8%	9.6%	8.7%

Figure 3.1.2: The average wind rose for Trondheim in 2021 [45]

As previously mentioned, when selecting wind farm sites, the wind speed is considered more important than the wind direction. However, understanding the wind direction is crucial for optimising the layout of the wind farm, particularly to minimise the wake effect. Minimising the wake effect is essential for optimising the power production of the wind farm. [20]

3.2 Variable Speed Wind Turbine

Variable speed wind turbines, as their name suggests, have the ability to adjust and control the rotational speed of the turbine to operate at the optimal level. This control flexibility is achieved through the use of generator types such as Doubly Fed Induction Generators (DIFGs) and Fully Rated Converters (FRCs). Variable speed wind turbines offers several advantages compared to the fixed speed counterpart, including greater control flexibility, improved system efficiency and enhanced power quality. This makes variable speed wind turbines the preferred choice in modern wind power plants. [22]

Wind turbines with doubly fed induction generators employ a wound rotor induction generator with slip rings to control the flow current into or out of the rotor. Variable speed operation is achieved by injecting a controllable voltage into the rotor at slip frequency. The rotor windings are fed through a power converter with variable frequency. This power converter decouples the rotor's mechanical frequency from the power system frequency, which enables variable speed operation. To safeguard the generator and converters, voltage limits are set using crowbar protection. [22] Figure 3.2.1 provides a line diagram illustrating the configuration of a DFIG.

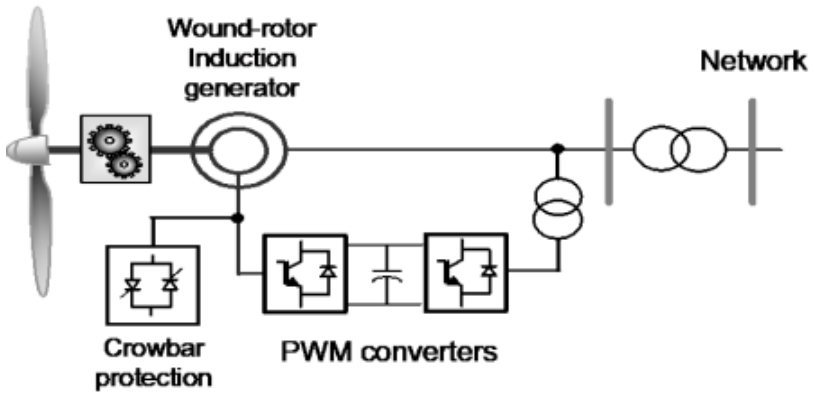

Figure 3.2.1: Line diagram of a DFIG [22]

Both DFIGs and FRCs have direct electrical links to the power grid. The key difference lies in the electrical link and power electronic interfaces. In the DFIG, the direct electrical link to the grid is established through the stator coils with no power electronic interface. Only the rotor circuit in the DFIG incorporated power electronic components. This link is the reason that the slip in a DFIG only can vary by about 30% since the rotating magnetic field of the stator needs to be considered. On the other hand, an FRC routes all the electrical power of the machine through the power electronic interface, which completely severs the generator side from the grid side. The complete separation of the generator and grid side gives independent control of the frequency and speed on the generator side. [22] Figure 3.2.2 provides a line diagram illustrating the configuration an FRC.

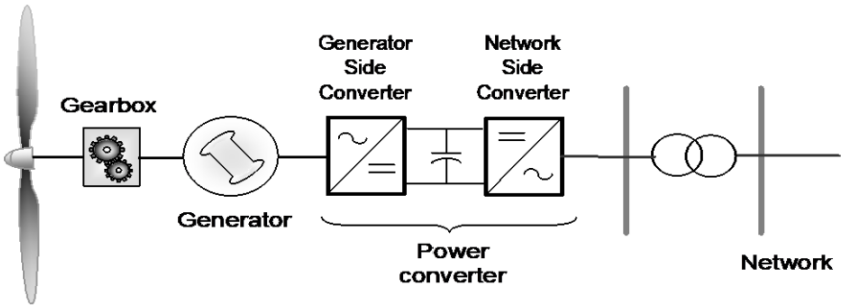

Figure 3.2.2: Line diagram of an FRC [22]

3.3 Synthetic Inertia

The vision for the future of energy production is purely renewable. This entails the closure of a significant number of power plants fuelled by fossil-fuel, while integrating renewable energy sources into the power grid. Unlike the power plants based on fossil-fuel, which have the advantage of being able to store the natural energy from the rotating mass of the synchronous generator[7] and provide a large amount of inertia to the grid, Renewable energy sources such as wind turbines inherently have low inertia due to the lack of reliable energy storage mechanisms. A lower system inertia results in more significant and faster frequency deviations in the occurrence of a disturbance in generation or load. [26]

Variable speed wind turbines have the capacity to provide more inertia to the grid compared to their fixed speed counterpart. The inertia of the variable speed wind turbine is still inherently low however. This is primarily due to the decoupling of the wind turbines and the power grid through power electronic converters, as depicted in figure 3.2.1. To address this limitation, an additional control loop can be implemented in the power electronic converters, enabling a direct connection of the turbine's inertia to the grid. [26] Control systems even facilitate the implementation synthetic inertia, where additional power can be injected into the grid during a frequency drop. The synthetic inertia can even surpass the contribution of real inertia. This additional power is provided by the stored kinetic energy in the rotating mass of the turbine. [26]

3.4 Energy and Power Production

Wind energy is captured by making the turbine rotate. The mechanical power generated from the movement of air through the turbine blades is given by equation 3.4.1. [34]

$$P_m = \frac{1}{2}\rho A U^3 C_p \tag{3.4.1}$$

ρ is the air density.
A is the swept area of the turbine.
U is the wind speed.
C_P is the power coefficient.

The equation and the corresponding parameters are depicted in figure 3.4.1

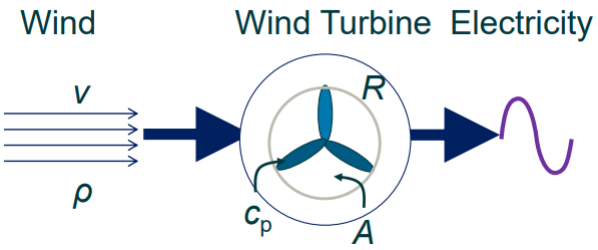

Figure 3.4.1: Visualisation of the relationship between wind and electricity generation [22]

The power curve of a wind turbine shows relationship between the power output P, and the wind speed U. An example of a power curve can be seen in figure 3.4.2.

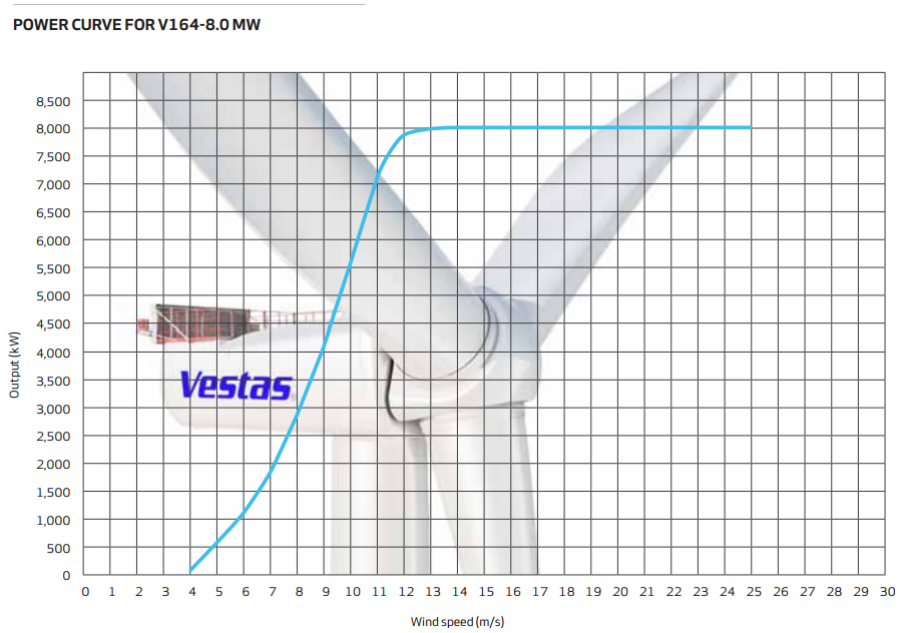

Figure 3.4.2: The power curve for Vestas V164 - 8.0MW

The power curve for the Vestas V164 turbine has a cut-in wind speed of 4 m/s and a cut-out wind speed of 25 m/s. The wind turbine will not operate for a wind speed lower than 4 m/s due to the excessively low force the wind applying to the turbine, making it unable to rotate. For a wind speed higher than 25 m/s, operation of the turbine can be dangerous due to the high force the wind applies. The operation of the turbine is therefore halted due to safety constrains. The optimal range of wind speeds for the V164 turbine is between 13 m/s and 25 m/s. In this region rated power production is achieved, which is 8 MW for this specific turbine. [34]

The capacity factor of a wind turbine is not to be confused with the power coefficient. The capacity factor is the average power output of the wind farm divided by its maximum power capability. Theoretically, this can be 100%, but in reality it varies greatly based on the wind farm location. Offshore wind farms typically have a capacity factor of greater value because the wind speeds have a generally higher magnitude and is less turbulent than onshore. The average capacity factor was 17% for onshore wind, and 23.1% for offshore wind in Europe in 2022. The highest values in Europe in 2022 were Denmark for onshore, with capacity factor of 31.1%, and Germany for offshore wind, with a capacity factor of 53.9%. [44]

Web pages such as https://www.renewables.ninja/ make rough calculations of the power coefficient in a specific region, which depict the difference. In figure 3.4.3 and 3.4.4, an onshore and offshore capacity factor for a 400MW wind farm is depicted respectively. The onshore wind farm, approximately located at Storheia in Norway, has a capacity factor of 27.7%. The offshore wind farm, located at Dogger Bank in the North Sea, has a capacity factor of 59.1%. The wind statistics are collected from the year 2019. [34]

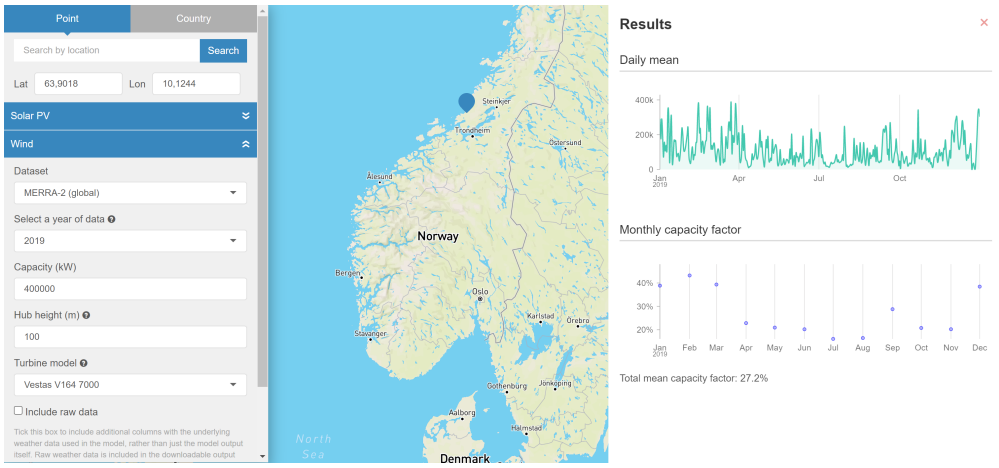

Figure 3.4.3: Capacity factor at Storheia for a 400MW wind farm

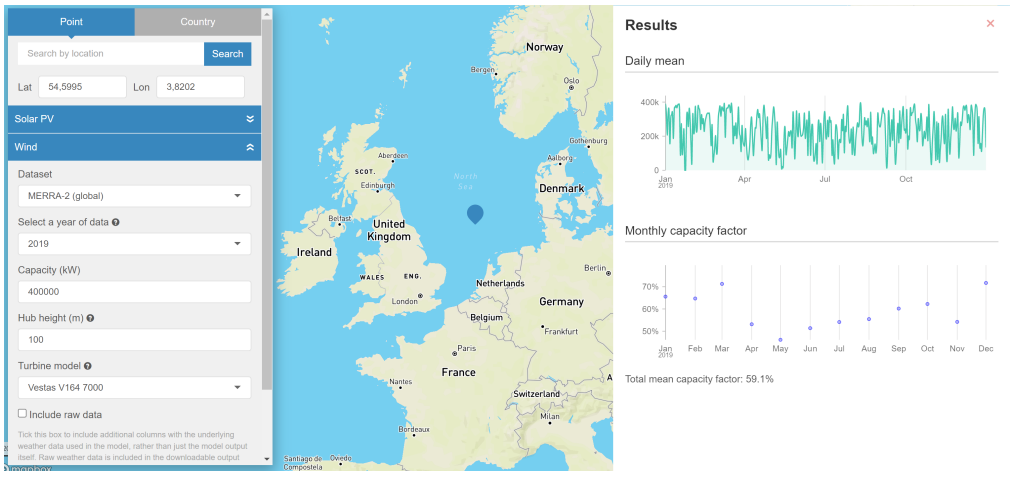

Figure 3.4.4: Capacity factor at Dogger Bank for a 400MW wind farm

The power coefficient C_p is a measure of how efficiently a wind turbine converts wind energy to electrical energy. This relation is simply the electrical power output of the wind turbine divided by the wind energy input. The theoretical limit of C_P is called Betz limit, and its value is presented in equation 3.4.2. [6]

$$C_{pBetz} = \frac{16}{27} = 0.593 \tag{3.4.2}$$

Wind turbines are unable to have a higher power extraction than this value due to losses in the generator and drive train. The energy contained in blade tip vortices and turbulence caused by turbine wakes are also factors which unaccounted for in Betz analysis. Consequently, Betz limit acts as an upper limit for power extraction from wind. [34]

The power coefficient is often visualised in relation to the tip speed ratio of the wind turbine as this describes the rotor performance. Equation 4.1.3 defines the tip speed ratio.

$$\lambda = \frac{\omega R}{U_{wind}} \tag{3.4.3}$$

These curves are referred to as $C_p - \lambda$ curves. The curve is a graphical representation of the wind turbine's rotor performance for various operating conditions. The curve illustrates the power coefficient during both during optimal and sub-optimal operation, in addition to the corresponding tip speed ratio. For a specific tip speed ratio, the power coefficient reaches its maximum value on the curve. This is the optimal operational value for both the power coefficient and tip speed ratio. The specific values for λ_{opt} and $C_{P,opt}$ vary depending on the turbine design. Figure 3.4.5 provides an example of a typical $C_p - \lambda$ curve. [34]

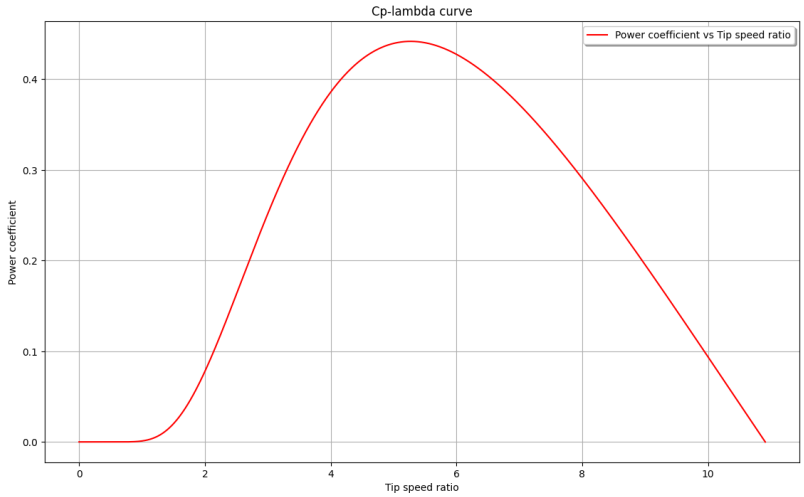

Figure 3.4.5: $C_p - \lambda$ curve for a wind turbine [22]

Extracting energy from wind changes its attributes. As the wind flows through the swept area of a turbine, the turbine exerts a force on the wind and the wind exerts a force on the turbine. Since the turbine is extracting energy from the wind, the wind's velocity is reduced. No mass or volume is consumed during the flow through the turbines swept area, as the principles of conservation apply. Due to the conservation of mass and volume, the wind-stream must expand as a consequence of the reduction in velocity. A portion of the wind-stream will also pass directly through the swept area without interfering with the blades, while some wind also diverts around the area as shown in figure 3.4.6. [34]

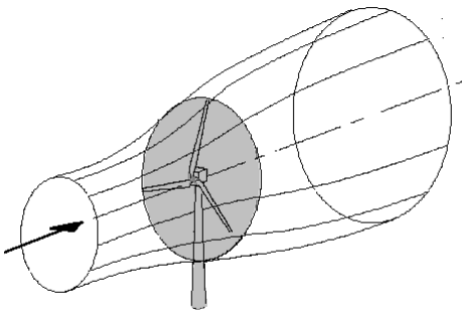

Figure 3.4.6: The expansion of the wind-stream because of extracted power [22]

3.5 Turbine Wakes

Turbine wakes emerge as a consequence of the expansion and deceleration of wind in the wake region of the turbine after energy extraction. Upstream of the turbine, the wind contains more energy compared to the downstream region. Additionally, the downstream airflow does not only experience a reduction in velocity, but also an increase in turbulence. This trail of downstream wind, characterised by turbulence, is known as the turbines wake. As the airflow continues beyond the turbine, the wind speed increases and the turbulence gradually diminishes until it eventually return to its original state. [20]

Figure 3.5.1: Visualisation of the turbine wake effect [43]

When planning the layout of offshore wind farms, careful examination of the wind direction is required. The wake causes a reduction in the energy contained in the wind. It is therefore essential to avoid aligning wind turbines directly behind each other, parallel to the wind direction, as this causes a reduced power production in subsequent wind turbines. Analysis of multiple wind roses spanning a longer period is necessary to identify the most frequent wind direction. It must be noted that the wind direction is erratic, and can change somewhat based on months or seasons. The spacing between turbines must also be optimised using the sites wind data, in case the wind deviates from the optimal flow direction. [34]

3.6 Grid Code Requirements for a Wind Power Plant

Grid codes are technical specifications that defines the criteria and standards for grid-connected facilities to ensure stability, efficiency and safety in the power system. The codes are formulated to facilitate maintenance, operation and development of efficient power systems. Additionally, the codes should encourage competition in the electricity market, as well as encourage general security for both generation and transmission of electrical energy. The facilities subject to grid codes include generation plants, energy consumers, or interconnected networks. In the context of wind farm models they are classified as generation facilities. Although specific grid code requirements for wind power integration may vary across different power systems, there are certain general requirements which are applicable for all wind power integration. [38]

Wind power plants are subject to certain operating conditions and requirements to ensure stable and safe operation of the power system. Grid frequency and voltage operating range are two critical parameters for maintaining stability in the power system. Wind power plants are expected to operate continuously during normal grid operation. Additionally, they must maintain connection to the grid for a specified duration in the event of a frequency deviation. One advantage of wind farms are the ability to remain connected to the grid over a wide range of frequencies, enabling them to provide support the power system during abnormal operating conditions. The operating conditions for wind power plants connected to the Nordic power gird are listed in figure 3.6.1. [38]

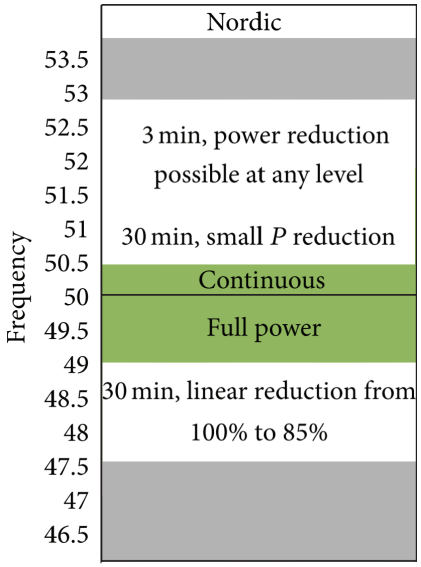

Figure 3.6.1: Required operating frequency range for the Nordic power grid [38]

Active and reactive power control is essential for a power system. For a wind farm, active power control involves the regulation of active power output to ensure the stability of power system frequency and to prevent overloading of transmission lines. Active power control is particularly important during faults, as it helps maintain transient stability. Over-speeding of the turbines can also be prevented by effective control of the active power after the occurrence of a fault. [38]

Reactive power control is important for maintaining stable and constant voltage levels in the power system. Maintaining voltage levels at a constant value is essential for ensuring the proper functioning and reliability of both utility equipment and consumers equipment, since these are

designed to operate at specific voltage levels. To regulate the voltage levels at the point of common coupling, the wind power plants must have the capability to both generate and absorb reactive power. The ability to actively manage reactive power contributes to maintaining reliability and safety in the power system. [38]

The integration of low voltage ride through (LVRT) requirements in grid codes has gained significant importance considering the growing integration of wind energy in the power system. LVRT specifically describes a generators capability to stay connected to the grid during short periods of low voltage. This requirement is critical for ensuring the stable and reliable operation of the power system, particularly in regions where wind energy contributes for a significant portion of the total generation. The occurrence of faults in the power system can result in wide-ranging voltage drops, leading to the disconnection of multiple generators. To address this challenge, recent grid codes require wind power plants to maintain grid connection in order to support both during and after a the occurrence of a fault. Consequently, the wind farms must be able to withstand severe drops in the voltage level. [38]

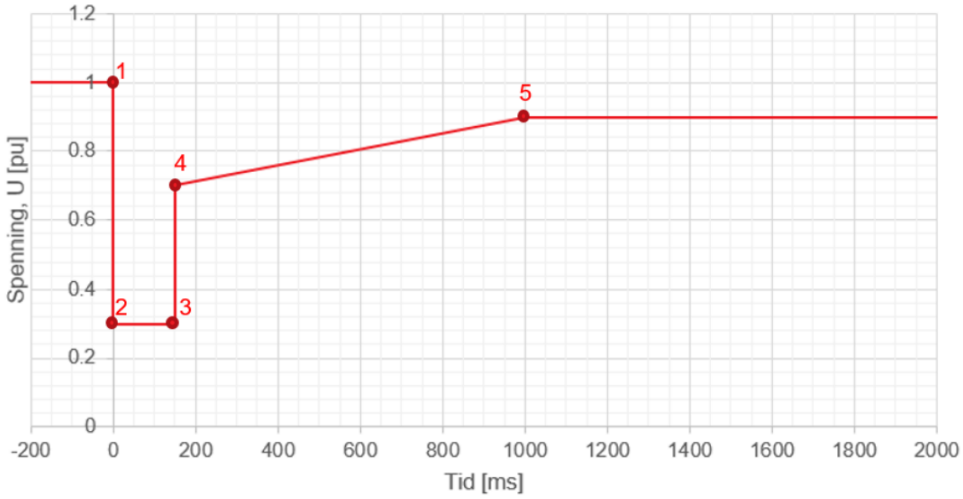

Figure 3.6.2: Example figure of Low-Voltage-Ride-Through [40]

Figure 3.6.2 illustrates the voltage limits for fault ride through requirement of specific production units in the Norwegian power system for a grid voltage $U_n < 110kV$. [40]

3.7 Offshore Wind Transmission Schemes

Offshore wind power plants are connected to the grid by transmission cables. High Voltage Alternating Current (HVAC) and High Voltage Direct Current (HVDC) are the two choices of transmission systems. There are both advantages and disadvantages for each transmission type. [34]

Offshore HVAC transmission typically include an offshore transformer substation on the turbine side and an onshore substation on the grid side. In situations where power need to be transmitted over long distances, HVAC transmission cables may need to be equipped with reactive power compensators due to the naturally high capacitance of HVAC cables. The high capacitance leads to generation of reactive power in the cables, resulting in significant power losses over long distances.

To mitigate this effect, the use of reactive power compensators becomes necessary. However, these compensators are very expensive and therefore contribute to the lower efficiency of HVAC compared to HVDC over long distances. For offshore wind farms located closer to shore HVAC may still be advantageous, as it is more cost-effective initially, and reactive power compensators are not needed for short distances. It is important to note that HVAC transmission systems must be synchronised with the grid at all times, as it does not decouple the wind power plant from the grid. [29]

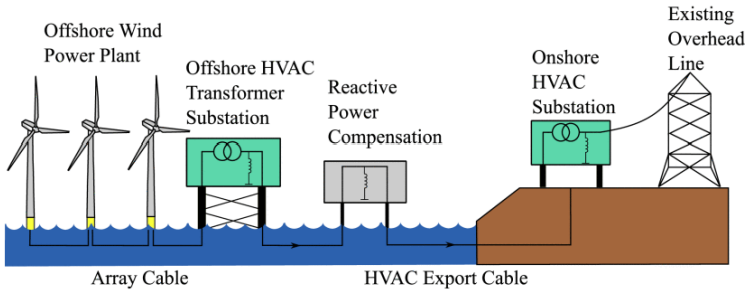

Figure 3.7.1: HVAC transmission scheme [8]

HVDC transmission is a preferred option for many offshore wind farms due to the superior efficiency over long distances, and enabling the decoupling of wind farm from the grid. The HVDC transmission scheme, as illustrated in figure 3.7.2, consists of an offshore HVDC converter and transformer substation on the turbine side, and an onshore HVDC converter and transformer substation on the grid side. With the incorporation of power converters that facilitate AC/DC or DC/AC voltage conversion, the wind farm becomes fully independent, as it is completely decoupled from the grid. This provides increased flexibility, as the wind farm no longer requires the synchronisation with the power system. HVDC cables do not posses any reactive power element, and consequently experience lower power losses compared to HVAC transmission cables over long distances. [29]

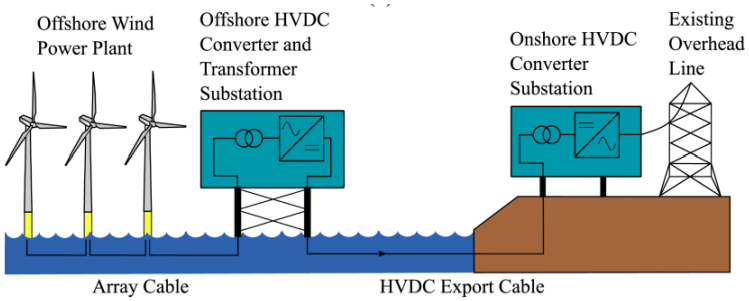

Figure 3.7.2: HVDC transmission scheme [8]

Initially, HVAC transmission is more cost-effective than HVDC transmission due of the high cost of voltage converters. However, the naturally high capacitance in the HVAC cables necessitates the use of expensive reactive power compensators in the transmission cables. Consequently, the overall cost of HVAC transmission exceeds that of HVDC for long distances. A specific distance exists, known as the break-even distance, where HVAC and HVDC transmission have an equal cost. Figure 3.7.3 visualises the cost-effective relationship between HVAC and HVDC transmission. [13]

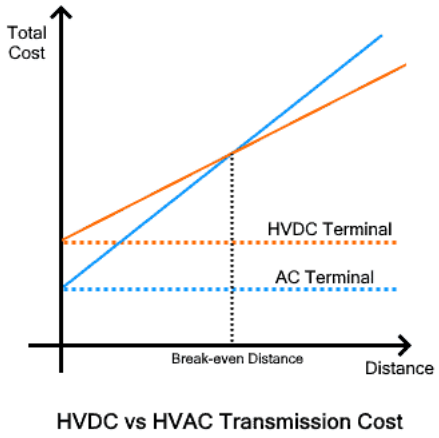

Figure 3.7.3: The transmission cost difference between HVDC and HVAC [13]

The selection of transmission scheme for offshore wind farms encompasses a range of factors beyond the consideration of transmission cost. While the overall cost of transmission is frequently a deciding factor in the planning of offshore wind farms, additional aspects also assume significant importance in determining the optimal transmission scheme. The flexibility of the decoupling from the HVDC scheme may prove more beneficial for a specific wind farm, and for another the simpler protection system of the HVAC scheme may be better suited. Given the distinctive attributes and demands of each wind farm, the process of decision making necessitates a comprehensive evaluation of multiple factors to achieve the most suitable transmission scheme for a specific project. [34]

3.7.1 LCC-HVDC

Line Commuted Converters (LCC) represent a significant branch within HVDC technology. These converters employ a configuration of thyristor valves interconnected in both series and parallel arrangements, enabling the attainment of a higher voltage and power levels. However, a prominent challenge associated with LCC technology arises from the simultaneous switching of all thyristors during operation, which cause transients in the system that necessitates the implementation of additional hardware to suppress the transients. [29]

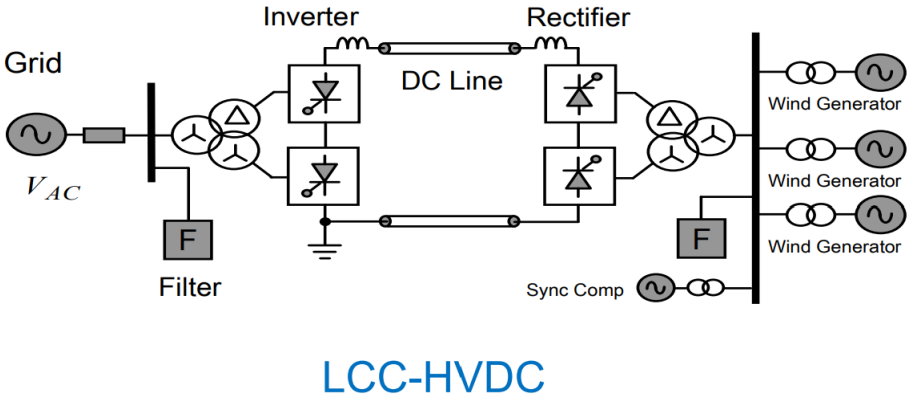

Figure 3.7.4: Offshore LCC-HVDC Technology [4]

3.7.2 VSC-HVDC

The advancements in power systems, particularly in terms of higher voltage levels, made way for the development of the Voltage Source Converter (VSC). These converters are self-commutated, characterised by their fast switching capabilities that serve as a link between HVAC and HVDC. VSC technology relies on the utilisation of insulated-gate bipolar transistors (IGBT), interconnected in both series and parallel arrangements. The fast switching frequency of the IGBTs results in a higher magnitude of switching losses. The distinctive advantage of VSC technology lies in its ability to independently control active and reactive power, which facilitates the decoupling of the generator and grid side. Additionally, a faster switching frequency produce a higher quality waveform of the AC signal during the conversion from DC to AC, surpassing the quality of the waveform produced by the LCC. Consequently, the filtering requirement is reduced on both the AC and DC side of the converter. [29]

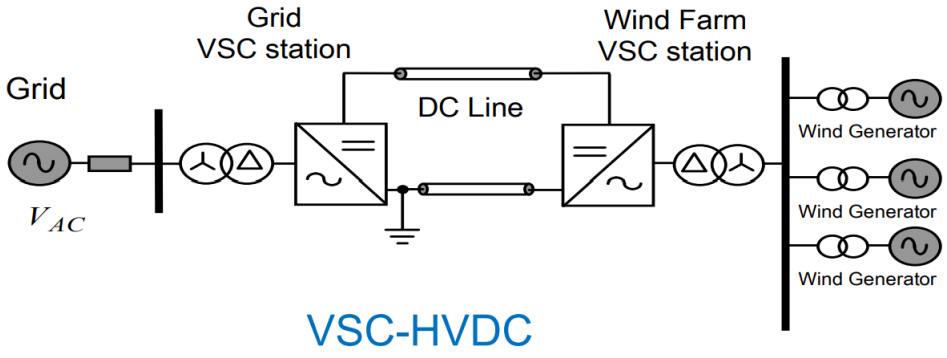

Figure 3.7.5: Offshore VSC-HVDC Technology[4]

Converter Levels

VSC-HVDC technologies encompasses multiple levels of converters. The initial implemented technology, and therefore most simple, is the two-level converter. This converter is capable of synthesising two discrete voltage levels, resulting in a square waveform. In modern power systems, such a waveform is unacceptable due to the high levels of harmonic distortion. To mitigate this issue, a pulse-width modulator (PWM) must be implemented to reduce the level of harmonic distortions. Three-level converters are a notable improvement compared the two-level converter. With this technology, the converter is capable of synthesising three discrete voltage levels leading to a staircase waveform with three steps. Although an improvement, the limited number of steps in the waveform still falls short for desired performance in the modern power system. [9]

Modular Multi-Level Converters (MMC) have emerged as the modern standard for VSC-HVDC technology. Initially introduced in 2003, MMC has become the most common type of VSC for HVDC applications. In a typical MMC, approximately 300 submodels are connected in a series arrangement in each valve, effectively creating the equivalent of a 301-level converter. This multitude of voltage levels eliminates harmonic distortion rendering the use of a pulse-width modulator unnecessary. Additionally, MMCs exhibit significantly lower power losses compared to the two-level or three-level converters. [9]

Chapter 4

Power System and Wind Turbine Modelling

4.1 Wind Turbine

To achieve the desired power output from a wind turbine, precise control mechanisms are needed. Among the various factors influencing power production in a wind turbine, wind speed is the most significant parameter. Additionally, the power coefficient substantially affects mechanical power generated by the turbine. Optimising the power coefficient is critical for good performance of the wind power plant, which can be accomplished by controlling the turbine's rotational speed and the blade pitch. This section covers the essentials of the wind turbine modelling in detail. [34]

4.1.1 Power Extraction

As described in chapter 3, the mechanical power extracted from a wind turbine is defined as in equation 4.1.1.

$$P_m = \frac{1}{2}\rho A U^3 C_p(\lambda, \beta) \tag{4.1.1}$$

Figure 4.1.1 illustrates each of the four regions of power output for a wind turbine. Region 1 is where the wind speed is less than the minimum threshold for the turbine. Region 2 is the section between the cut-in and the rated wind speed. In this region, the power output grows rapidly. This is also the region where maximum power is extracted by using MPPT. [27] Region 3 is where constant rated power is produced up until the cut out wind speed. Region 4 consists of all wind speeds higher than the cut-out wind speed. Beyond this limit operation of the turbine is not safe, and it is therefore taken out of operation. [37] Speed control is important in all regions of the curve.

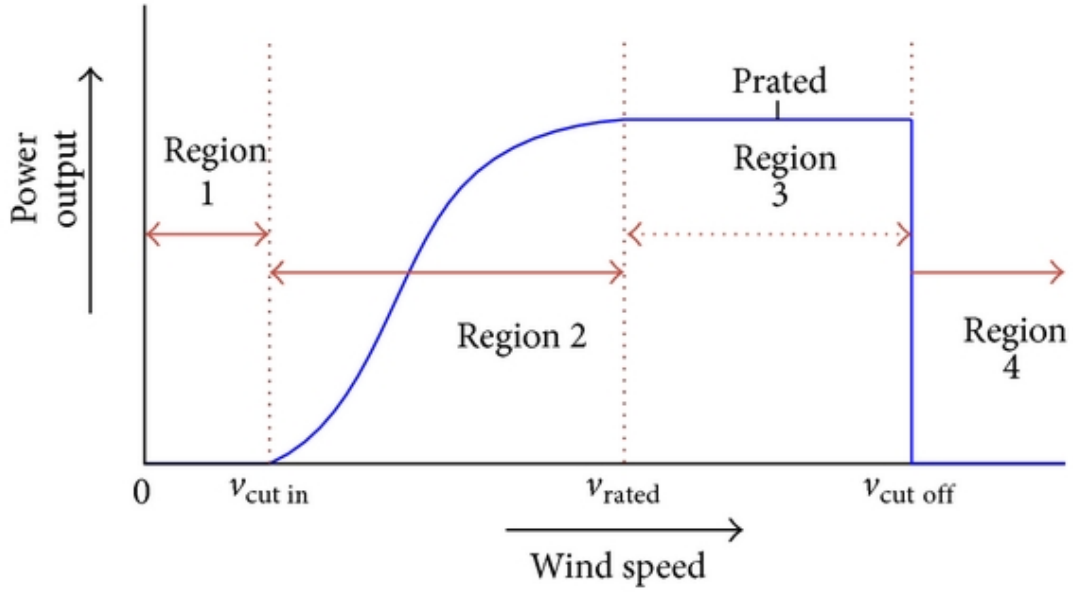

Figure 4.1.1: The wind power curve for a wind turbine [37]

From figure 4.1.1, the power output of a wind turbine can be expressed as

$$P_m = \begin{cases} 0 & v_{wind} < v_{cut-in} \\ p(v) & v_{cut-in} \leq v_{wind} < v_{rated} \\ P_{rated} & v_{rated} \leq v_{wind} \leq v_{cut-out} \\ 0 & v_{wind} > v_{cut-out} \end{cases} \tag{4.1.2}$$

The relationship between power output and wind speed is non-linear in region 2 between cut-in wind speed and rated wind speed. This can be approximated by using mathematical expressions. The simples approximation for $p(v)$ is a linear expression. However, for more accuracy, a a multi-polynomial expression can be employed. In region 3, where wind speeds are higher, the power output remains constant by adjusting the pitch of the turbine blades. This allows for consistent power generation despite increasing wind speeds [37]

From equation 4.1.1, it can be observed that the power output of a wind turbine is highly dependent on the wind speed, as it scales with power of three.

Additionally, the mechanical power is influenced by the power coefficient, which varies based on a relationship with the tip speed ratio λ, and the pitch angle of the turbine blades β. The tip speed ratio is defined in equation 4.1.3.

$$\lambda = \frac{\omega_m R}{U_{wind}} \tag{4.1.3}$$

Where ω_m is the rotational speed of the turbine, R is the radius of the turbine, and U_{wind} is the wind speed. [10]

C_p can be expressed as an empirical formula as in equation 4.1.4, with constant values for $c_1...c_9$ applicable to a variable speed wind turbine. [10]

$$C_p(\lambda, \beta) = c_1 \left(\frac{c_2}{\lambda_i} - c_3\beta - c_4\beta^{c_5} - c_6 \right) e^{-\frac{c_7}{\lambda_i}} \tag{4.1.4}$$

Where $c_1...c_7$ are constants found in table 4.1.1, β is the pitch angle on the turbine blades, and λ_i is defined in equation 4.1.5.

$$\lambda_i = \frac{1}{\frac{1}{\lambda + c_8\beta} - \frac{c_9}{\beta^3+1}} \tag{4.1.5}$$

Where c_8, c_9 are constants found in table 4.1.1 and β is the pitch angle on the turbine blades.

The maximum value for the power coefficient occurs when $\beta = 0$. By using the value zero for β in equation 4.1.4 and 4.1.5.

$$\lambda_i = \lambda \tag{4.1.6}$$

$$C_p(\lambda, \beta) = c_1 \left(\frac{c_2}{\lambda} - c_6 \right) e^{-\frac{c_7}{\lambda}} \tag{4.1.7}$$

The values of the C_P constants are defined in table 4.1.1.

Parameter	**Value**
c_1	0.73
c_2	151
c_3	0.58
c_4	0.002
c_5	2.14
c_6	13.2
c_7	18.4
c_8	-0.02
c_9	-0.003

Table 4.1.1: Power coefficient equation constants [10]

4.1.2 Maximum Power Point Tracking

To get the highest possible value C_p for optimal power production, maximum power point tracking is introduced.

Maximum power point tracking, MPPT in short, is used to extract the maximum amount of wind power for different wind speeds. Maximum wind power capture is achieved by controlling the rotational speed and the pitch of the wind turbine to maintain the optimal tip speed ratio at any given time.

Assuming constant wind speed, the optimal tip speed ratio is found at the point of the $C_P - \lambda$ curve where $\frac{dC_P}{d\lambda} = 0$. This is depicted in figure 4.1.2.

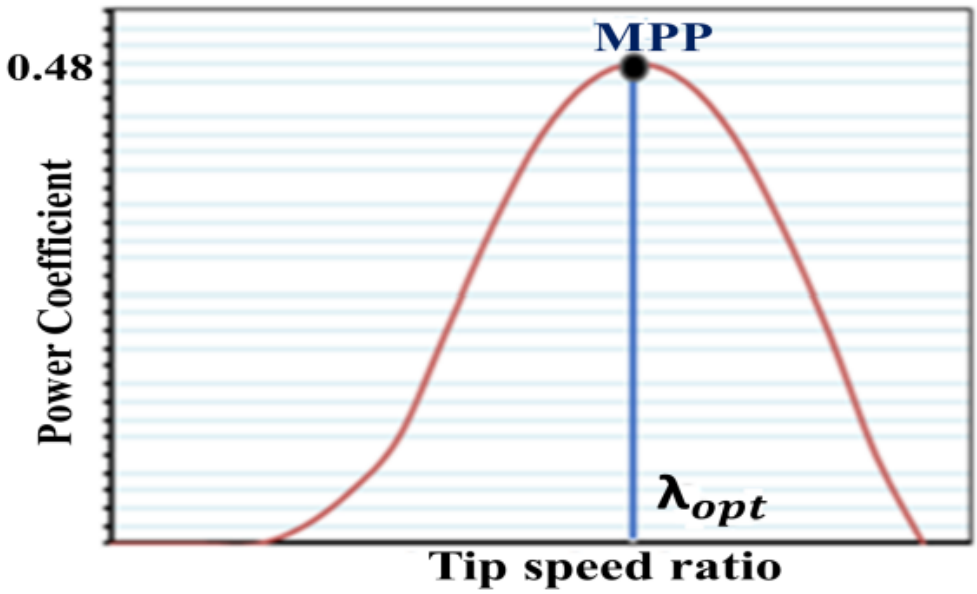

Figure 4.1.2: $C_p - \lambda$ curve with the optimal tip speed ratio [27]

4.1.3 Speed Control

Speed control is the main source of control for the wind turbines power coefficient. This is achieved by making sure the tip speed ratio corresponds to the optimal tip speed ration at any given time.

The block diagram for speed control using TSR MPPT is given in fig 4.1.3. The TSR MPPT algorithm is used for regulation of the rotor speed under changing wind conditions. The optimal reference speed of the rotor, ω_{ref}, is generated by estimating the rotor and wind speed. The advantage of the TSR MPPT algorithm is the rapid response and simplicity.[27]

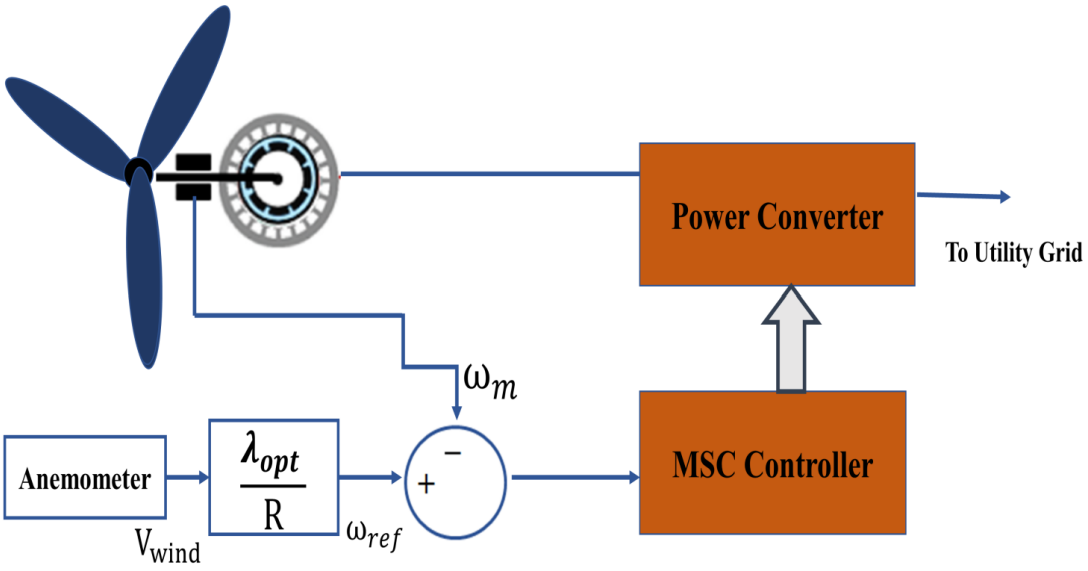

Figure 4.1.3: Block diagram for the TSR MPPT algorithm [27]

V_{wind} is the estimated wind speed.
λ_{opt} is the optimal tip speed ratio.
R is the radius of the turbine.
ω_{ref} is the estimated turbine rotor speed.
ω_m is the actual turbine rotor speed.

4.1.4 Pitch Control

Controlling the pitch of the turbine blades are essential for keeping the rated power output for wind speeds in region 3 of the power curve. Reducing the pitch of the turbine blades results in the wind transferring less of its power onto the blades, which makes it easier to keep the power constant for wind speeds varying between rated and cut-out values.

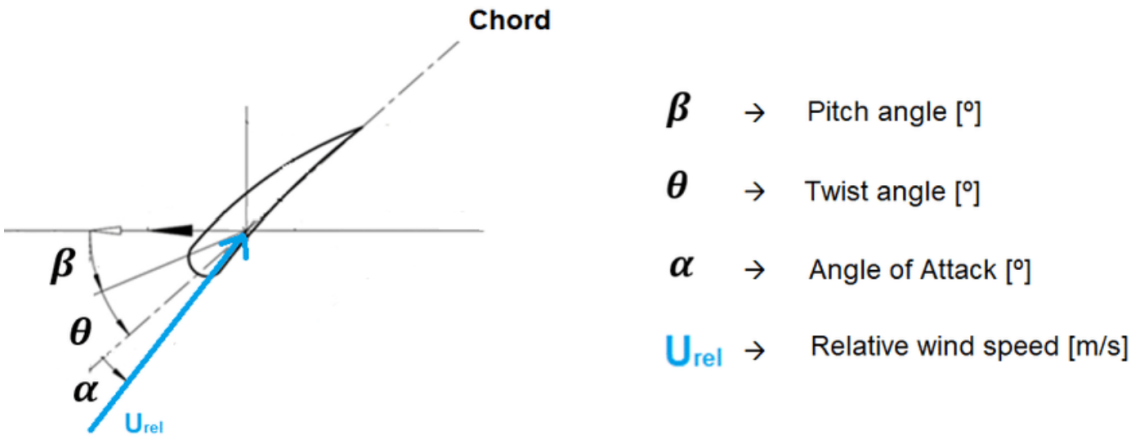

Figure 4.1.4: The aerodynamics of a turbine blade [35]

The pitch of the turbine blades is also an essential part of power coefficient equation. Changing the pitch angle will change the $C_P - \lambda$ curve as a whole, allowing for more freedom to control the turbine speed and output power. An example of this is visualised in figure 4.1.5.

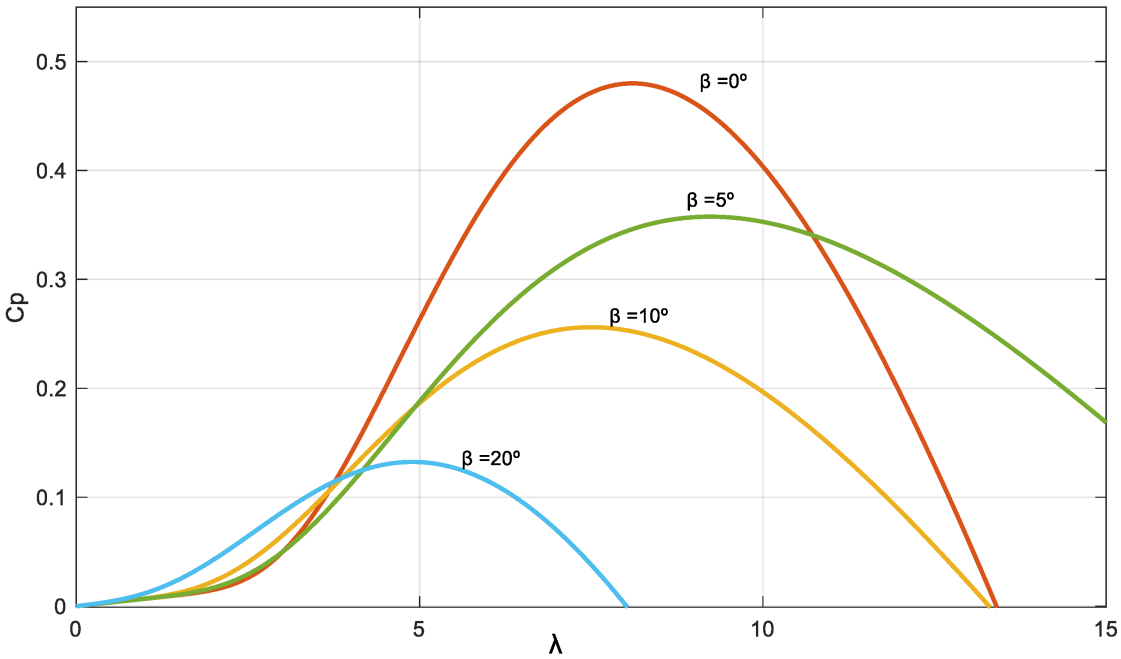

Figure 4.1.5: $C_p - \lambda$ curves for different values of β [24]

4.2 Wind Power Plant

The wind power plant is considered as one large generator. This generator, and its connection to the VSC, makes for the swing equation. For the modelling case, this is expressed as in equation 4.2.1.

$$J\dot{\omega} = P_{mech} - P_{el} \tag{4.2.1}$$

Where J is the moment of inertia in the rotating mass, $\dot{\omega}$ is the angular rotor acceleration, P_{mech} is the turbine mechanical power, and P_{el} is the electrical power from the VSC.

The block diagram for a wind power plant connected to the power grid is presented in figure 4.2.1.

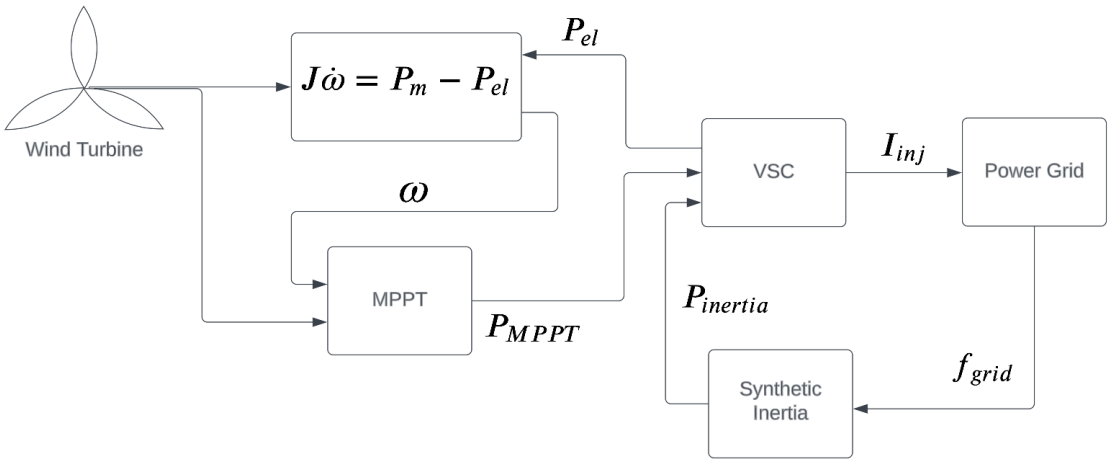

Figure 4.2.1: A simple block diagram of a wind power plant connected to the power grid

The only input value for the wind turbine model is the wind speed, which decides the base mechanical power. The turbines rotational speed is computed using the swing equation, and together with the wind speed it is used to find the optimal TSR using MTTP. The optimal TSR gives the maximum C_P for optimal power production. The power reference from the MTTP feeds into the VSC as a power reference, and is used to control the current injection to the power grid.

When simulating a scenario for the wind farm, it is reasonable to consider the wind speed as constant as the simulation has a duration of seconds to minutes. The pitch angle is also constant in this time frame, and is chosen to be 0° for simplicity. P_{mech} only changes with C_P, and $C_P(\lambda, \beta)$ only depends on the rotor speed ω as derived from the equations below.

$$P_{mech}(U_{wind}, C_P) \rightarrow P_{mech}(C_P) \tag{4.2.2}$$

$$\lambda(\omega, U_{wind}) \rightarrow \lambda(\omega) \tag{4.2.3}$$

$$C_P(\lambda, \beta) \rightarrow C_P(\lambda) \rightarrow C_P(\omega) \tag{4.2.4}$$

The rotor speed is subject to change after a disturbance to the active power supplied to the grid. Increased active power supply from the turbine causes a deceleration of the rotor speed. The chosen working point is critical for the efficient production of mechanical power. A working point higher than the optimal can be beneficial, as the turbine will decelerate to optimal speed, and achieve higher value of C_P for the mechanical power production. The wind farm will aso be able to sustain power production for longer in this scenaio, as depicted in figure 4.2.2.

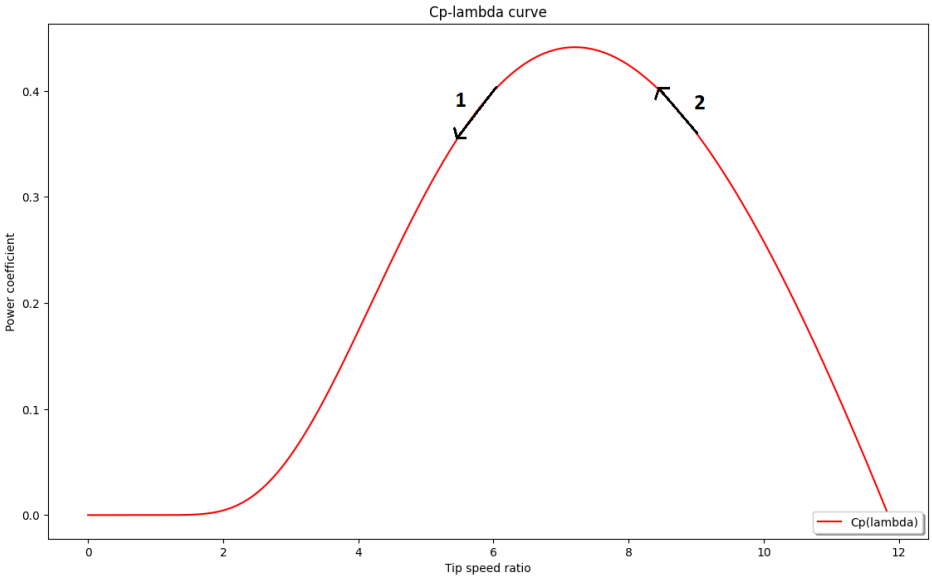

Figure 4.2.2: Working point of the $C_P - \lambda$ curve as a result of a disturbance to the active power

Initially working on the left side of the curve will cause a decrease of mechanical power when supplying the grid with additional active power. Initially working on the right side of the curve will cause an increase of mechanical power as rotor speed decreases and active power is injected into the grid.

Figure 4.2.3 and 4.2.4 depicts the rotor speed and wind turbines mechanical power for an initial working point at the left side of the curve.

Figure 4.2.5 and 4.2.6 depicts the rotor speed and wind turbines mechanical power for an initial working point at the right side of the curve.

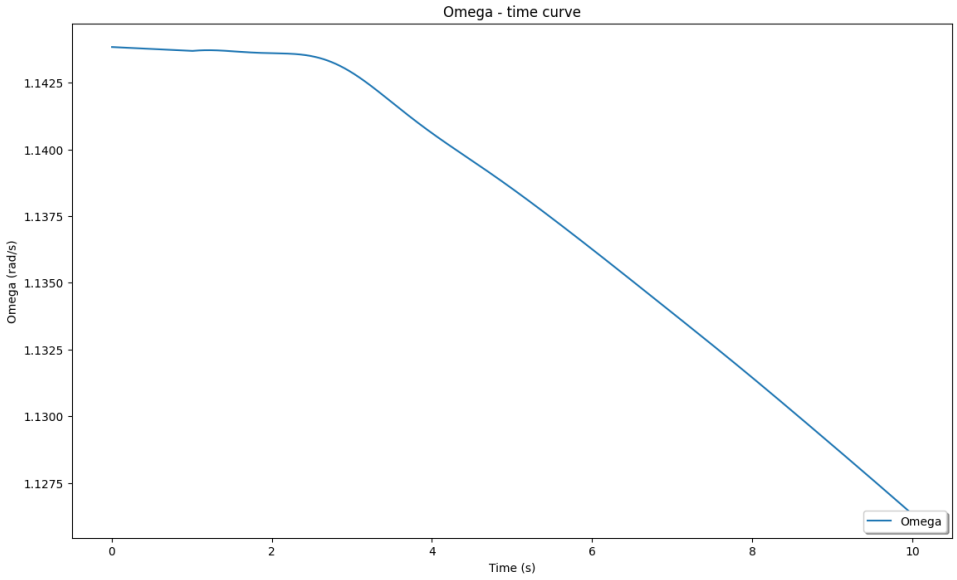

Figure 4.2.3: The resulting rotor speed for an increase in active power supply to the grid starting at the left side of the curve

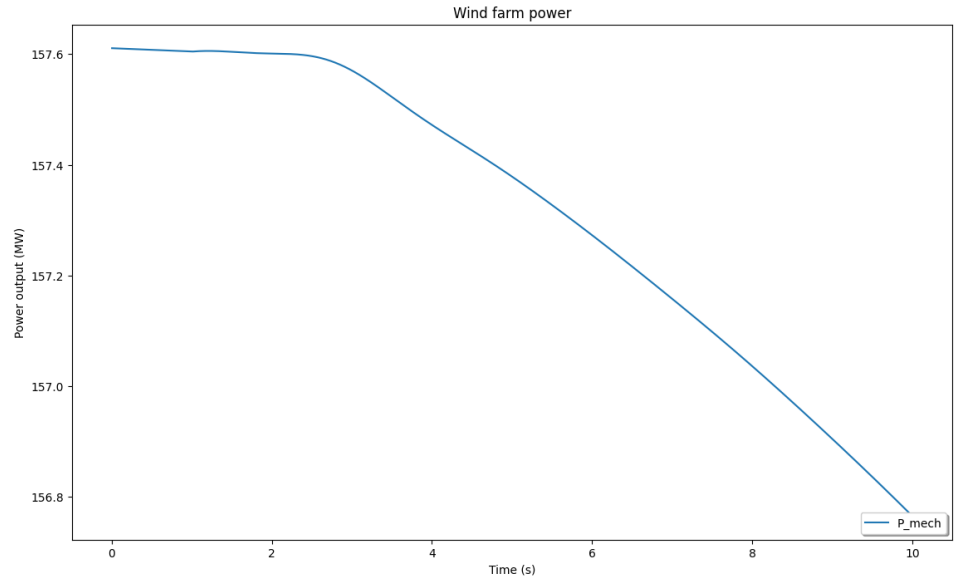

Figure 4.2.4: The resulting mechanical power for an increase in active power supply to the grid starting at the left side of the curve

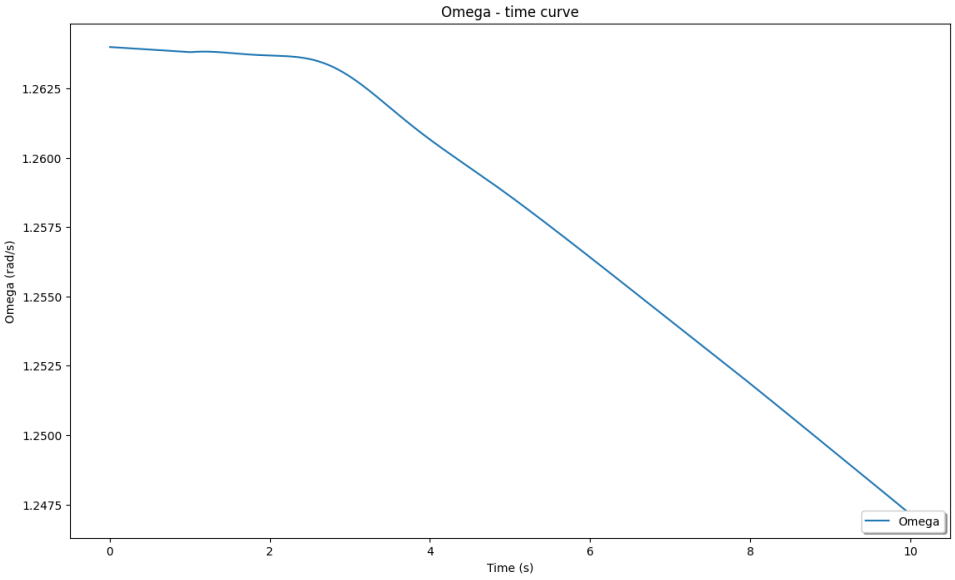

Figure 4.2.5: The resulting rotor speed for an increase in active power supply to the grid starting at the right side of the curve

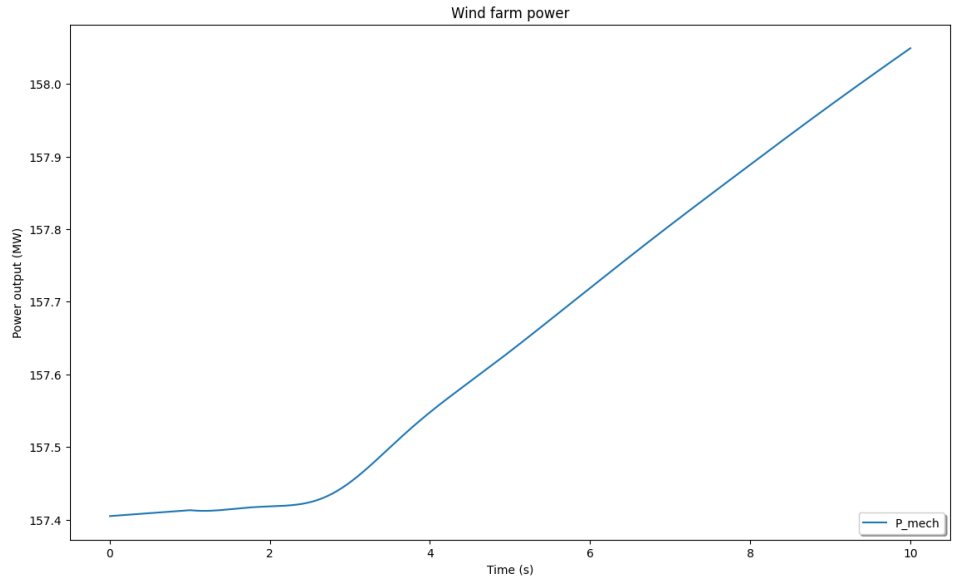

Figure 4.2.6: The resulting mechanical power for an increase in active power supply to the grid starting at the right side of the curve

4.3 Synthetic Inertia

Wind turbines do not provide inertia to the system naturally like fossil-fuelled or nuclear powered synchronous generators do. However, it is possible for the wind turbine to provide synthetic inertia to the power system by augmentation of an auxiliary control loop to the power reference of the active power controller. [10]

A requirement for the synthetic inertia scheme is the identification of the system event being above or below nominal frequency. If the event is above nominal frequency, the inertia contributes by decreasing the active power reference. If the event is below nominal frequency, the inertia contributes by increase in the active power reference.

The block diagram for the synthetic inertia process is given in figure 4.3.1.

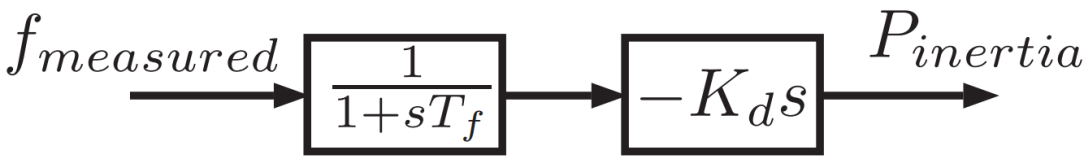

Figure 4.3.1: Block diagram for synthetic inertia control [10]

$f_{measured}$ is the measured grid frequency.
$P_{inertia}$ is the active power reference contribution.
K_d is the derivative controller gain.
T_f is the time constant of the low-pass filter.

4.4 Voltage Source Converter

The model for the Voltage Source Converter consists of multiple blocks and functions. It includes control modules for the active and reactive power, in addition to a Phase-Locked Loop to filter the signal. The reference and measured signal are processed through a PI controller, which generates the reference values for I_d and I_q. Additionally, a time constant T_i employed to produce a lag in the signal.

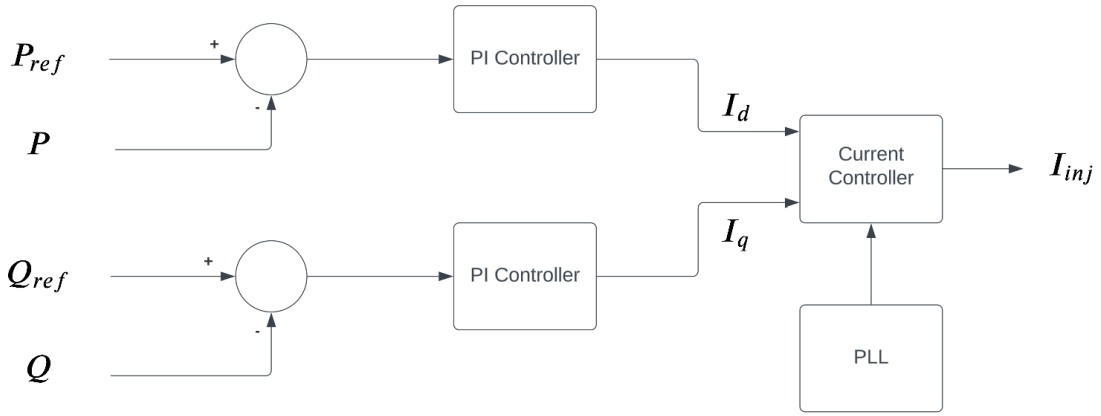

Figure 4.4.1: A simple block diagram of a VSC

The Phase-Locked Loop included in the VSC consists of a Phase Detector block, which receives the input and the feedback signal, and processes the signal through a Low Pass Filter and a Voltage Controlled Oscillator.

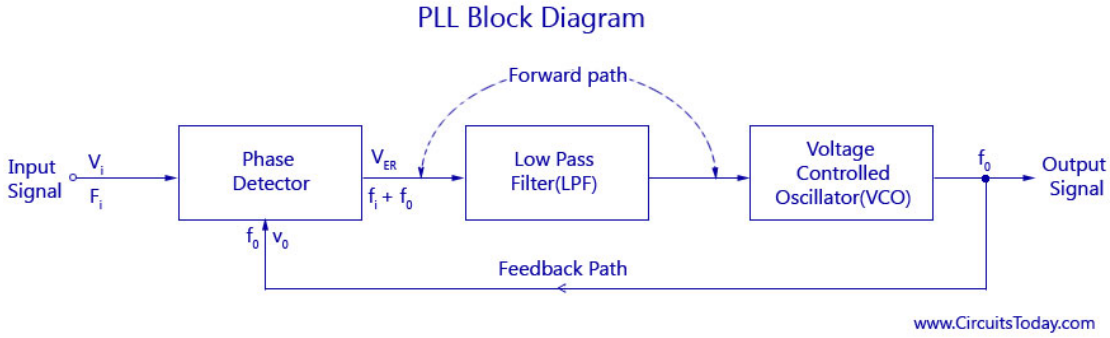

Figure 4.4.2: A simple block diagram of a PLL

4.5 Turbine Governor Model

The governor in the turbine control system regulates the rotational speed in response to deviations in load conditions. It ensures that the turbine operates at the desired speed to meet the changing power demands in the system. [28]

TGOV1 is the governor model used in the simulation model. It is a simplified representation of a turbine control system, and is implemented as in figure 4.5.1.

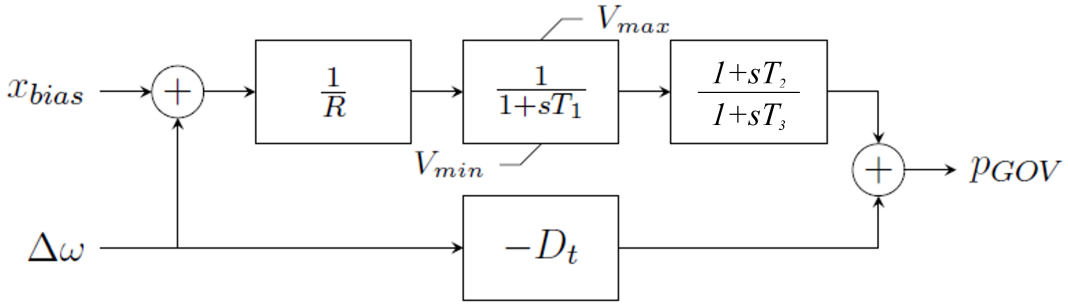

Figure 4.5.1: Turbine Governor Model TGOV1

R is the permanent droop in.
r is the temporary droop, and is defined by the equation $r = R\frac{T_3}{T_2}$.
T_1 is the steam bowl time constant.
T_2 is the governor time constant.
T_3 is the re-heater time constant.
D_t is the turbine damping coefficient.

4.6 Automatic Voltage Regulator

The Automatic Voltage Regulator regulates the voltage at the terminal of the generator. This is achieved by controlling the current flowing through the rotor field windings. By adjusting the excitation current, the AVR controls the output voltage of the generator through regulation of the magnetic field strength. This ensures that the generated voltage remains within the desired range, even for varying load conditions. [19]

The Automatic Voltage Regulator model utilised in the simulation model is the AVR model SEXS, implemented as in figure 4.6.1.

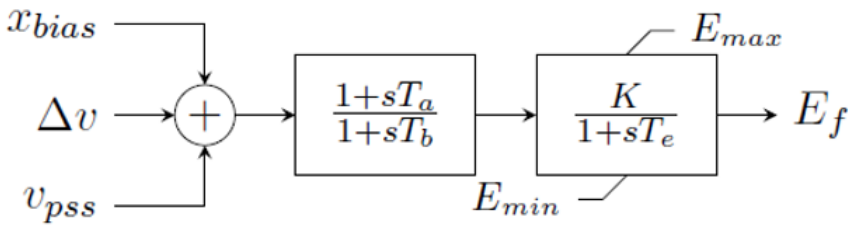

Figure 4.6.1: AVR Model SEXS

K is the gain.
T_A, T_B and T_C are time constants.
Δv is the measured voltage.
v_{pss} is the voltage reference from the PSS.
x_{bias} is the reference value.

4.7 Power System Stabiliser

The Power System Stabiliser is a control system implemented on the generation units in the power system. The PSS continuously monitors current, voltage and shaft speed. Its main purpose is to mitigate frequency deviations and stabilise the system. The PSS control deviations in frequency by analysing the referenced parameters, and sends appropriate control signals to the voltage regulator in order to damp the system oscillations. The PSS enhances the dynamic response of the generators and overall stability of the system. [15]

The model for the Power System Stabiliser utilised in the simulation model is the PSS model STAB1, implemented as in figure 4.7.1.

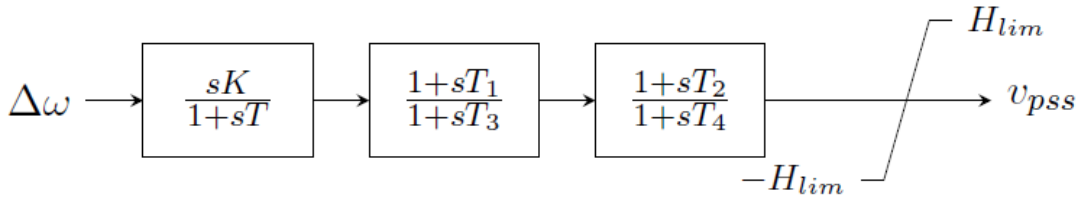

Figure 4.7.1: PSS Model STAB1

K is the gain.
T is the derivator time constant.
T_1, T_2, T_3 and T_4 are filter time constants.
H_{lim} is the output limit.
$\Delta\omega$ is the measured speed.
v_{pss} is the voltage reference contribution from the PSS.

4.8 Synchronous Generator Model

A mathematical model is employed to simulate the dynamic behaviour of the synchronous generator. The synchronous generator model is characterised by a sixth order model, consisting of the differential equations 4.8.1 to 4.8.6. [21]

$$M\Delta\dot{\omega} = P_m + P_e - D\Delta\omega \tag{4.8.1}$$

$$\dot{\delta} = \Delta\omega \tag{4.8.2}$$

$$T_{d0}^{'}\dot{E}_q^{'} = E_f - E_q^{'} + I_d(X_d - X_d^{'}) \tag{4.8.3}$$

$$T_{q0}^{'}\dot{E}_d^{'} = -E_d^{'} + I_q(X_q - X_q^{'}) \tag{4.8.4}$$

$$T_{d0}^{''}\dot{E}_q^{''} = E_q^{'} - E_q^{''} + I_d(X_d^{'} - X_d^{''}) \tag{4.8.5}$$

$$T_{q0}^{''}\dot{E}_d^{''} = E_d^{'} - E_d^{''} + I_q(X_q^{'} - X_q^{''}) \tag{4.8.6}$$

Where E is the emf, T is the time constant, and X is the reactance. The subtext d and q refers to the d- and q-axis in the abc/dq0-transformation. The notation $'$ refers to the transient version of the parameter and $''$ refers to the subtransient version of the parameter. E_f refers to the field emf of the generator.

The electrical power in the synchronous generator is given by equation 4.8.7. [21]

$$P_e = E_d^{''} I_d + E_q^{''} I_q \tag{4.8.7}$$

4.9 Power Flow

The power flow equations are used to calculate active- and reactive power at each bus in the power system. Equation 4.9.1 express the apparent power flow, equation 4.9.2 express the active power flow, and equation 4.9.3 express the reactive power flow. The equations are derived from the Y_{bus}, which represents the admittance matrix of the system.

$$S_i = \sum_{k=1}^{n} |V_i||V_k|(cos\delta_{ik} + jsin\delta_{ik})(G_{ik} + B_{ik}) \tag{4.9.1}$$

$$P_i = \sum_{k=1}^{n} |V_i||V_k|(G_{ik}cos\delta_{ik} + B_{ik}sin\delta_{ik}) \tag{4.9.2}$$

$$Q_i = \sum_{k=1}^{n} |V_i||V_k|(G_{ik}sin\delta_{ik} - B_{ik}cos\delta_{ik}) \tag{4.9.3}$$

Where V_i and V_k is the voltage at bus i and bus k respectively, G_{ik} and B_{ik} is the conductance and susceptance on the line connecting bus i and bus k, and δ_{ik} is the difference in voltage angle between bus i and bus k.

4.10 Grid-Following and Grid-Forming

Grid-following and grid-forming are two control approaches for the power electronics in the energy storage systems. In grid-following mode, the inverter of the energy storage system adjusts the output based on the voltage angle of the grid. The inverter essentially follows the grid's voltage angle to regulate its output. In grid-forming mode, the inverter of the energy storage system actively controls the frequency and voltage output. The key difference between the two control modes lies in the active role of the inverter of the energy storage system in maintaining stable frequency and voltage levels in grid-forming mode, while in grid-following mode, corrections will only be made if the frequency deviates outside the specified bandwidth. [32]

Grid-Following

Grid-following converters follow a reference signal, typically the voltage angle. The converter control is synchronised with the grid through a phase-locked loop, which determines the voltage angle in the system. [31] By following the voltage angle, grid-following converters function as current sources, injecting active and reactive power into the grid. In order to achieve accurate power injection, the converter control utilises a PLL to synchronise with the grid. The converter control structure consists of the main current control loop, which operates in conjunction with an outer voltage control loop. The voltage control loop feeds the reference signal back to the current control loop, enabling precise regulation of the converter's output. [33]

The abc/dq0-transformation is a useful technique for controlling the converter. To correctly control the output during this transformation, accurate information about the grid frequency is needed. The reference signal must align with the frequency of the AC voltage signal. The necessary information about phase angle and frequency needed in the transformation is obtained from the PLL. [46] As a result, the dq-voltages V_d and V_q can be determined based on the input of a three-phase abc voltage, expressed in equation 4.10.1 and 4.10.2.

$$V_d(t) = \hat{V} cos(\omega t + \theta_0 - \phi) \tag{4.10.1}$$

$$V_q(t) = \hat{V} sin(\omega t + \theta_0 - \phi) \tag{4.10.2}$$

Where $\hat{V}$ is the voltage magnitude, θ_0 is the initial voltage angle, and ϕ is the rotation of the dq-frame.

The rotation of the dq-frame is synchronised with the grid when the rotation of the dq-frame equals to $\phi = \omega t + \theta_0$. Substituting this into equation 4.10.2, gives $V_q = 0$. Therefore, by regulating V_q to zero, the correct rotation can be obtained for the dq-transformation. The feedback loop is given by equation 4.10.3.

$$\omega = H(s)V_q(t) \tag{4.10.3}$$

Where $H(s)$ is a linear transfer function and is easily implemented as a PI-regulator. Additionally, an integrator must be included since $\frac{d\phi}{dt} = \omega$. This will result in the feedback signal being ϕ.

Grid-Forming

Grid-forming converters behaves like an AC voltage source with a characteristic voltage amplitude, phase shift and frequency. By behaving like a voltage source behind a reactance, the converter with grid-forming control resembles a synchronous generator. This concept is known as a virtual synchronous machine. Unlike a grid-following converter, which synchronises based on the voltage angle and the PLL, a grid-forming converter synchronises based on the active power transfer and the swing equation. The voltage angle is calculated in the same way as for a synchronous machine, enabling the converter to maintain synchronisation with the grid. [30]

The swing equation for a synchronous machine transformed to the Laplace domain is given in equation 4.10.4.

$$P_m - P_e = \left(\frac{2HS_{base}}{\omega_s}s + D\right)\omega \tag{4.10.4}$$

Where P_m and P_e are mechanical and electrical power, H is the inertia constant, S_n is the nominal power of the synchronous generator, ω_s is the nominal angular speed, D is he damping factor and ω is the output angular speed. [47]

If the converter is connected to the grid, equation 4.10.4 gets some modifications.

$$\omega = \omega_{ref} + \frac{1}{(2HS_N/\omega_s + D)}(P_{ref} - P) \tag{4.10.5}$$

Where ω_{ref} and P_{ref} are the angular speed reference and active power reference.

Once power balance has been achieved in the swing equation, the rate of change of frequency becomes zero. Demonstrated in equation 4.10.5, the RoCoF is dependent on the inertia constant H. A larger the value of the inertia constant, will result in a slower change in frequency. This approach simplifies the establishment of the power angle in the grid. Calculation of the voltage magnitude can be accomplished by using any reactive power or voltage control scheme. By utilising these strategies, grid-forming converters can effectively regulate frequency and voltage similar to a synchronous generator. [31]

Chapter 5

Simulation

5.1 Dynamic Power System Simulator in Python

The power system simulation software employed in this thesis is DynPSSimPy, which is developed by PhD student Hallvar Haugdal. [21] DynPSSimPy is an open source software package implemented in the programming language Python. It is specifically designet to perform dynamic RMS simulations of small- to medium-sized power systems. The primary objective of the program is to facilitate fast prototyping of new wide area monitoring, control and protection application for future power systems by allowing for integration with other tools that are available in the Python open source community. [21]

The program is mainly employed for conducting simulations on the electric power grid, specifically the transmission network. In encompasses multiple valuable features that cater both steady state and dynamic studies of the network. These features include load flow calculations and fault applications, among others. DynPSSimPy facilitates comprehensive studies and evaluations of a power systems performance and behaviour under varying conditions.

In the dynamic analysis of large-scale power systems, voltages and currents are typically represented as phasors. The relevant models applied for this simulation are known as RMS-models. The main objective of the RMS-model simulator is to integrate the differential equations of the dynamic models in the system, while simultaneously ensuring that the algebraic equations of the network are satisfied. [21]

Differential algebraic equations are used for describing the dynamics of the system. The two equations utilised are equation 5.1.1 and 5.1.2.

$$\dot{x} = f(x, y) \tag{5.1.1}$$

$$0 = g(x, y) \tag{5.1.2}$$

Function f describes the differential equation for all states of the system, and function g describes the algebraic equations that represents the network equations. Furthermore, x is the vector of the state variables, and y is the vector of the algebraic equations. [34]

5.1.1 Model Implementation

All of the dynamic models in the system are implemented as individual and separate classes in Python. This includes the generators, governors, AVR, PSS, and VSC, which are implemented as presented in the corresponding sections in chapter 4. Each individual class contains state derivatives that are calculated for each iteration, updating the states of the dynamic models.

The model of the wind power plant is implemented as a hard coded script. The script contains the generated $C_P - \lambda$ and mechanical power curve, in addition to the equations to correctly update the rotor speed, power coefficient, mechanical and electrical power for each iteration of the simulation. The power coefficient is calculated using the rotor speed, which decides the mechanical power. The electrical power is delivered by the VSC connected to the grid, which together with the mechanical power is used to calculate the new rotor speed.

5.2 Kundur's Two Area System

Kundur's Two Area System is an example system presented by Prabha Kundur in the textbook *Power System Stability and Control*.

The systems layout is visualised in figure 5.2.1.

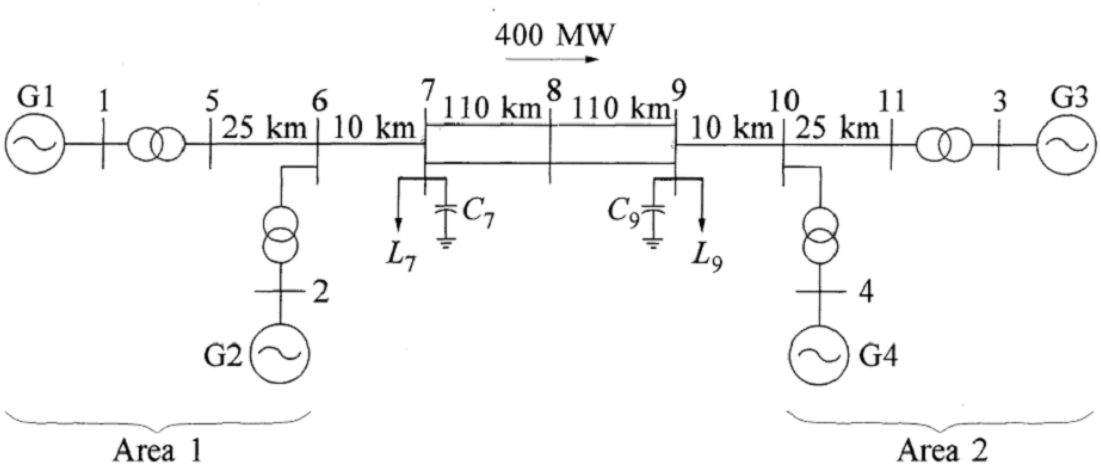

Figure 5.2.1: A line diagram of Kundur's Two Area System

The system consists of eleven buses, divided in to two areas. The system is divided in to two areas by weak link between bus 7 and 9. Additionally, two shunt capacitors and two loads are also directly connected to bus 7 and 9. The system operates for with base apparent power of 900 MVA and a nominal frequency of 50 Hz. There are four generators in total, each with a rating of 900 MVA and a voltage of 20 kV. The slack bus, responsible for maintaining system balance, is located at bus 3.

All necessary variables of the system base, buses, lines, transformers, loads, shunts, generators, governors, AVR and PSS are given in table A1 to A10 in appendix A respectively.

5.3 Simulation Initialisation and Power Curves

The $C_P - \lambda$ curve and the wind turbines power curve are essential for the initialisation of the wind farm dynamic simulation. The curve is generated using equation 4.1.4, with the coefficients listed in table 4.1.1 and a pitch angle β equal to zero. All values of C_P used to calculate mechanical power in the simulation follows the curve in figure 5.3.1.

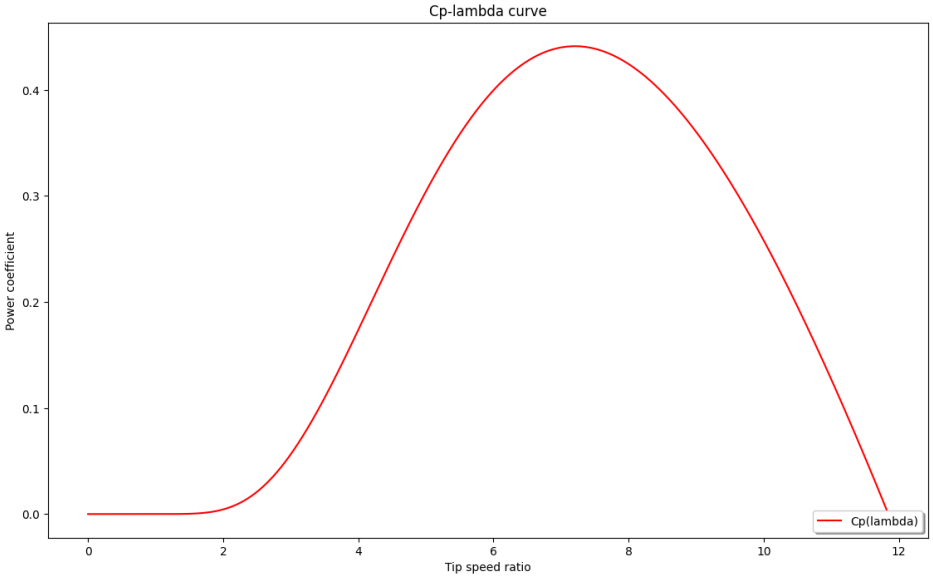

Figure 5.3.1: The simulated $C_P - \lambda$ curve

The wind turbine power curve is generated using constant values and equation 4.1.2. The turbine has a cut-in wind speed of 4 m/s and a cut-out wind speed of 25 m/s. The mechanical power in region 2 is calculated using equation 4.1.1, and the rated power of the wind turbine is 8 MW. Using a constant wind speed of 10 m/s for the simulation, the operational area of mechanical power will be in region 2.

The linear relationship between wind speed and rotor speed in equation 5.3.1 is used to plot mechanical power against rotor speed.

$$\omega_r = \frac{\lambda U_{wind}}{R} \tag{5.3.1}$$

Working with constant wind speed does not result in a constant rotor speed. The tip speed ratio will vary based on the $C_P - \lambda$ curve and MPPT. The rotor speed will as a result vary based on λ, since the wind speed and turbine radius are constant. The working point on the curve will still be in region 2, since $\omega_{opt} \approx 1.2$ refers to the same point on the power curve as $U_{wind} = 10$. The wind turbine power plotted against rotor speed is depicted in figure 5.3.2.

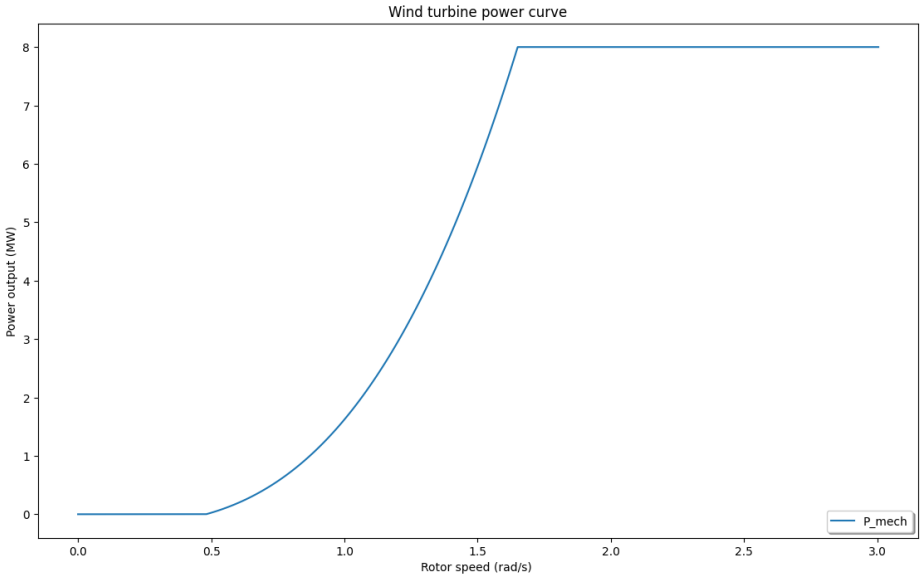

Figure 5.3.2: The simulated $P_{mech} - \omega_r$ curve for a single wind turbine

5.4 Voltage Source Converter

The VSC connects the wind farm to the grid, allowing for transmission of power. Depending on the control strategy, the VSC can accept an active or reactive power reference depending on our choice of frequency or voltage control. Figure 5.4.1 and 5.4.2 depicts the VSC power output and generator speeds for an active power injection of 400 MW to the VSC connected at bus 9. The active power input is introduced one second into the simulation, with no control effect.

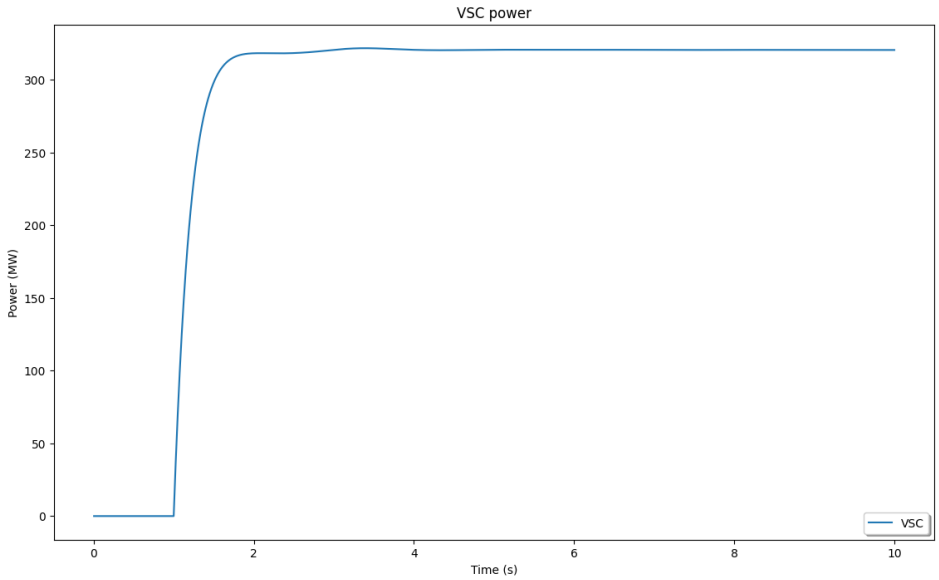

Figure 5.4.1: The VSC power for an set active power injection of 400 MW after 1 second

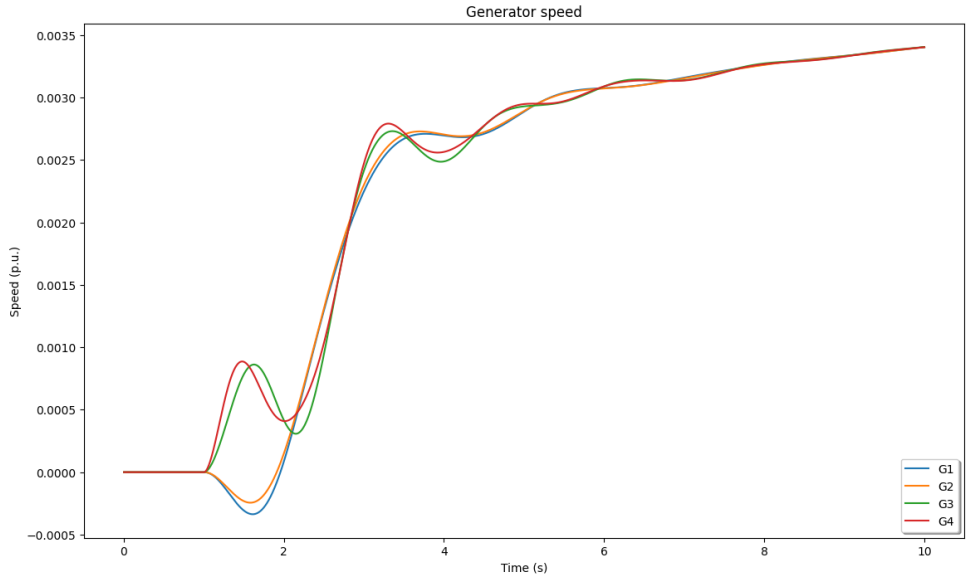

Figure 5.4.2: The generator speeds for an active power injection of 400 MW after 1 second

Figure 5.4.3 and 5.4.4 depicts the VSC power and generator speed for an active power injection of 400 MW to the VSC connected at bus 9 one second into the simulation, and active power control two seconds into the simulation. Active power control is achieved by extracting the generator speed from all other generators in the power system, calculating the active power, finding the average of all generators and using it as the input for the VSC set power.

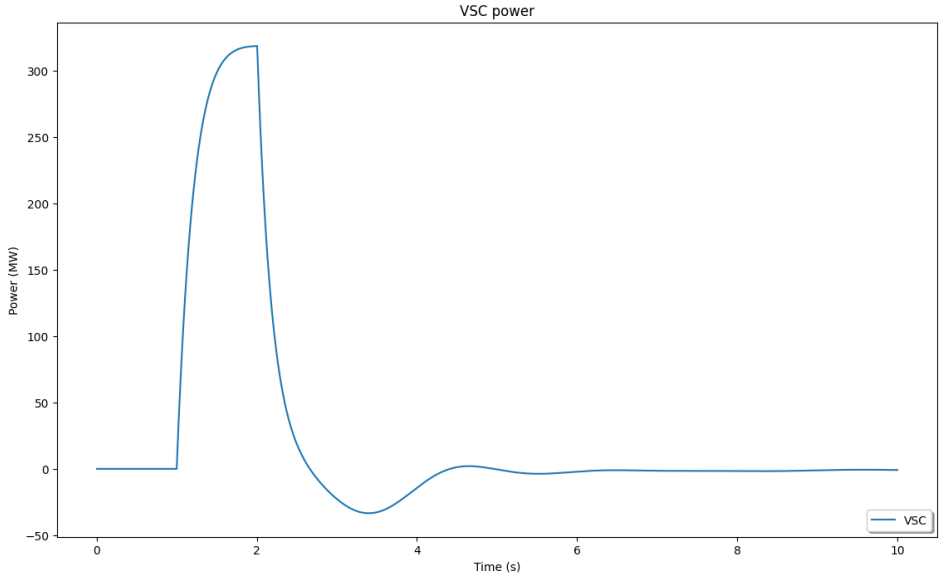

Figure 5.4.3: The VSC power for an active power injection of 400 MW after 1 second and active power control after 2 seconds

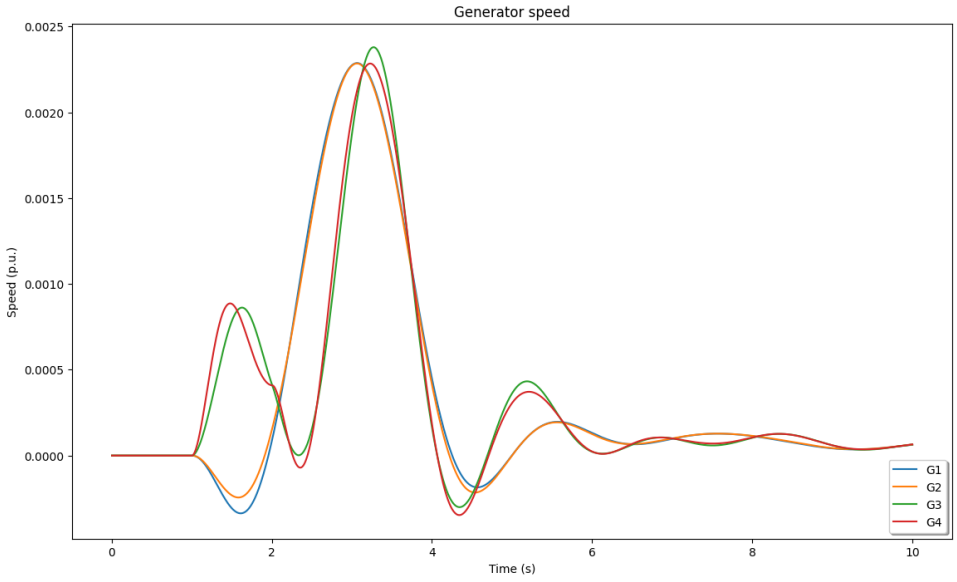

Figure 5.4.4: The generator speeds for an active power injection of 400 MW after 1 second and active power control after 2 seconds

5.5 Wind Farm Test Scenarios

In addition to the $C_P - \lambda$ curve and power curve, the initial constants of the wind power plant and the power system must be decided. The wind farm constants are listed in table 5.5.1, the wind speed constants are listed in table 5.5.2, the VSC constants are listed in table 5.5.3, and the power system constants for the K2A network are listed in appendix A.

Parameter	Value	Unit
R	60	m
A	11 310	m^2
ρ	1.273	kg/m^3
$P_{turbine}$	8	MW
Turbines	50	-
P_{rated}	400	MW

Table 5.5.1: Wind farm constants

Parameter	Value	Unit
U_{cut-in}	4	m/s
U_{wind}	10	m/s
U_{rated}	13.733	m/s
$U_{cut-out}$	25	m/s

Table 5.5.2: Wind speed constants

Parameter	Value	Unit
T_{PLL}	0.1	s
T_i	1	s
P_{Kp}	0.01	-
P_{Ki}	10^{-12}	-
Q_{Kp}	0.1	-
Q_{Ki}	0.1	-
P_{ref}	158.37	MW
Q_{ref}	0	MVAr

Table 5.5.3: Voltage Source Converter constants

The initial value of P_{ref} in the VSC is equal to the wind farms total mechanical power for the given wind speed and at the corresponding C_P value. This is calculated using equation 4.1.1.

The initial value of the rotor speed ω_0 is higher than the optimal value, to give a operating point on the right side of the curve. This achieves an increase in power production in the event of a disturbance, as explained in figure 4.2.2.

The new rotor speed, expressed by equation 5.5.1, is found by utilising a simplified version of equation 4.10.5 with some modifications to match the block diagram 4.2.1 for the wind power plant.

$$\omega = \omega_0 + \frac{1}{(2HS_N/\omega_s)}(P_{mech} - P_{el}) \tag{5.5.1}$$

New values for λ and C_P is then calculated based on the new value for ω, using equation 4.1.5 and 4.1.4. C_P is then used to calculate the new mechanical power.

The total kinetic energy available in the power system is found by equation 5.5.2.

$$E_{k,sys} = \sum_{i=1}^{N} S_{n,i} H_i = 23.4GW \tag{5.5.2}$$

The system frequency bias is calculated using equation 2.3.4 and inserting the droop values from the governors. This gives a value of $\beta_{p.u.} \approx 33.33$. Multiplying by the system base apparent power of 900 MVA gives the system frequency bias of $\beta_{sys} = 600$ MW/Hz.

$$\beta_{sys} = \frac{1}{R_{sys}} \cdot \frac{S_{base}}{f_{base}} = 600MW/Hz. \tag{5.5.3}$$

The frequency bias of each generator in the power system is calculated by using the droop of each individual generator. With a droop of 12% for all generators in the K2A system, the resulting frequency bias is $\beta_{gen} = 150$ MW/Hz.

$$\beta_{gen} = \frac{1}{R_{gen}} \frac{S_{base}}{f_{base}} = 150MW/Hz \tag{5.5.4}$$

The wind farms frequency bias can be manipulated within a reasonable range. In this case, it is set to $\beta_{wind} = 200$ MW/Hz. The resulting droop of the wind farm is 9%.

The total load of the system is 2734 MW, and the system frequency bias is 600 MW/Hz.

The wind farm is connected to bus 9 for all scenarios.

5.6 Load Deviation

The simulation of the base case and wind case aims to study the response of the power system to a sudden increase in load.

A sudden increase in the system's load causes a drop in frequency. The change in system frequency is proportional to the total change in active power, shown by equation 5.6.1.

$$\Delta f_\infty = \frac{-\Delta P_{gen} + \Delta P_{load} + \Delta P_{loss}}{\beta_{sys}} \tag{5.6.1}$$

Where ΔP_{gen}, ΔP_{load} and ΔP_{loss} are the deviation in active power for generation, load and losses in the system respectively, and β_{sys} is the system frequency bias.

The sudden increase in the system's load also causes a voltage drop at the buses. The increase in load causes the generators to increase the production of power. The load deviation is proportional to the square of the voltage drop. The load model for an arbitrary bus in the system is shown by equation 5.6.2.

$$P_{load} = P_0 \left(\frac{V_{load}}{V_0} \right)^2 \tag{5.6.2}$$

Where P_{load} is the load active power after the deviation, P_0 is the active power before the deviation, V_{load} is the load voltage after the deviation, and V_0 is the load voltage before the deviation. The deviation causes the the active power to decrease by the square of the voltage, meaning that a voltage drop of 2% results in an active power deviation of 4%.

As a consequence of voltage drop at the buses, the system may not receive the full effect of the intended load deviation from the simulation.

5.6.1 Base Case

For the base case, all generators have their normal value of active power, as listed in table 5.6.1.

Generator	Power	Unit
$G1$	700	MW
$G2$	700	MW
$G3$	719	MW
$G4$	700	MW

Table 5.6.1: Base Case Generator Rated Power

In this scenario, the load at bus 7 is increased by 180 MW. This load increase results in a theoretical frequency drop of 0.006 per unit, which corresponds to 0.30 Hz.

$$\Delta f_\infty = -\frac{\Delta P_{load}}{\beta_{sys}} = -\frac{180MW}{600MW/Hz} = -0.30Hz \tag{5.6.3}$$

This results in a new steady state frequency of $f_\infty = 49.70$ Hz.

The theoretical maximum RoCoF is estimated to be 0.1923 Hz/s.

$$RoCoF = \frac{\Delta P_{load} f_{base}}{2E_{k,sys}} = \frac{180MW \cdot 50Hz}{2 \cdot 23.4GWs} = 0.1923Hz/s \tag{5.6.4}$$

The theoretical increase in power for each generation unit is 0.05 per unit, which corresponds to 45 MW.

$$\Delta P_{gen} = -\beta_{gen} \Delta f_{p.u.} S_{base} = \frac{1}{0.12} \cdot 0.006 \cdot 900 = 45MW \tag{5.6.5}$$

Simulation

The system frequency, depicted in figure 5.6.1, drops steeply after the load increase one second into the simulation. After running the simulation for 60 seconds, the system frequency has stabilised at a value of 49.75 Hz. This corresponds well with the theoretical value of 49.70 Hz considering the system don't receive the full effect of the load deviation due the voltage drops at the buses and losses in the system.

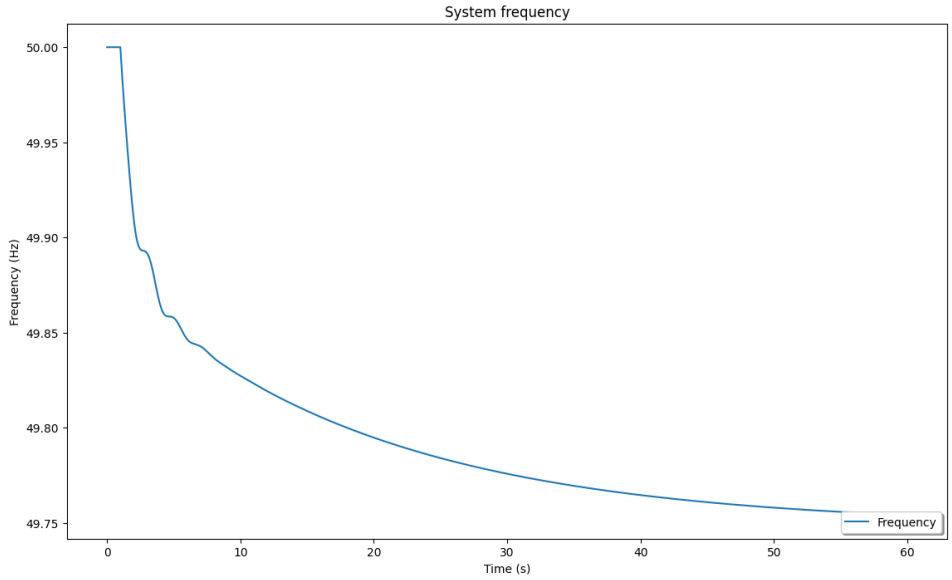

Figure 5.6.1: The system frequency after a load deviation at bus 7 for the base case

The relation between ΔP and Δf is given by the plot of the generator speed and power. The simulated value is 164 MW/Hz, which corresponds well with the theoretical value of 150 MW/Hz.

$$\frac{\Delta P}{\Delta f} = \frac{P_{gen,end} - P_{gen,start}}{\Delta \omega_{gen} \cdot f_{base}} = \frac{741 - 700}{0.005 \cdot 50} = 164MW/Hz \tag{5.6.6}$$

Figure 5.6.2 and 5.6.3 represents the generator speed and power respectively. The reduction in generator speed is 0.005 per unit, which corresponds to a reduction in generator frequency of 0.25

Hz. The increase in generator power is 0.046 per unit, which corresponds to an increase of 41 MW in each generator. This gives a simulated change in load of 164 MW.

$$\Delta P_{load} = \Delta P_{gen} \cdot N_{gen} = 41MW \cdot 4 = 164MW \tag{5.6.7}$$

The simulated maximum RoCoF is 0.1752 Hz/s.

$$RoCoF = \frac{\Delta P_{load} f_{base}}{2E_{k,sys}} = \frac{164MW \cdot 50Hz}{2 \cdot 23.4GWs} = 0.1752Hz/s \tag{5.6.8}$$

These are acceptable results as the voltage drop at the buses reduces and losses in the system the effect of the intended load deviation.

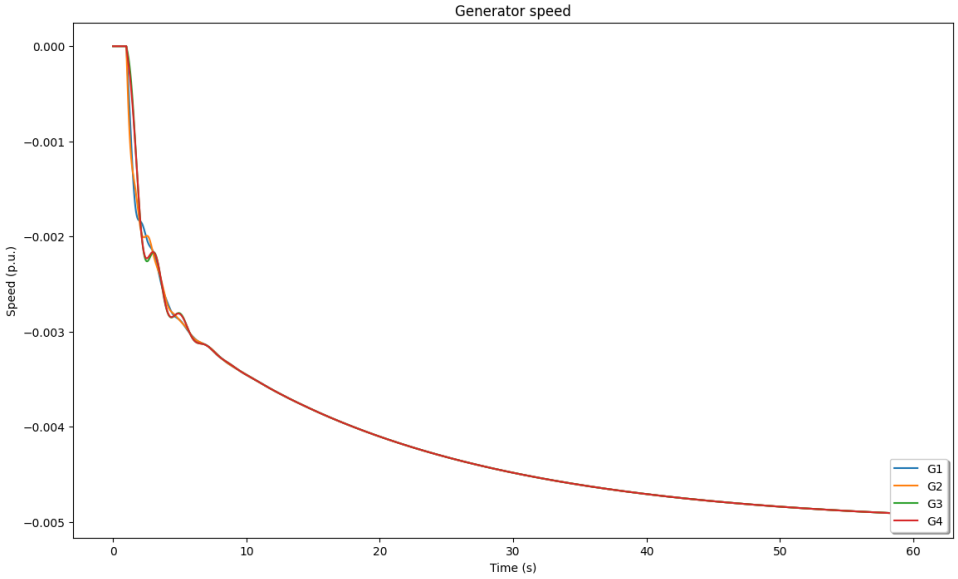

Figure 5.6.2: The generator speed after a load deviation at bus 7 for the base case

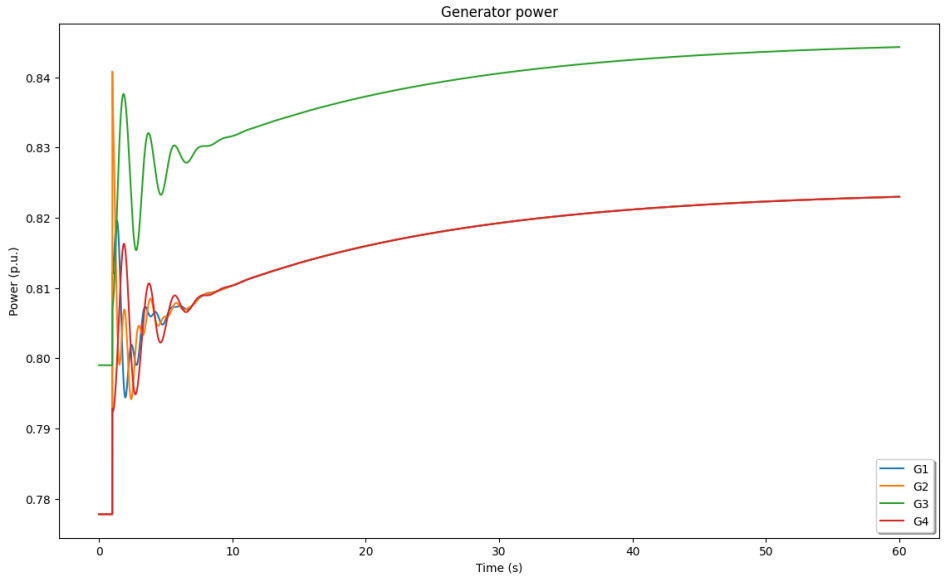

Figure 5.6.3: The generator power after a load deviation at bus 7 for the base case

Figure 5.6.4 depicts the voltage levels at each individual bus in the system. The voltage level is slightly reduced at all buses, except for bus 8 which has a small increase in its voltage level. This is due to the reduction in load flow between the two areas of the K2A system, depicted in figure 5.2.1. The increase in load at bus 7 results in a demand for generation in area 1. As a consequence, there is a reduction in the load flow from area 1 to area 2.

In addition to losses in the system, the drop in voltage level for ten of the eleven buses are the reason for the reduced effect of the intended load deviation.

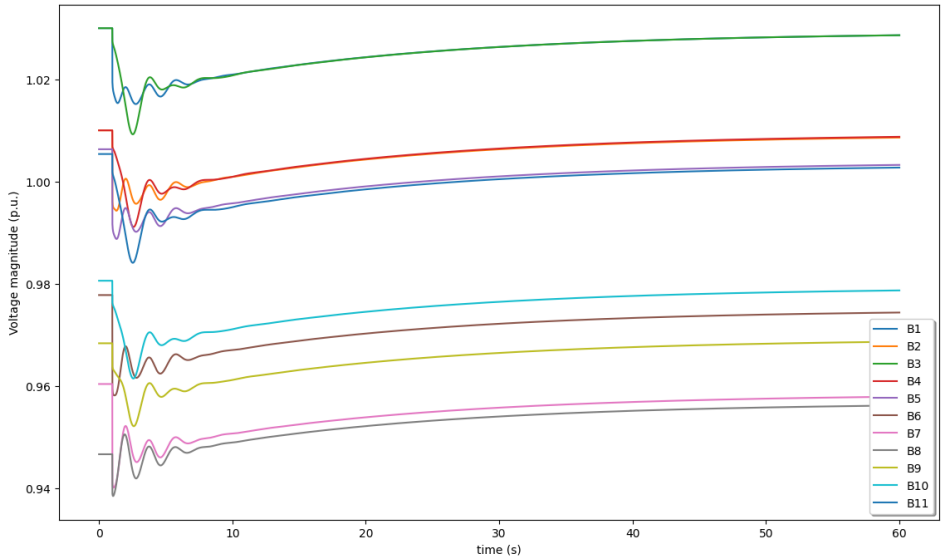

Figure 5.6.4: The bus voltages after a load deviation at bus 7 for the base case

5.6.2 Wind Case

For the wind case, the rating of generator 4 is decreased due to the integration of the wind power plant at bus 9. The three remaining generators have their normal value of active power, as listed in table 5.6.2. The reduction in power rating for generator 4 is necessary because the wind farm would hinder the the power production in generator 3 and 4 if they were to retain their their original rating. Given that bus 3 is the slack bus, it is more advantageous to maintain generator 3 at its original rating while adjusting the rating of generator 4.

Generator	Value	Unit
$G1$	700	MW
$G2$	700	MW
$G3$	719	MW
$G4$	625	MW
$W1$	400	MW

Table 5.6.2: Wind Case Generator Rated Power

In this scenario, the load at bus 7 is increased by 180 MW. This load increase results in a frequency drop of -0.225 Hz.

$$\Delta f = -\frac{\Delta P_{load}}{\beta_{sys}} = -\frac{180MW}{800MW/Hz} = -0.225Hz \tag{5.6.9}$$

This results in a new steady state frequency of $f_\infty = 49.70$ Hz.

The theoretical maximum RoCoF is estimated to be 0.1923 Hz/s.

$$RoCoF = \frac{\Delta P_{load} f_{base}}{2E_{k,sys}} = \frac{180MW \cdot 50Hz}{2 \cdot 23.4GWs} = 0.1923Hz/s \tag{5.6.10}$$

The increase in power for each generation unit is 0.05 per unit, which corresponds to 45 MW.

$$\Delta P_{gen} = -\beta_{gen} \Delta f_{p.u.} S_{base} = \frac{1}{0.12} \cdot 0.0045 \cdot 900 = 33.75MW \tag{5.6.11}$$

Simulation

The system frequency, depicted in figure 5.6.1, drops steeply after the load increase one second into the simulation. After running the simulation for 60 seconds, the system frequency has stabilised at a value of 49.80 Hz. This corresponds well with the theoretical value of 49.70 Hz considering the system don't receive the full effect of the load deviation due the voltage drops at the buses and losses in the system.

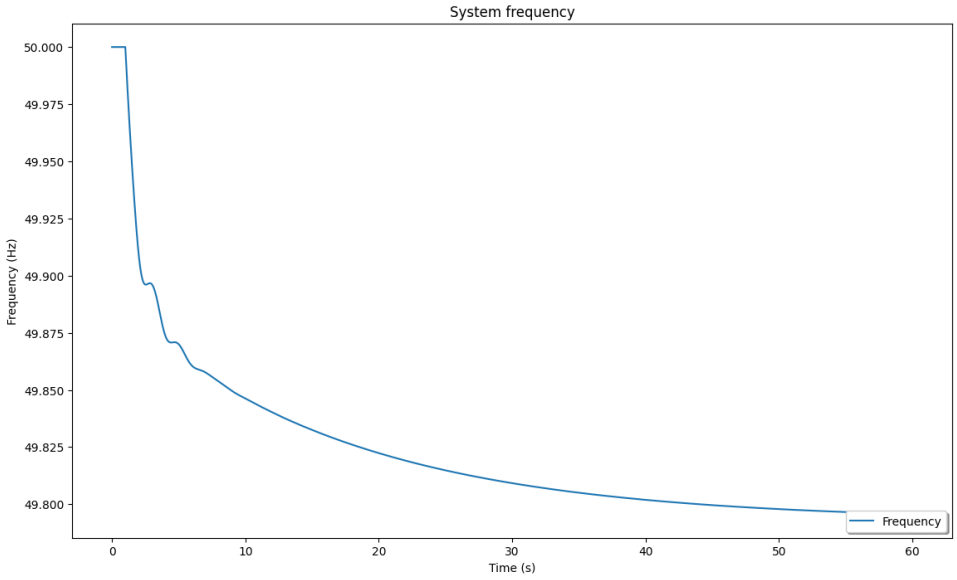

Figure 5.6.5: The system frequency after a load deviation at bus 7 for the wind case

The relation between ΔP and Δf is given by the plot of the generator power. The simulated value is 165 MW/Hz, which corresponds well with the theoretical value of 150 MW/Hz.

$$\frac{\Delta P}{\Delta f} = \frac{P_{gen,end} - P_{gen,start}}{\Delta\omega_{gen} \cdot f_{base}} = \frac{733 - 700}{0.004 \cdot 50} = 165MW/Hz \tag{5.6.12}$$

The relation between ΔP and Δf can also be identified by the plot of the wind farms electrical power provided by the VSC. The simulated value is identical, at 165 MW/Hz. This corresponds well with the value of the theoretical wind farm value of 200 MW/Hz.

$$\frac{\Delta P}{\Delta f} = \frac{P_{vsc,end} - P_{vsc,start}}{\Delta\omega_{gen} \cdot f_{base}} = \frac{187 - 154}{0.004 \cdot 50} = 165MW/Hz \tag{5.6.13}$$

Figure 5.6.6 and 5.6.7 represents the generator speed and generator power respectively. Figure 5.6.8 represents the mechanical and electrical power for the wind farm. The reduction in generator speed is 0.004 per unit, which corresponds to a reduction in generator frequency of 0.2 Hz. The increase in generator power is 0.037 per unit, which corresponds to an increase of 33 MW in each generator. The increase in electrical power in the VSC is identical. This gives a simulated change in load of 164 MW.

$$\Delta P_{load} = \Delta P_{gen} \cdot N_{gen} + \Delta P_{vsc} = 33MW \cdot 4 + 33MW = 165MW \tag{5.6.14}$$

The simulated maximum RoCoF is 0.1762 Hz/s.

$$RoCoF = \frac{\Delta P_{load} f_{base}}{2E_{k,sys}} = \frac{164MW \cdot 50Hz}{2 \cdot 23.4GWs} = 0.1762Hz/s \tag{5.6.15}$$

These are acceptable results as the voltage drop at the buses reduces and losses in the system the effect of the intended load deviation.

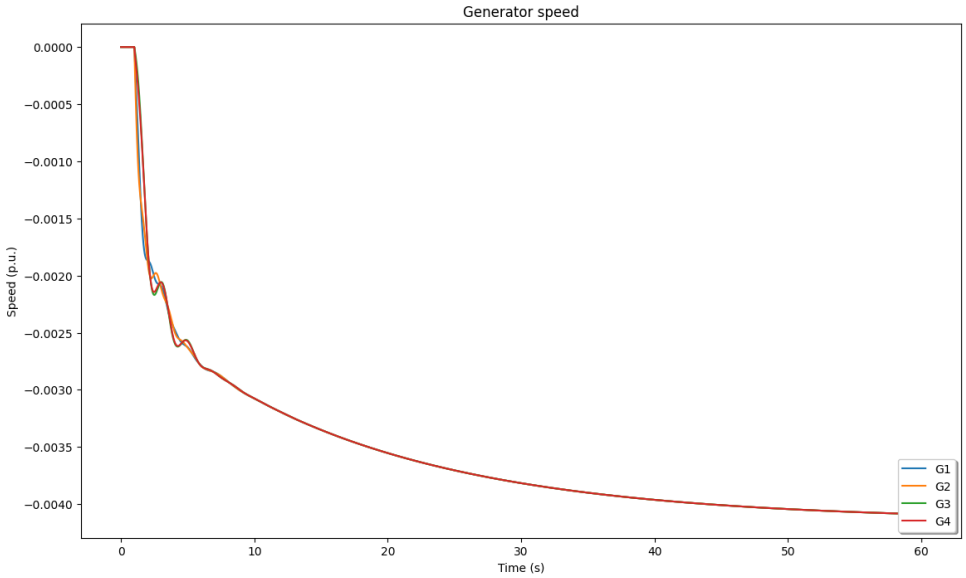

Figure 5.6.6: The generator speed after a load deviation at bus 7 for the wind case

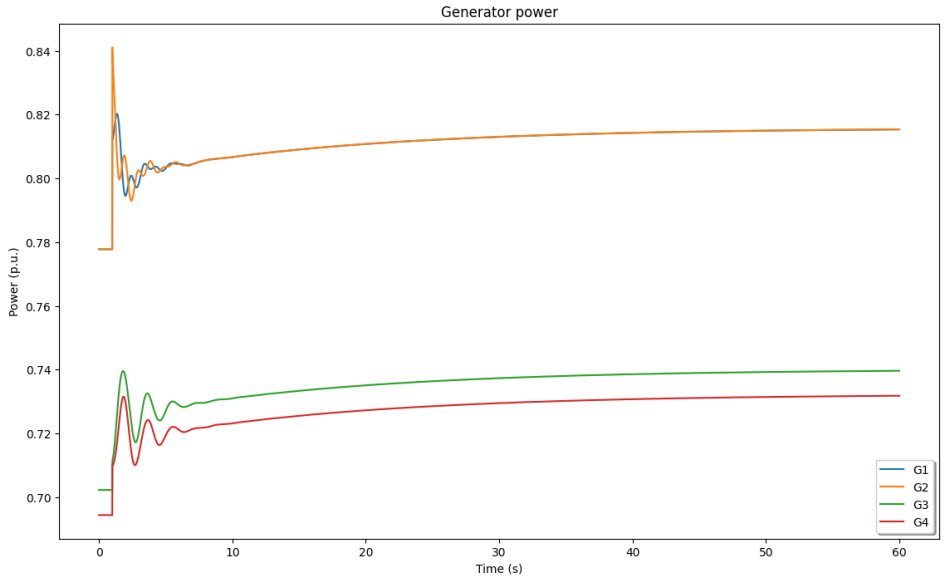

Figure 5.6.7: The generator power after a load deviation at bus 7 for the wind case

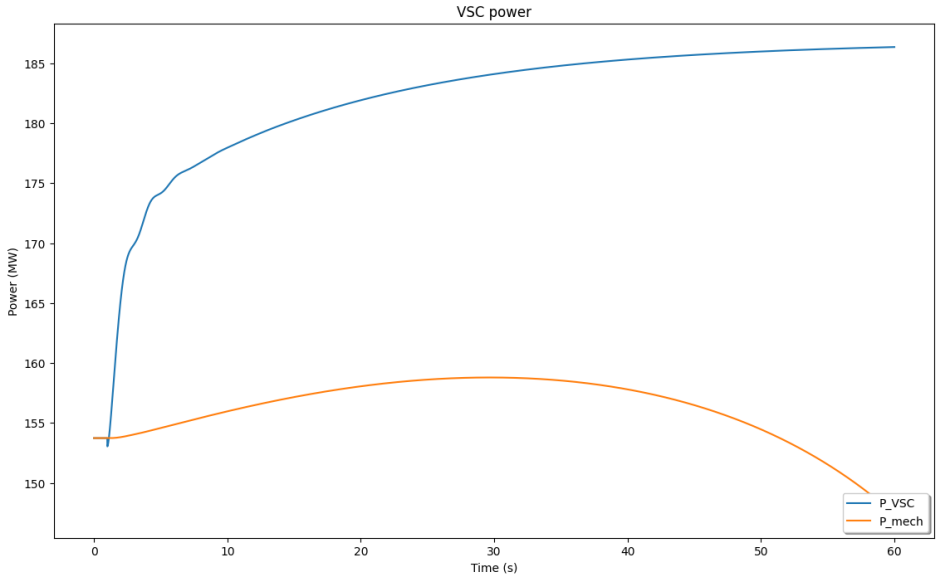

Figure 5.6.8: The wind farm power after a load deviation at bus 7 for the wind case

Figure 5.6.9 is an enhanced depiction of the wind turbines mechanical power. For this scenario the the wind farm provides power to the grid for the full simulation of the load deviation. In reference to figure 4.2.2, having an initial operating point larger than ω_{opt} is beneficial as the wind farm is able to provide generation for a longer period. Figure 5.6.10 depicts the turbines rotor speed. As expected, the rotor speed starts declining after the load increase due to the difference between the wind farms mechanical and electrical power. The deceleration of rotor speed is only temporary and the consequence of reaching excessively low levels will be addressed in the next section.

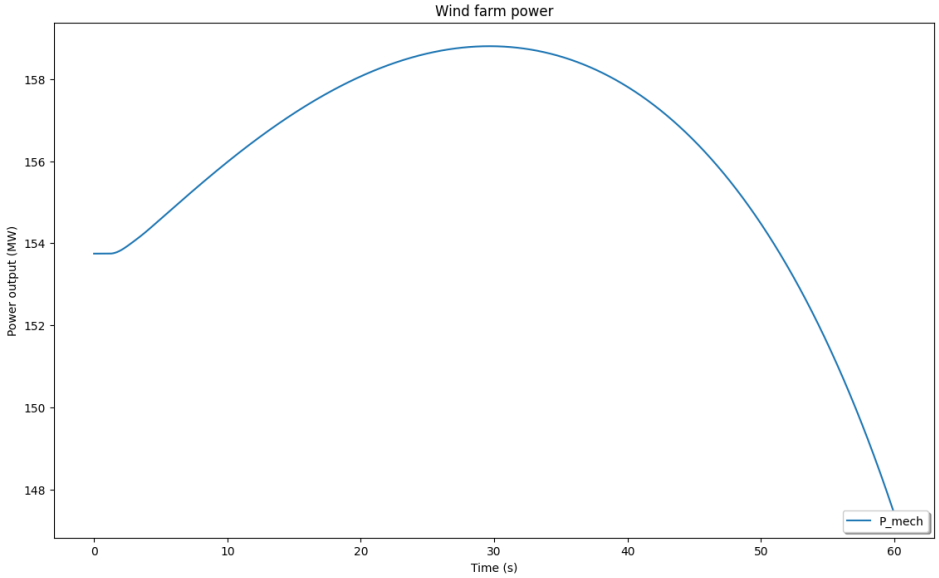

Figure 5.6.9: The mechanical power after a load deviation at bus 7 for the wind case

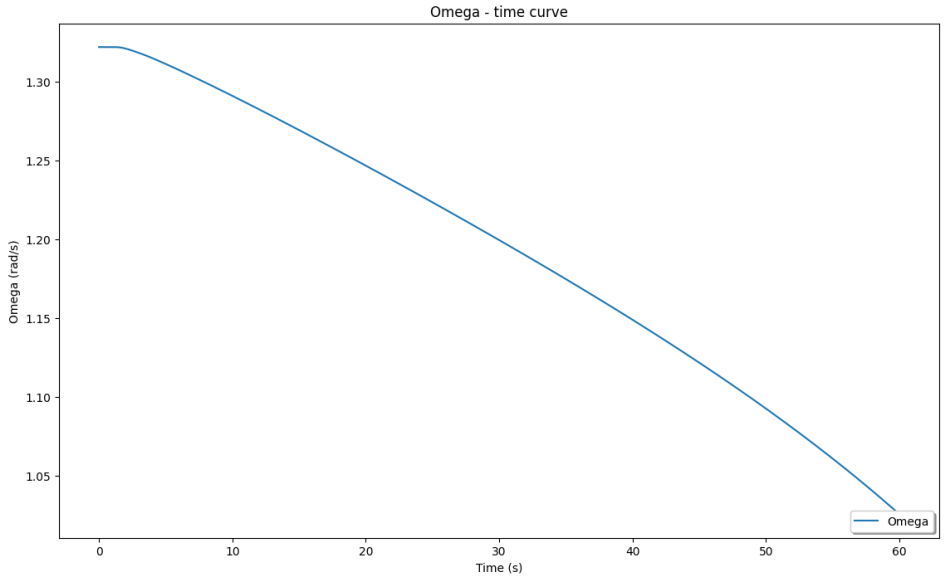

Figure 5.6.10: The rotor speed after a load deviation at bus 7 for the wind case

Figure 5.6.11 depicts the voltage levels at each individual bus in the system. The voltage level is slightly reduced at all buses, except for bus 8 which has a small increase in its voltage level. As with the base case, this is due to the reduction in load flow between the two areas of the K2A system, depicted in figure 5.2.1. The increase in load at bus 7 results in a demand for generation in area 1. As a consequence, there is a reduction in the load flow from area 1 to area 2.

In addition to losses in the system, the drop in voltage level for ten of the eleven buses are the reason for the reduced effect of the intended load deviation.

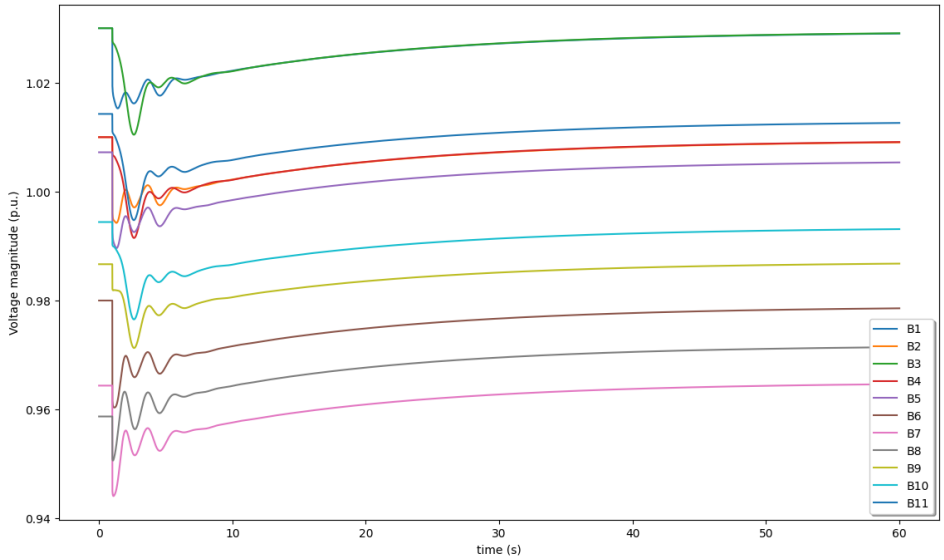

Figure 5.6.11: The bus voltages after a load deviation at bus 7 for the wind case

5.6.3 Extended Wind Case

The extension of the wind case maintains the same rating of all generators, and the same results for changes frequency and power due to the load deviation of 180 MW at bus 7. The objective of the extended simulation is to capture the events of the wind farm recovery stage. The first event is reduction of active power supply to the grid, and the second event is the self recovery stage if additional frequency restoration reserves are introduced. Both the base case and wind case were simulated for a total time of 60 seconds. In the extended simulation, the time frame is doubled, spanning 120 seconds. The preceding subsections have already addressed the initial events, and the focus of this case will be the subsequent events.

In the case of the rotor speed control, a limitation is set for parameter. The initial value, as with the previous cases, is set to 1.32 rad/s. When the rotor speed drops below 0.90 rad/s, the active power supply from the wind farm is reduced. This is achieved by reducing the active power reference by 100 MW in the wind farm controller.

In the case of the self recovery analysis of the wind farm, additional frequency restoration reserves are introduced after 40 seconds. These reserves replace the primary frequency control provided by the wind farm, allowing for autonomous recovery of the wind farm.

Simulation - Power Reduction

The system frequency, depicted in figure 5.6.12, drops steeply after the load increase one second into the simulation. After running the simulation for 60 seconds, the system frequency has stabilised at a value of 49.80 Hz. After 74 seconds the rotational speed of the wind turbines drops below the set limit of 0.9 rad/s and must reduce the active power contribution to the grid. The reduction in active power supply from the wind farm results in a further drop in frequency, giving a new stabilised value of 49.73 Hz.

The active power contribution of the wind farm to the grid reduces the initial drop in frequency by 0.05 Hz during the load deviation compared to the base case. For the wind case this is 49.80 Hz, and for the base case this is 49.75 Hz. After the rotor speed limit is surpassed the new frequency becomes 49.73 Hz, which is a lower than the base case due to the lower contribution of active power from the wind farm.

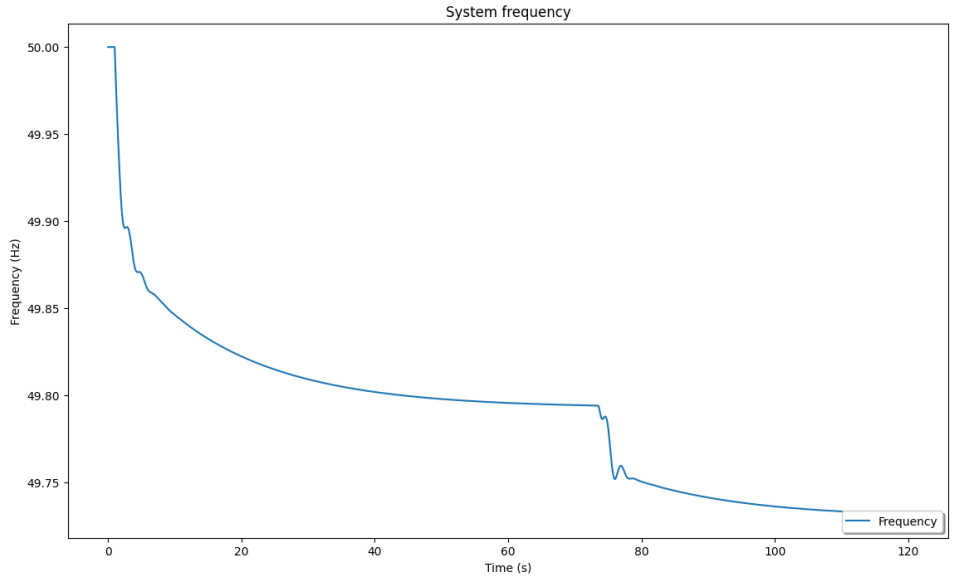

Figure 5.6.12: The system frequency after a load deviation at bus 7 utilising power reduction

Figure 5.6.13 and 5.6.14 represents the generator speed, generator power, and VSC electrical power respectively. The total reduction in generator speed is 0.0054 per unit, which corresponds to a reduction in generator frequency of 0.27 Hz. The total increase in generator power is 0.050 per unit, which corresponds to an increase of 45 MW in each generator.

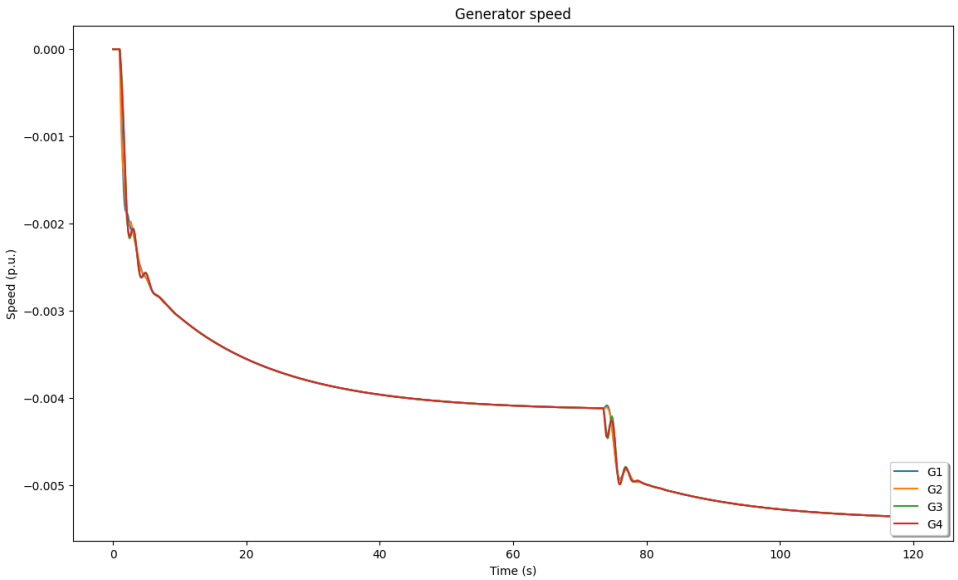

Figure 5.6.13: The generator speed after a load deviation at bus 7 utilising power reduction

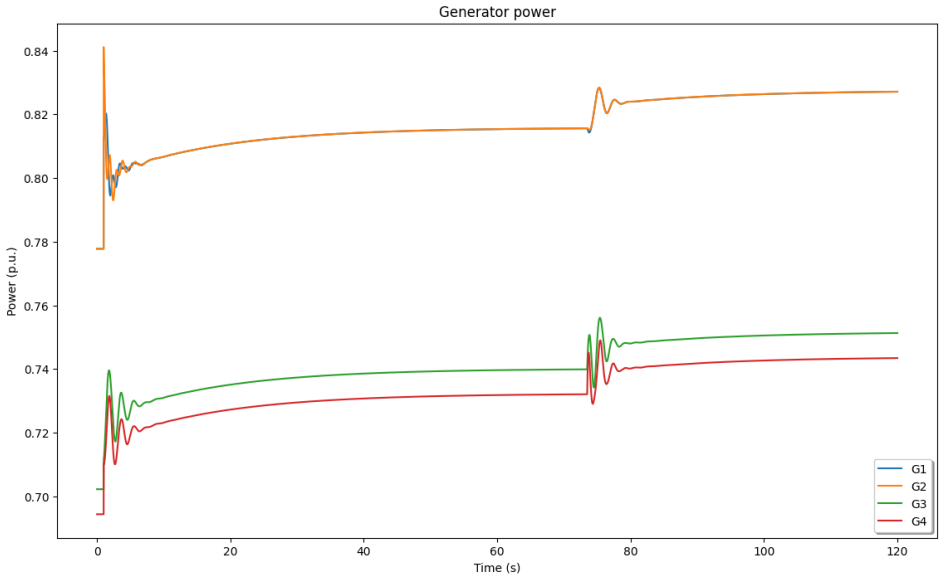

Figure 5.6.14: The generator power after a load deviation at bus 7 utilising power reduction

Figure 5.6.15 is the main focus of this simulation, as it depicts the wind farms mechanical and electrical power. Figure 5.6.23 is an enhanced depiction of the mechanical power, and 5.6.24 depicts the rotor speed. The initial load deviation requires additional power from the wind farm. This causes the electrical power to increase by 33 MW to a value of 187 MW, before decreasing by 70 MW to a new value of 117 MW after the active power supply is reduced. The rotor speed initially decelerates, but after 74 seconds the limit for the rotor speed is reached. After this event, the electrical power output is reduced to a value lower than the mechanical power. This causes the rotor speed to re-accelerate, resulting in an increase of the mechanical power.

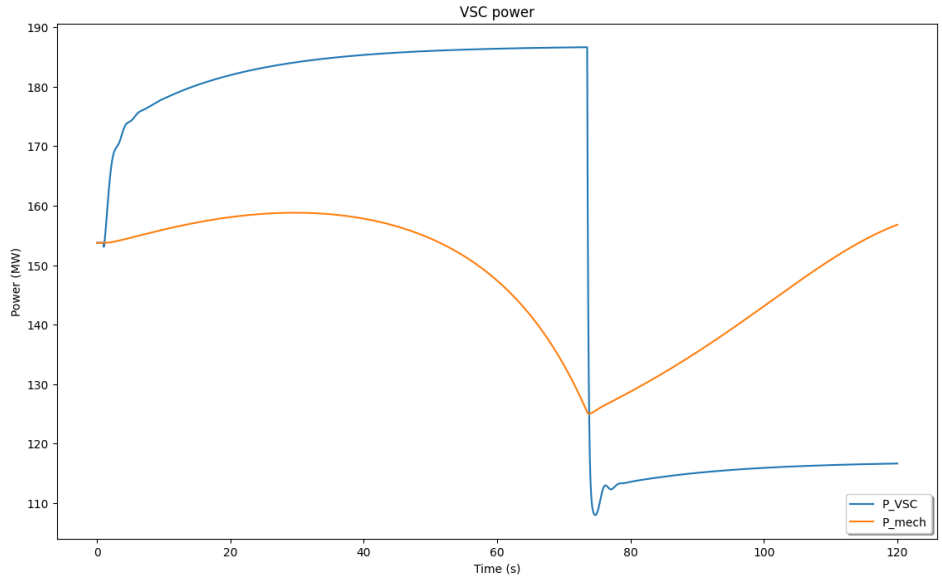

Figure 5.6.15: The wind farm power after a load deviation at bus 7 utilising power reduction

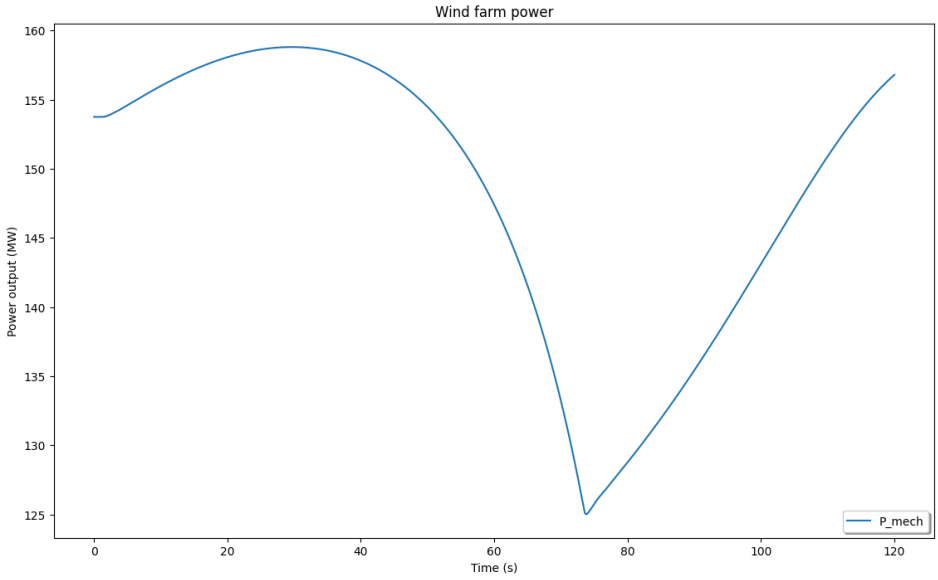

Figure 5.6.16: The mechanical power after a load deviation at bus 7 utilising power reduction

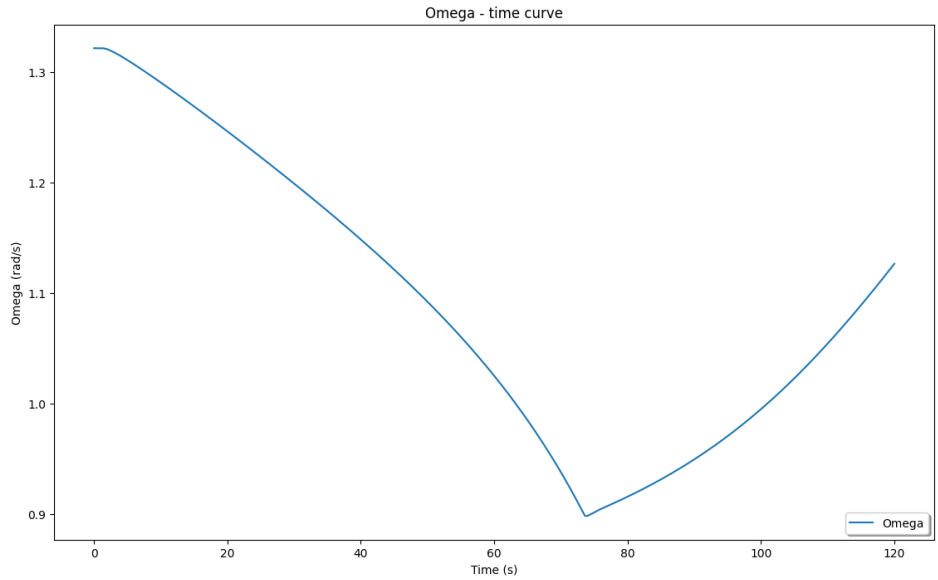

Figure 5.6.17: The rotor speed after a load deviation at bus 7 utilising power reduction

Figure 5.6.18 depicts the voltage levels at each individual bus in the system. The voltage level is slightly reduced at all buses, except for bus 8 which has a small increase in its voltage level. As with the previous cases, this is due to the reduction in load flow between the two areas of the K2A system, depicted in figure 5.2.1. The increase in load at bus 7 results in a demand for generation in area 1. As a consequence, there is a reduction in the load flow from area 1 to area 2.

The extension of the wind case includes a second drop in voltage during the reduction in active

power contribution from the wind farm. All buses have a small reduction in their voltage levels. Bus 8 has a larger reduction in voltage level, as the system receives less power from the wind farm located in area 2, increasing the load flow from area 1 to area 2.

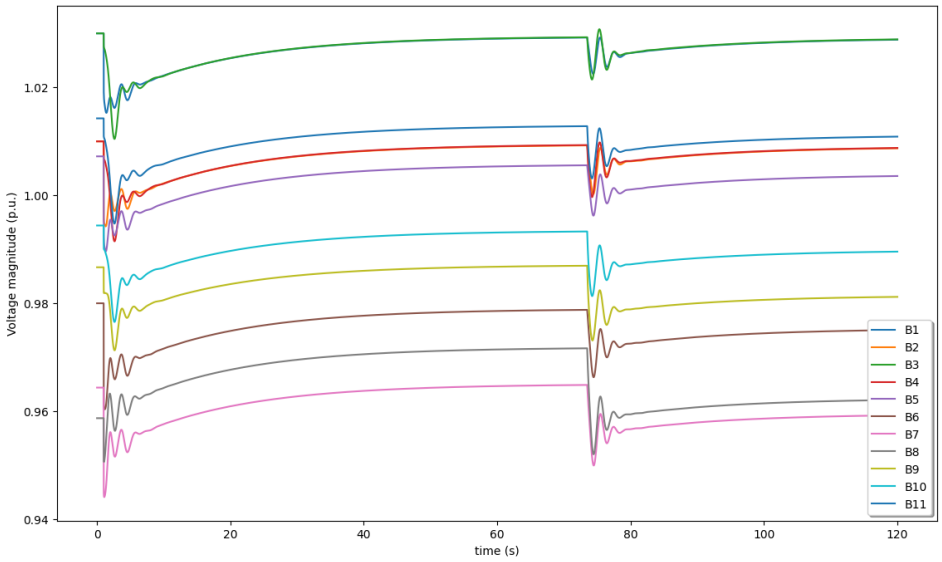

Figure 5.6.18: The bus voltages after a load deviation at bus 7 utilising power reduction

Simulation - Self Recovery

The system frequency, depicted in figure 5.6.19, drops steeply after the load increase one second into the simulation and reaches a value of 49.80 Hz. As with the previous case, the active power contribution of the wind farm to the grid reduces the initial drop in frequency during the load deviation compared to the base case. After 40 seconds additional frequency restoration reserves are introduced, replacing the primary frequency control provided by the wind farm, and the system frequency is restored.

Figure 5.6.19 depicts the system frequency following the initial load increase, and the additional frequency reserves to restore the system's frequency to nominal value.

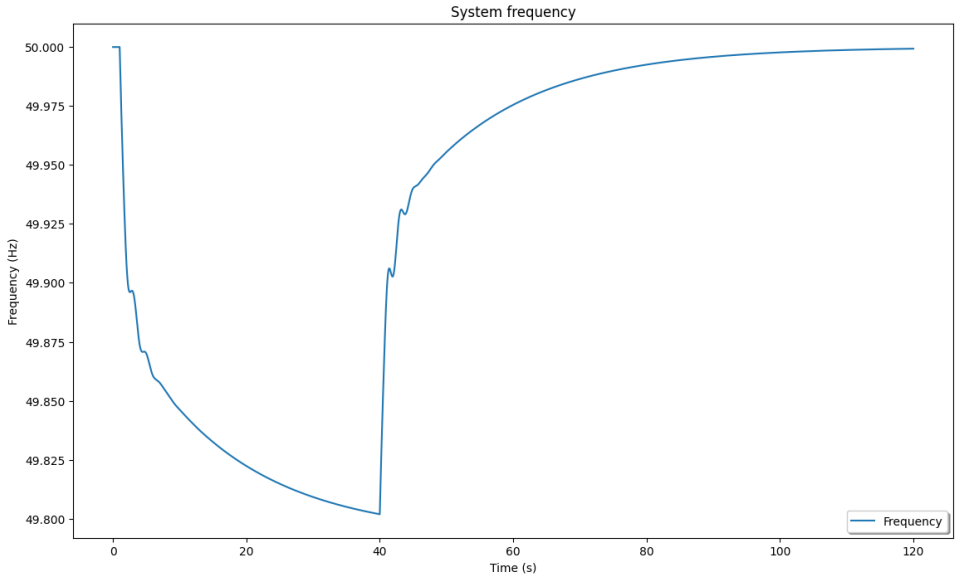

Figure 5.6.19: The system frequency after a load deviation at bus 7 utilising additional FRR

Figure 5.6.20 and 5.6.21 represents the generator speed and power respectively. The generator speed decreases as a consequence of the initial load increase, and is increased to normal value after the introduction of FRR. The generator power is increased as a consequence of the initial load increase, and is reduced to normal value after the introduction of FRR.

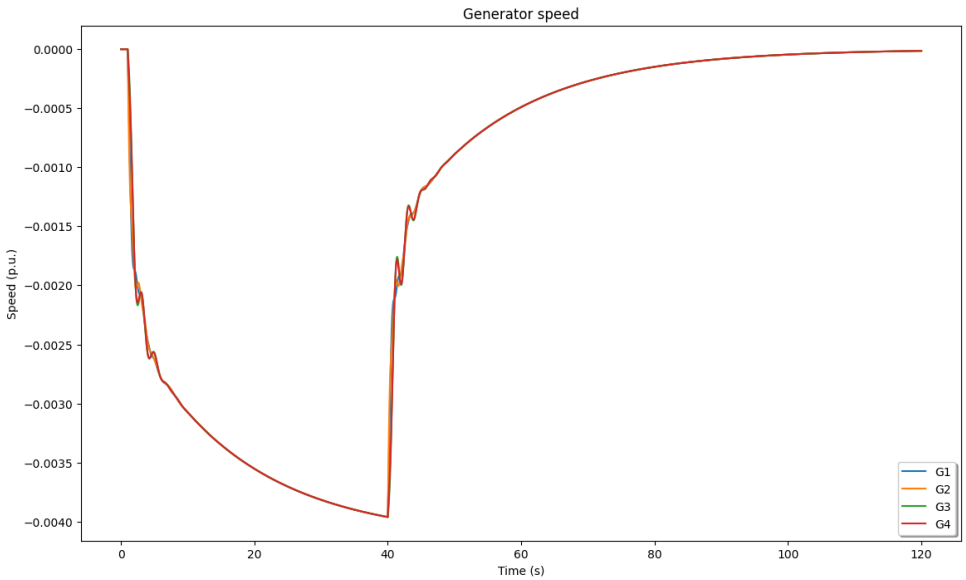

Figure 5.6.20: The generator speed after a load deviation at bus 7 utilising additional FRR

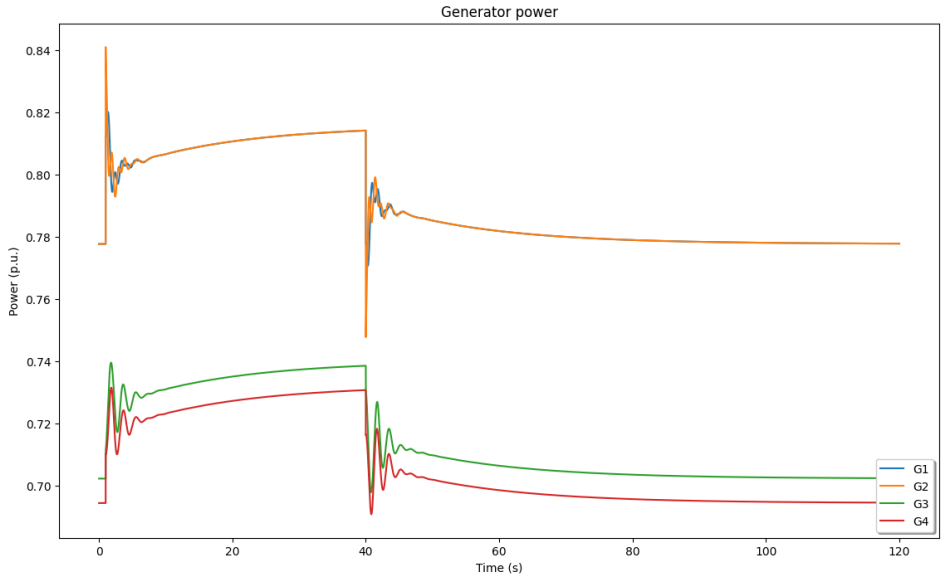

Figure 5.6.21: The generator power after a load deviation at bus 7 utilising additional FRR

Figure 5.6.22 is the main focus of this simulation, as it depicts the wind farms mechanical and electrical power. Figure 5.6.23 is an enhanced depiction of the mechanical power, and 5.6.24 depicts the rotor speed. The initial load deviation requires additional power from the wind farm. This causes the electrical power to increase, which causes the rotor speed to decelerate. The mechanical power initially increases due to the initial operating point on the $C_P - \lambda$ curve, but decreases after the passing of the optimal rotor speed. After 40 seconds frequency restoration reserves are introduced, and the grid no longer requires the provision of synthetic inertia from the wind farm. The electrical power returns to normal value, and the mechanical power increases.

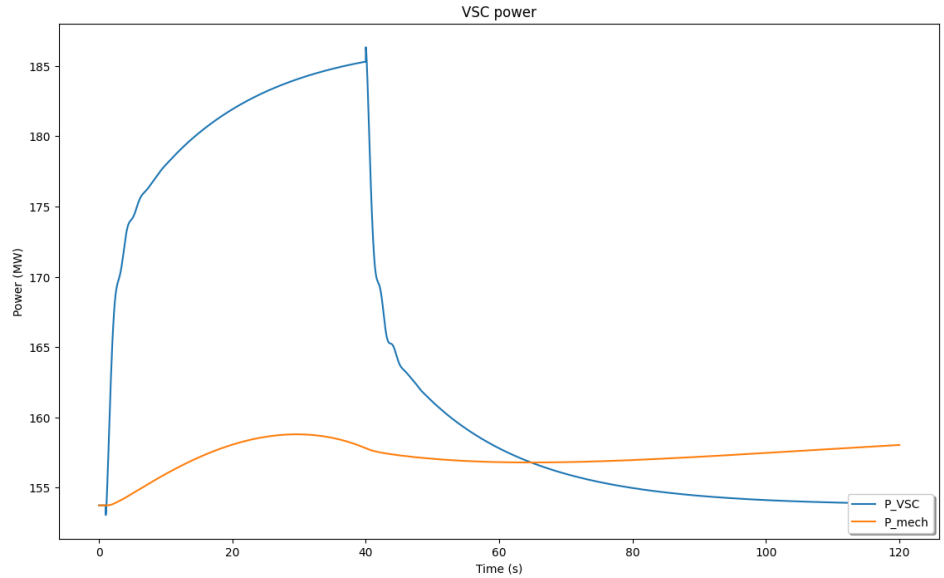

Figure 5.6.22: The wind farm power after a load deviation at bus 7 utilising additional FRR

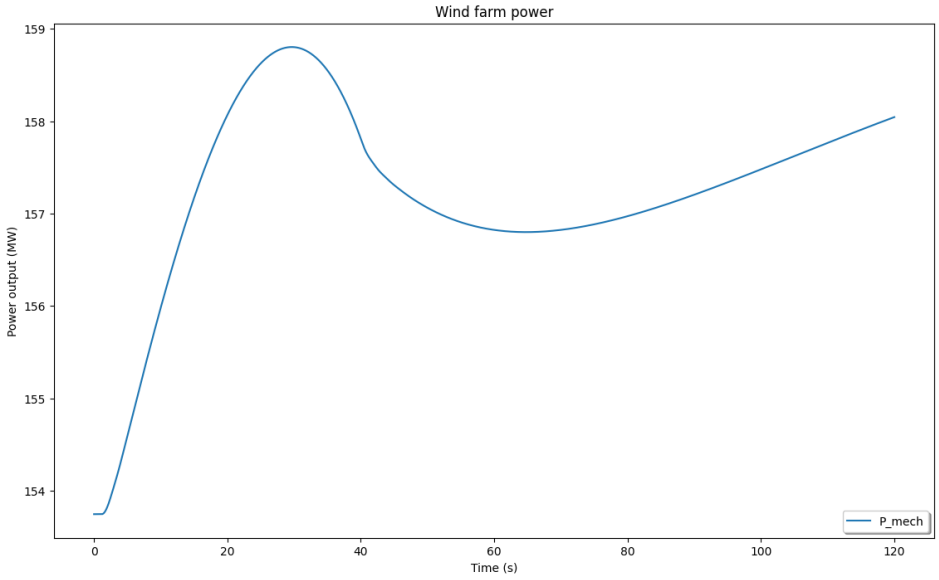

Figure 5.6.23: The mechanical power after a load deviation at bus 7 utilising additional FRR

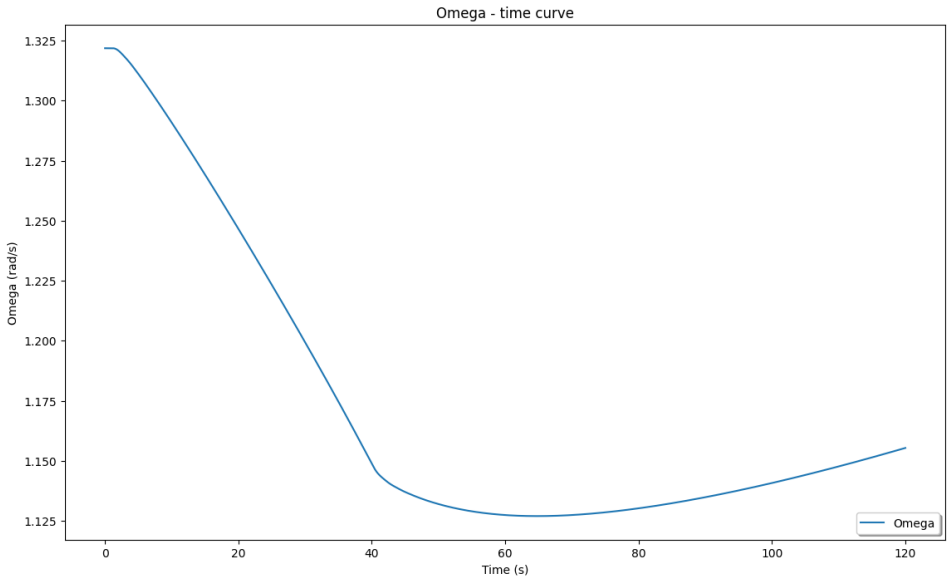

Figure 5.6.24: The rotor speed after a load deviation at bus 7 utilising additional FRR

Figure 5.6.25 depicts the voltage levels at each individual bus in the system. The voltage level is initially reduced at all buses, except for bus 8 which has an increase in its voltage level. As with the previous cases, this is due to the reduction in load flow between the two areas of the K2A system, depicted in figure 5.2.1. The increase in load at bus 7 results in a demand for generation in area 1. As a consequence, there is a reduction in the load flow from area 1 to area 2.

The self recovery simulation of the wind case includes a rise in voltage levels for all buses, except

for bus 8 which gets a reduction in voltage level after the introduction of frequency restoration reserves at 40 seconds, as all buses returns to their initial voltage levels.

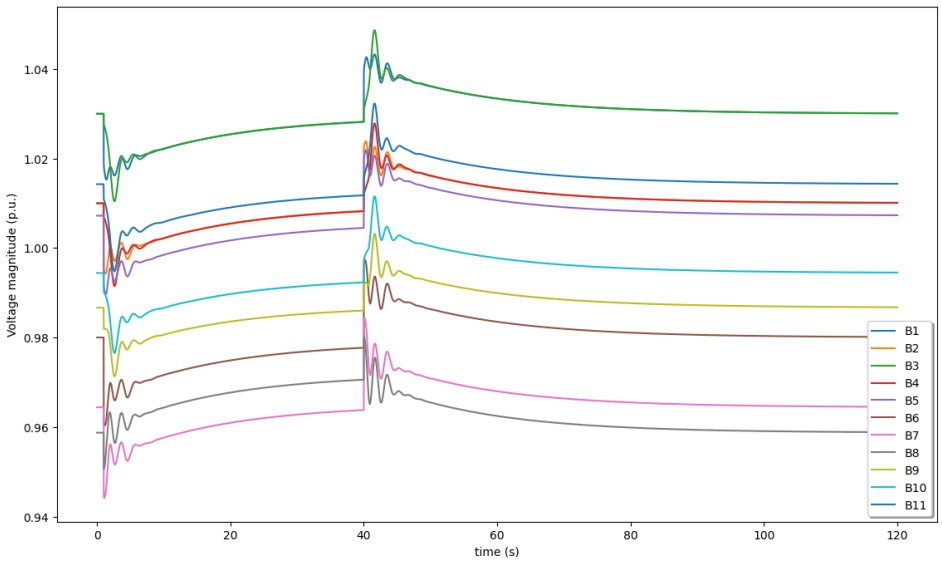

Figure 5.6.25: The bus voltages after a load deviation at bus 7 utilising additional FRR

Chapter 6

Discussion

The proposed wind farm model is used to emulate frequency control and inertia in the power system. Even for it's simplicity, it is useful in the provision of frequency support during both planned and unplanned events in the power system. Several simulations have been carried out using the well known Kundur's Two-Area System. At the rated power output of 400 MW, the wind farm would account for nearly 15% of generation in the system. For the simulation, a more realistic value of generation is used. Due to the short duration of the simulation, a constant wind speed was used to calculate the mechanical power of the wind turbines. Using the average wind speed at Dogger Bank as a reference, the simulation was carried out with a wind speed of 10 m/s, which gives a power output in the area of 150 MW depending on the power coefficient. This accounts for 5-6% of the total generation in the K2A system. Even with a relatively low percentage of power contribution, the presence of the wind farm in the system contributes to the robustness and stability of the system.

Additionally, all simulated results align with the theoretical values within reason, accounting for power system losses, voltage levels, and measurement errors. This consideration ensures that the simulated outcome remain consistent with the expected behaviour of the system, despite accounting for various factors that may cause deviations in the measurements.

6.1 Wind Farm Contribution

For the simulation, a load increase of 180 MW at bus 7 was studied. This represents an increase of approximately 6.5% of the system's total load. The active power contribution from the wind farm proved beneficial for frequency control, granting a higher steady state frequency after the load deviation.

For the base case, the load increase of 180 MW initially produced a frequency drop of -0.25 Hz. Including the wind farm in the simulation, this frequency deviation was reduced to -0.20 Hz. The inclusion of the wind farm reduces the stress on the other generators in the system during the load deviation, making for a lower reduction in the generator frequency. Although the wind farm's frequency support, regarded as primary frequency control, reduces the initial impact of the load deviation, additional services must be provided to restore the system frequency to nominal value.

In the base case, the power output of each generator is increased by 41 MW. This gives a total generation increase of 164 MW for the system containing four generators. When incorporating the wind farm, the power output of each generator is increased by only 33 MW. The total increase in generation remains roughly the same, as five generators contributing 33 MW gives a total of 165 MW. The base case and wind case therefore yield consistent results.

It is important to note that the theoretical load increase for the simulation is 180 MW. This does not perfectly correspond with the simulated generation increase of 165 MW. Several factors contribute to the difference between simulated and theoretical values. For both the base case and the wind case, the voltage levels for all buses are reduced slightly, except bus 8 which experiences an increase in voltage level due to the reduction in load flow between the two areas of the system. The reduction in voltage level can introduce deviations in the simulation results compared to the theoretical values.

Measurement errors represent another significant factor contributing to the deviation between simulated and theoretical values. The simulated values are obtained from plots which may introduce inaccurate readings and subsequently impact the overall accuracy of the simulated outcomes.

6.2 Contribution for an Extended Time Period

In response to the load deviation, the wind farm increases its contribution of power to the grid by receiving an active power reference in the voltage source converter, provided by the synthetic inertia regulator. The sudden increase in load releases a portion of the kinetic energy stored within the rotating masses present in the system, causing a deviation in the system frequency. The synthetic inertia regulator monitors the frequency deviation actively, and subsequently signals the wind farm to provide additional power to the grid in order to compensate for the deviation.

During the provision of synthetic inertia to the grid as a response to the load deviation, kinetic energy is extracted from the wind turbines. As a consequence, the rotor speed of the turbine starts decelerating, leading to changes in the mechanical power according to the $C_P - \lambda$ characteristic. When the initial rotor speed value is situated on the left side of the $C_P - \lambda$ curve, there is a direct decrease in mechanical power due of the continuous deceleration of rotor speed. Conversely, when the initial rotor speed value is situated on the right side of the $C_P - \lambda$ curve, there is an initial increase in mechanical power until the optimal rotor speed is achieved, after which the mechanical power starts decreasing. This is beneficial for the provision of synthetic inertia as the wind farm is able to provide support for an extended duration.

Without control of the wind farms rotor speed, deceleration would continue until the turbine eventually stalls due to reaching excessively low levels. To prevent this from happening, governor control is introduced for the wind turbines. A control action is implemented, reducing the active power output after the transient contribution of the wind farm is completed, or when the rotor speed reaches a limit set by the governor. In this simulation, the load increase is permanent and a the rotor speed becomes the limit for the wind farm. Reducing the active power output allows the wind farm to enter a recovery state, where the turbines mechanical power is larger than the electrical power. This causes the rotor speed to accelerate, according to equation 5.5.1. During the re-acceleration of the rotor speed, the mechanical power starts increasing according to the $C_P - \lambda$ characteristic, and kinetic energy is recovered. Once the kinetic energy has reached a satisfying

level, the wind farm can resume normal operation at optimal rotor speed again.

Another advantage of having the initial rotor speed value on the right side of the $C_P - \lambda$ curve is the case where the load returns to its normal value after a few seconds. In this case, a reduction of active power in the wind farm is not necessary as the wind turbines are able to re-accelerate by themselves. After the initial decrease rotor speed, the turbines mechanical power increases before reaching optimal speed, resulting in a decreasing value of mechanical power. If the load is reduced back to normal value before the point corresponding to the starting point on the left side of the $C_P - \lambda$ curve is reached, the turbines mechanical power is greater than the electrical power. This stops the deceleration of the turbines, and the wind farm is able to recover by itself without reducing its active power output.

6.3 Modelling and Software

The DynPSSimPy software has been utilised to represent the wind farm dynamics within an isolated power system. The simulations have been conducted using Kundur's Two Area Test system as the power system model. Employing the developed wind farm model within the DynPSSimPy, provides the necessary tools and capabilities to accurately model and analyse the behaviour of both the wind farm and the power systems dynamics for the specific power system configuration. The combination of the software and the power system model contributes for a deeper understanding of their behaviour and performance,

6.3.1 DynPSSimPy

The utilisation of DynPSSimPy has provided considerably flexibility for this thesis, as it is a non-commercial open source software package designed for performing dynamic simulations of small- and medium-sized power systems. While the software offers many advantages, there are also a few drawbacks to consider. The software being written entirely in the Python contributes to its user-friendliness and ease of use, due to the widespread popularity and familiarity of the programming language. In addition, the open source nature of the software enables the implementation of various simulation models without any boundaries.

On the other hand, it is worth noting that getting familiar with the software is time consuming, due to the large amount of different variables and functions involved. Additionally, validation of the written code and corresponding results has presented its own set of challenges. Still, through working effort, these challenges have been overcome, leading to satisfying outcomes.

Overall, the utilisation of DynPSSimPy has provided a useful platform for dynamic power system simulations, and has proven to be an incredible valuable asset in this thesis.

6.3.2 Kundurs's Two Area System

Kundur's Two Area System, being a small-sized power system, is well-suited to the DynPSSimPy software. Despite the simplicity of the system, it provides an effective mean to capture a realistic depiction of the behaviour of both the wind farm and the power system during a transient event.

Chapter 7

Conclusion

The growing proportion of renewable energy sources in the overall generation mix has significant implications for frequency regulation in modern power systems. As renewable energy sources are unable to act as spinning reserves in the power system, the system's total inertia is reduced. However, due to the fast response capabilities of the electronic controllers, some renewable energy sources can provide frequency support during a transient event in the power system.

In this thesis, the frequency control has been evaluated for a variable speed wind power plant connected to an isolated grid. Initially, a base case was established using Kundur's Two Area System to examine the systems behaviour during a load deviation. Subsequently, the wind farm model was incorporated in the same power system configuration to examine the frequency support and impact of synthetic inertia provided by the wind farm.

Additionally, two scenarios involving continuous support from the wind farm over an extended time period was examined. In the first scenario, continuous support was provided until the wind farm controller is forced to take action due to the excessively low rotational speed of the turbines, reducing the active power output to allow the wind farm to recover. In the second scenario, frequency restoration reserves were introduced, subsequently replacing the primary control reserve provided by the wind farm. This enabled the autonomous restoration of the wind farm without external intervention after providing synthetic inertia.

The provision of frequency support from a variable speed wind power plant shows promising results in enhancing the stability of the power system. The integration of the wind farm in the power system reduces the initial drop in frequency during the load deviation. In larger commercial power systems, frequency restoration reserves are more abundant, enabling the self-recovery of the wind farm in most scenarios. When the wind farm can autonomously restore its operation, it can quickly resume the providing support to the power system in case of a new transient event.

It is important to acknowledge the advantage of initially operating on the right side of the $C_P - \lambda$ curve. Even though the wind farm operates below optimal level during normal conditions, it is advantageous in the case of a loss of generation or a load increase, as the wind farm must provide support to the grid. By initially operating on the right side of the curve, the wind farm can provide support for a significantly longer duration compared to initially operating on the left side. This is true for both cases of the extended simulation. Operating on the right side allows the wind farm to avoid reaching the rotor speed limit quickly, enabling it to provide support for a longer

duration. The same principle applies when introducing frequency restoration reserves to replace the primary control. By operating on the right side of the curve, the wind farm takes time to reach the corresponding point on the left side, allowing it to autonomously recover without reducing its power output if the replacing reserves are introduced early enough.

It is still important to note the extensive drop in system frequency in the absence of additional frequency restoration reserves. Reducing the wind farms active power output to prevent the turbines from stalling causes an increase in the frequency drop compared to the base case. This highlights the importance of having other sources of frequency reserves to ensure safe and stable operation of the power system. While the wind farm can provide valuable support during abnormal conditions, it must be noted that the contribution is only temporary. Relying solely on the wind farm for frequency control is not sufficient for maintaining the frequency levels over an extended period.

Further Work

The wind farm model employed in this thesis represents a simplified configuration compared to the actual setup of a wind farm. The voltage source converter is the main controller responsible for the interaction between the wind farm and the grid. The converter is modelled to use both frequency and voltage control. In reality, wind turbines are typically interfaced with converters using pulse width modulation. Including this level of detail in the model would provide a more realistic depiction of the frequency support capabilities provided by the wind farm.

The time frame for the simulation is very short, which serves the specific objective of this thesis. Maintaining a constant wind speed for the duration of the simulation, the need for speed or pitch control of the turbines is removed. However, simulation for an extended period incorporating varying wind speeds would allow for a more comprehensive analysis of the wind farms performance by the use of speed and pitch control. Implementing speed control techniques, such as maximum power point tracking, would enable the turbines to optimise power production by adjusting the rotor speed and the operating point on the wind power curve accordingly. Additionally, integrating pitch control, modifying the pitch angle β would alter the $C_P - \lambda$ curve, resulting in an enhanced variation of the mechanical power produced in the wind turbines.

Kundur's Two Area System is a simple power system. While it serves useful for conducting simulations of specific objectives like in this thesis, exploring the effects of wind energy and synthetic inertia in a larger power system would be interesting. The contribution of a single wind farm has limited impact in a larger power system due to its relatively small capacity. However, integrating multiple wind farms in the system would lead to a significant aggregated contribution of synthetic inertia. This could play a crucial role in enhancing the stability in the power system during a transient event, as the system would benefit from the increased availability of synthetic inertia, which helps mitigate frequency deviations.

Bibliography

[1] Mahamat A. Abdraman et al. 'Wind resource assessment in the city of N'Djamena in chad'. In: *International Journal of Renewable Energy Research* 6.3 (2016). ISSN: 13090127. DOI: 10.20508/ijrer.v6i3.4066.g6885.

[2] AEMO. *Energy Explained: Frequency Control*. July 2020.

[3] Olimpo Anaya-Lara. *EE967 Power System Design, Operation and Protection - Frequency control*. University of Strathclyde, 2022.

[4] Olimpo Anaya-Lara. *TET4575 Power System Operation and Analysis*. NTNU, 2022.

[5] Maggie Mae Armstrong. *Cheat sheet: What is Digital Twin?* 2020.

[6] Center for Sustainable Systems. *Wind Energy Factsheet*. Tech. rep. University of Michigan, 2022.

[7] Peiyuan Chen et al. *Inertial Support from Variable Speed Wind Turbines*. Tech. rep. Energiforsk, 2018.

[8] Jovana Dakic et al. 'HVAC Transmission System for Offshore Wind Power Plants including Mid-Cable Reactive Power Compensation: Optimal Design and Comparison to VSC-HVDC Transmission'. In: *IEEE Transactions on Power Delivery* 36.5 (Oct. 2021), pp. 2814–2824. ISSN: 19374208. DOI: 10.1109/TPWRD.2020.3027356.

[9] Sawata R. Deore, Pranav B. Darji and Anil M. Kulkarni. 'Switching function analysis of half- and full-bridge modular multi-level converters for HVDC applications'. In: *IET Generation, Transmission and Distribution* 7.11 (2013). ISSN: 17518687. DOI: 10.1049/iet-gtd.2012.0034.

[10] Hasala Dharmawardena, Kjetil Uhlen and Sverre S. Gjerde. 'Modelling wind farm with synthetic inertia for power system dynamic studies'. In: *2016 IEEE International Energy Conference, ENERGYCON 2016*. Institute of Electrical and Electronics Engineers Inc., July 2016. ISBN: 9781467384636. DOI: 10.1109/ENERGYCON.2016.7514098.

[11] Stuart Burnet Donovan. 'Wind flow modelling and wind farm layout optimisation'. PhD thesis. Auckland: Univeristy of Auckland, Feb. 2016.

[12] Electrical Academia. *Swing Equation in Power System*. 2023. URL: https://electricalacademia.com/electric-power/swing-equation-power-system/.

[13] Electrical Technology. *Difference between hvac and hvdc*. June 2020. URL: https://www.electricaltechnology.org/2020/06/difference-between-hvac-hvdc.html.

[14] Electricity Maps. *Warm weather and energy efficiency decreased electricity consumption in Europe - 2022 review*. Feb. 2023. URL: https://www.electricitymaps.com/blog/2022-europe-review#:~:text=%E2%80%8D2022%20REVIEW%3A%20In%202022%2C%20electricity,one%20reason%20for%20this%20decrease..

[15] Enerdynamics. *Power system stabilizer (PSS)*. 2022. URL: https://www.energyknowledgebase.com/topics/power-system-stabilizer-pss.asp#:~:text=A%20power%20system%20stabilizer%20(PSS,does%20not%20stray%20beyond%20tolerances..

[16] International Energy Agency. *Offshore Wind Outlook 2019: World Energy Outlook Special Report*. Tech. rep. 2019. URL: www.iea.org/t&c/.

[17] Mircea Eremia and Mohammad Shahidehpour. *Handbook of Electrical Power System Dynamics: Modeling, Stability, and Control*. John Wiley and Sons, Feb. 2013. ISBN: 9781118497173. DOI: 10.1002/9781118516072.

[18] European Environment Agency. *Share of energy consumption from renewable sources in Europe (8th EAP)*. June 2023. URL: https://www.eea.europa.eu/ims/share-of-energy-consumption-from#:~:text=Europe%20(8th%20EAP)-,Share%20of%20energy%20consumption%20from%20renewable%20sources%20in%20Europe%20(8th,same%20level%20as%20in%202020..

[19] Jeewan Garg. *Automatic Voltage Regulator*. June 2017. URL: https://circuitglobe.com/automatic-voltage-regulator.html.

[20] F. González-Longatt, P. P. Wall and V. Terzija. 'Wake effect in wind farm performance: Steady-state and dynamic behavior'. In: *Renewable Energy* 39.1 (Mar. 2012), pp. 329–338. ISSN: 09601481. DOI: 10.1016/j.renene.2011.08.053.

[21] Hallvar Haugdal, Kjetil Uhlen and Hjortur Johannsson. 'An Open Source Power System Simulator in Python for Efficient Prototyping of WAMPAC Applications'. In: *2021 IEEE Madrid PowerTech, PowerTech 2021 - Conference Proceedings*. 2021. DOI: 10.1109/PowerTech46648.2021.9494770.

[22] Graeme Hawker and Julian Feuchtwang. *EE977 Wind Energy and Distributed Energy Resources - Wind Resource*. 2021.

[23] Muhammad Nizam Kamarudin et al. 'Review on load frequency control for power system stability'. In: *Telkomnika (Telecommunication Computing Electronics and Control)* 19.2 (Apr. 2021), pp. 638–644. ISSN: 23029293. DOI: 10.12928/TELKOMNIKA.v19i2.16118.

[24] Camilo I. Martínez-Márquez et al. 'Small wind turbine emulator based on lambda-Cp curves obtained under real operating conditions'. In: *Energies* 12.13 (2019). ISSN: 19961073. DOI: 10.3390/en12132456.

[25] Met Office. *How we measure wind*. 2022. URL: https://www.metoffice.gov.uk/weather/guides/observations/how-we-measure-wind#:~:text=Wind%20speed%20is%20normally%20measured,causes%20the%20spindle%20to%20rotate..

[26] Johan Morren, Jan Pierik and Sjoerd W.H. de Haan. 'Inertial response of variable speed wind turbines'. In: *Electric Power Systems Research* 76.11 (July 2006), pp. 980–987. ISSN: 03787796. DOI: 10.1016/j.epsr.2005.12.002.

[27] Jayshree Pande et al. *A review of maximum power point tracking algorithms for wind energy conversion systems*. 2021. DOI: 10.3390/jmse9111187.

[28] Petrotech. *What Is the Function of a Governor in a Steam Turbine?* 2017. URL: What%20Is%20the%20Function%20of%20a%20Governor%20in%20a%20Steam%20Turbine?.

[29] Syed Rahman et al. *A comparison review transmission mode for onshore integration of offshore wind farms: HVDC or HVAC—A comparison review*. June 2021. DOI: 10.3390/electronics10121489.

[30] Joan Rocabert et al. 'Control of power converters in AC microgrids'. In: *IEEE Transactions on Power Electronics* 27.11 (2012). ISSN: 08858993. DOI: 10.1109/TPEL.2012.2199334.

[31] Ebrahim Rokrok. 'Grid-forming control strategies of power electronic converters in transmission grids: application to HVDC link'. PhD thesis. 2022.

[32] Rolls Royce. *What is the difference between grid forming and grid following?* 2022. URL: https://rolls-royce-solutions.de/ufaqs/what-is-the-difference-between-grid-forming-and-grid-following/.

[33] Pontus Roos. 'A Comparison of Grid-Forming and Grid-Following Control of VSCs'. PhD thesis. Uppsala University, 2020.

[34] Jonas Eidsvåg Rostad. 'Power System Response to a Variable Speed Wind Power Plant'. PhD thesis. Trondheim: NTNU, 2022.

[35] Aitor Saenz-Aguirre et al. 'Kharitonov Theorem Based Robust Stability Analysis of a Wind Turbine Pitch Control System'. In: *Mathematics* 8.6 (June 2020), p. 964. ISSN: 2227-7390. DOI: 10.3390/math8060964.

[36] Sandip Sharma, Shun-Hsien Huang and N.D.R. Sarma. 'System Inertial Frequency Response estimation and impact of renewable resources in ERCOT interconnection'. In: *2011 IEEE Power and Energy Society General Meeting*. IEEE, July 2011, pp. 1–6. ISBN: 978-1-4577-1000-1. DOI: 10.1109/PES.2011.6038993.

[37] Vaishali Sohoni, S. C. Gupta and R. K. Nema. 'A Critical Review on Wind Turbine Power Curve Modelling Techniques and Their Applications in Wind Based Energy Systems'. In: *Journal of Energy* 2016 (2016), pp. 1–18. ISSN: 2356-735X. DOI: 10.1155/2016/8519785.

[38] Constantinos Sourkounis and Pavlos Tourou. 'Grid Code Requirements for Wind Power Integration in Europe'. In: *Conference Papers in Energy* 2013 (June 2013), pp. 1–9. ISSN: 2314-4009. DOI: 10.1155/2013/437674.

[39] Statnett. *Fast frequency reserves - FFR*. 2023. URL: https://www.statnett.no/for-aktorer-i-kraftbransjen/systemansvaret/kraftmarkedet/reservemarkeder/ffr/.

[40] Statnett. *NVF 2022 - Nasjonal veileder for funksjonskrav i kraftsystemet*. Tech. rep. Statnett, 2022, pp. 119–122. URL: https://www.statnett.no/globalassets/for-aktorer-i-kraftsystemet/systemansvaret/retningslinjer-fos/systemansvaret---vedlegg-til-retningslinjer-fos--14---nvf.pdf.

[41] Pietro Tuminio. *Frequency Control in a Power System*. 2020.

[42] Kaleem Ullah et al. *Automatic generation control strategies in conventional and modern power systems: A comprehensive overview*. May 2021. DOI: 10.3390/en14092376.

[43] Nadia Weekes. *Offshore wind clusters to lower energy production - study*. 2021. URL: https://www.windpowermonthly.com/article/1719266/offshore-wind-clusters-to-lower-energy-production-%e2%80%93-study.

[44] WindEurope. *Capacity Factors*. May 2023. URL: https://windeurope.org/about-wind/daily-wind/capacity-factors.

[45] World-Weather. *Weather archive in Trondheim*. 2022. URL: https://world-weather.info/archive/norway/trondheim/.

[46] Amirnaser Yazdani and Reza Iravani. *Voltage-Sourced Converters in Power Systems: Modeling, Control, and Applications*. 2010. DOI: 10.1002/9780470551578.

[47] Weiyi Zhang, Daniel Remon and Pedro Rodriguez. 'Frequency support characteristics of gridinteractive power converters based on the synchronous power controller'. In: *IET Renewable Power Generation* 11.4 (Mar. 2017), pp. 470–479. ISSN: 17521424. DOI: 10.1049/iet-rpg.2016.0557.

Appendix

A Kundur's Two Area System Parameters

Base Parameters

The base parameters for Kundur's Two Area System are presented in table A1.

Parameter	Value	Unit
S_{base}	900	MVA
f_{base}	50	Hz
Slack bus	B3	-

Table A1: K2A Base Parameters

Bus Parameters

The bus parameters for Kundur's Two Area System are presented in table A2.

Bus	Voltage
B1	20
B2	20
B3	20
B4	20
B5	230
B6	230
B7	230
B8	230
B9	230
B10	230
B11	230

Table A2: K2A Bus Parameters

Line Parameters

The line parameters for Kundur's Two Area System are presented in table A3.

Line	From	To	Length	S_n	V_n	Unit	R	X	B
L5-6	B5	B6	25	100	230	p.u.	0.0001	0.001	0.00175
L6-7	B6	B7	10	100	230	p.u.	0.0001	0.001	0.00175
L7-8-1	B7	B8	110	100	230	p.u.	0.0001	0.001	0.00175
L7-8-2	B7	B8	110	100	230	p.u.	0.0001	0.001	0.00175
L8-9-1	B8	B9	110	100	230	p.u.	0.0001	0.001	0.00175
L8-9-2	B8	B9	110	100	230	p.u.	0.0001	0.001	0.00175
L9-10	B9	B10	10	100	230	p.u.	0.0001	0.001	0.00175
L10-11	B10	B11	25	100	230	p.u.	0.0001	0.001	0.00175

Table A3: K2A Line Parameters

Transformer Parameters

The transformer parameters for Kundur's Two Area System are presented in table A4.

Transformer	From bus	To bus	S_n	V_{nfrom}	V_{nto}	R	X
T1	B1	B5	900	20	230	0	0.15
T2	B2	B6	900	20	230	0	0.15
T3	B3	B11	900	20	230	0	0.15
T4	B4	B10	900	20	230	0	0.15

Table A4: K2A Transformer Parameters

Load Parameters

The load parameters for Kundur's Two Area System are presented in table A5.

Load	Bus	P	Q	Model
L1	B7	967	100	Z
L2	B9	1767	100	Z

Table A5: K2A Load Parameters

Shunt Parameters

The shunt parameters for Kundur's Two Area System are presented in table A6.

Load	Bus	V_n	Q	Model
C1	B7	230	200	Z
C2	B9	230	350	Z

Table A6: K2A Shunt Parameters

Generator Parameters

The generator parameters for Kundur's Two Area System are presented in table A7.

Gen	Bus	S_n	V_n	P	V	H	D	X_d	X_q	$X_d^{'}$	$X_q^{'}$	$X_d^{''}$	$X_q^{''}$	$T_{d0}^{'}$	$T_{q0}^{'}$	$T_{d0}^{''}$	$T_{q0}^{''}$
G1	B1	900	20	700	1.03	6.5	0	1.8	1.7	0.3	0.55	0.25	0.25	8.0	0.4	0.03	0.05
G2	B2	900	20	700	1.01	6.5	0	1.8	1.7	0.3	0.55	0.25	0.25	8.0	0.4	0.03	0.05
G3	B3	900	20	719	1.03	6.5	0	1.8	1.7	0.3	0.55	0.25	0.25	8.0	0.4	0.03	0.05
G4	B4	900	20	700	1.01	6.5	0	1.8	1.7	0.3	0.55	0.25	0.25	8.0	0.4	0.03	0.05

Table A7: K2A Generator Parameters

Governor Parameters

The governor parameters for Kundur's Two Area System are presented in table A8.

Gov	Gen	R	D_t	V_{min}	V_{max}	T_1	T_2	T_3
GOV1	G1	0.12	0.02	0	1	0.1	0.09	0.2
GOV2	G2	0.12	0.02	0	1	0.1	0.09	0.2
GOV3	G3	0.12	0.02	0	1	0.1	0.09	0.2
GOV4	G4	0.12	0.02	0	1	0.1	0.09	0.2

Table A8: K2A Governor Parameters

AVR Parameters

The AVR parameters for Kundur's Two Area System are presented in table A9.

AVR	Gen	K	T_a	T_b	T_e	E_{min}	E_{max}
AVR1	G1	100	2.0	10.0	0.5	-3	3
AVR2	G2	100	2.0	10.0	0.5	-3	3
AVR3	G3	100	2.0	10.0	0.5	-3	3
AVR4	G4	100	2.0	10.0	0.5	-3	3

Table A9: K2A AVR Parameters

PSS Parameters

The PSS parameters for Kundur's Two Area System are presented in table A10.

PSS	Gen	K	T	T_1	T_2	T_3	T_4	H_{lim}
PSS1	G1	50	10.0	0.5	0.5	0.05	0.05	0.03
PSS2	G2	50	10.0	0.5	0.5	0.05	0.05	0.03
PSS3	G3	50	10.0	0.5	0.5	0.05	0.05	0.03
PSS4	G4	50	10.0	0.5	0.5	0.05	0.05	0.03

Table A10: K2A PSS Parameters

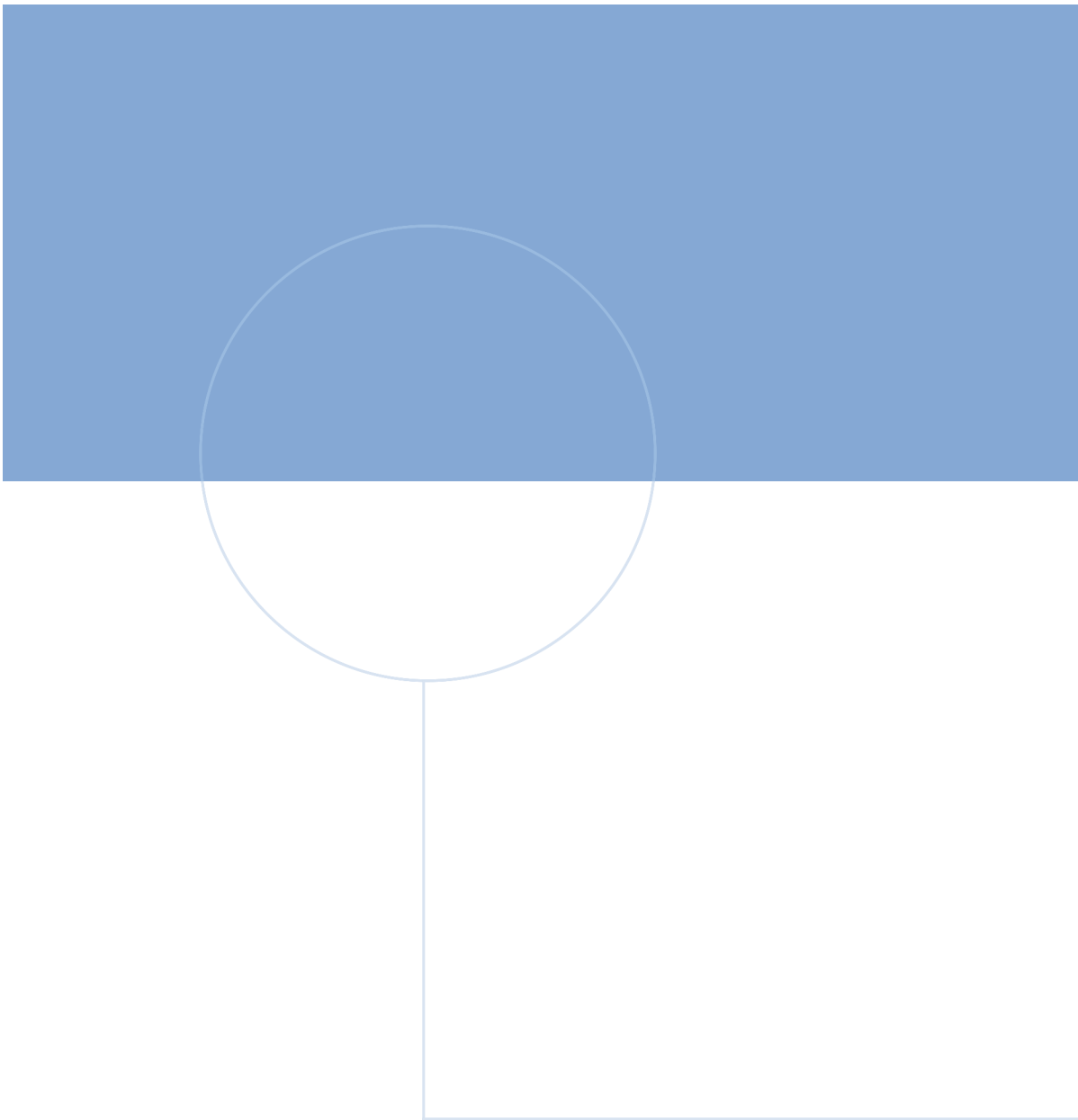

NTNU

Norwegian University of
Science and Technology